BEHAVIOR AND CAPACITY OF THERMALLY RESTRAINED MOMENT FRAME MEMBERS DURING COMPARTMENT FIRE

by

Supriya Nagraj Chinivar

A Thesis submitted to the Graduate Faculty of
Auburn University
in partial fulfillment of the
Requirements for the Degree of
Master of Science

Auburn, Alabama
August 7, 2021

Keywords: fire response, steel beam-to-column moment connections, bending moment and axial force, finite element analysis, modeling, connection behavior, elevated temperatures

Approved by

Kadir C. Sener, Chair, Assistant Professor of Civil & Environmental Engineering
Robert W. Barnes, Brasfield and Gorrie Associate Professor of Civil & Environmental Engineering
Justin D. Marshall, Associate Professor of Civil & Environmental Engineering

ACKNOWLEDGMENTS

I want to express my deep sense of gratitude to my advisor Dr. Kadir Sener, for giving me the incredible opportunity to study structural subjected to fire. Little did I know that our brief conversation would leave me with an intriguing research topic. Thank you for your continuous guidance, constant encouragement, and valuable feedback during the time, which has played a significant role in improving my self-esteem and the outcome of my research work. The learning environment created by you enabled me to think out of the box, which helped me handle multiple challenges. I would also like to thank Dr. Robert W. Barnes and Dr. Justin D. Marshall for serving on my graduate committee and contributing to my academic and professional development.

I express profound gratitude to the administrative staff in the Department of Civil and Environmental Engineering at Auburn University for always being kind and supportive.

I want to express my profound appreciation to Anjan Mogali for his friendship, helpful nature, and knowledge-sharing attitude. Your timely priceless advice has made my journey very memorable at Auburn University. Hongyang Wu and Pablo Hurtado, thank you for solving all queries related to Abaqus. I want to acknowledge further the motivation offered by all my friends that I made in Auburn.

Finally, I would like to thank my unwavering husband, Aditya Kamath, for his enduring love and belief in me and for allowing me to experience this incredible learning journey that we call graduate school. Your positive attitude has inspired me to face every challenge with a smile. You are the best person I have ever met. I am incredibly grateful to have you as my better half.

ABSTRACT

In the event of a fire hazard, structural resistance depends on the ability to resist a comprehensive set of load combinations comprising the gravity loads and the thermally induced fire loads without undergoing failure. Structural floor beams and connections of moment frames are typically designed against flexural demands from gravitational or lateral loads, and axial loads induced due to restrain against thermal expansion (thermal restraint) are generally not part of the design considerations. Prior studies on the fire behavior of structural steel frames have indicated that the thermally induced axial loads on beams and connections are dependent on the temperature change and connection type. Due to the high stiffness of moment (rigid) connections, these thermally-induced axial loads, in addition to beam bending moments due to gravity loads, can lead to various failure modes such as local buckling, plastic hinging, or other instabilities in the member or connection. Although there have been research studies on the flexural response of moment connection at elevated temperatures, the combined effect of axial force-bending moment interaction at elevated temperature under a thermal restraint condition has not been thoroughly investigated.

This thesis focuses on investigating the structural behavior of floor beams and moment connections that are part of moment frames under the combined effect of bending moment and thermally-induced axial force during a fire event. Finite element analysis method was employed to investigate the structural behavior of members and connections under elevated temperatures as a result of compartment fire. Benchmark finite element models were first developed to verify the modeling approach using data from past experimental research. The numerical models accounted

for temperature-dependent material models by Eurocode and NIST developed models, and also incorporated damage and failure criteria in the constitutive material models.

Member level studies of typical floor beams (slender sections for compression) under combined bending and axial loading were conducted to investigate strength through finite element analysis. The analysis results were used to develop interaction capacity curves for combined axial and bending moment cases at elevated temperature (M-N-T) and compared against the member strength equations provided in the AISC specification Appendix 4 for elevated temperature design of steel structures. It was observed that the AISC equations overestimate the strength of slender members for compression at low slenderness ratios. The analysis results also demonstrated that the beam-column design equations including the combined effects of axial-load and bending moment provided reasonable strength estimate for slenderness ratio of 60 and above.

Connection capacity studies were conducted on a typical welded unreinforced flange-bolted web (WUF-B) connection as a representative moment connection. The moment connection behavior was primarily governed by the failure modes exhibited at the ends of the connecting floor beams, therefore the interaction curves developed for beam-column member strength using the AISC provisions resulted in providing conservative estimates and are recommended for usage in moment connections capacity calculations during fire conditions.

TABLE OF CONTENTS

LIST OF TABLES

LIST OF FIGURES

1. INTRODUCTION

1.1 General Introduction

Steel is a popular construction material because of its structural properties, such as high strength and ductility, making it a safe choice in seismic-prone areas. The steel-framed buildings commonly use structural systems in seismic-prone areas because of their ability to provide a cost-effective way to provide large span elegance, fast erection speed, and adaptability [1]. The strength-to-weight ratio of steel is highest compared to the other construction material, making it one of the lighter construction materials. With the innovation of new construction methods, steel has become a well-liked choice for buildings with intricate architectural details. Despite these benefits, however, it has been observed that steel is adversely affected under fire events because of degradation in strength and stiffness, leading to large deformations followed by the collapse of the structure.

Fire is a hazardous event that subjects the structure to a distinctive set of demands during its performance to resist the enormous forces and excessive deflections and rotations with extensive damage. The structures are often subjected to an extensive set of different load combinations. The prescriptive design approach relies on load combinations where envelope demands from one hazard type typically govern the design, thus preventing the interaction of hazard scenarios. This may lead to lacking knowledge regarding the performance interactions between fire and significant lateral load demands from earthquakes or severe windstorms. In the event of a fire hazard, the structure's resistance is solely dependent on its ability to resist these extensive sets of load combinations comprising the service loads such as structural gravity loads, lateral loads, and induced thermal loads yielding satisfactory performance concerning

resilience under fire demands. This developed an interest in understanding structure's response at elevated temperature in fire conditions [2]. A few researchers focused on innovating new materials and methods to protect the structural members by delaying the onset of critical failure temperature, thereby enhancing their performance. These fire protection materials may prove to be advantageous in delaying the collapse. However, from an engineering perspective, it was rational to analyze and design the structure to withstand fire events without considering fire protection rather than analyzing the structure under normal conditions and then applying for fire protection. This has intrigued researchers to perform studies involving the overall response of individual structural elements in isolation or a complete form under fire conditions. As such, there has been new interest in development in engineering methods of analysis and design of structural steel under fire hazard reducing the fire protection requirement and positively impacting the construction process [3].

1.2 Beam-to-Column Connections

Connections are structural components used for fastening different members of the structural steel. With the help of its sufficient strength and stiffness, they facilitate the transfer of forces and moments between the individual structural members. These steel connections typically comprise bolts, welds, endplates, shear-tab, web, and flanges of beams and columns. The connection defines the actual behavioral mechanism between the beam and the column, which significantly influences connection rigidity on the beam response. A connection can be categorized as moment (rigid), shear (simple), or partially rigid connection. Due to the wide range of connection types, understanding the connection response has become necessary and complicated. However, there have been advancements towards the standardization of the design and detailing of connections [4]. Even though experimental testing is the most definitive way of

getting proper connection behavior [5], testing all types of connections proves expensive. Due to limitations of testing, this research project was directed towards developing numerical methods for capturing the key features of connection behavior in the structural system through computational studies.

1.3 Behavior of Connections at Elevated Temperatures

Beam-to-column connections have played a significant role in the design of steel structures as they enhance the overall structural behavior at both ambient and elevated temperatures. These connections are generally designed as simple (shear) connections in the case of having a separate lateral load resisting system. Simple connections resist insignificant moments at ambient temperature by allowing large rotations [6]. These deformations are significantly more prominent in fire, and the forces generated through the beam are transferred to the other structural members via connections. Some fire tests conducted on the Cardington full-scale test frame [7] and observations from actual fire events [8] have illustrated the significance of studying the connection behavior at elevated temperatures as the influence of connection rigidity has a more significant impact on increasing the survival time of the structure [8] as compared to the structural members. Due to the relative size and shielded locations, connections tend to heat up slower than the material within the span, allowing higher load resistance within the connection [6].

1.4 Motivation and Research Need

While prior experimental research focused on the behavior of structural steel-framed building components and simple (shear) connections subjected to fire, only a limited number of research studies focused on the behavior of moment connections at elevated temperatures. The simple (shear) connections are predominantly more flexible than moment connections, but these

studies reveal a severe amount of induced thermal forces approaching the beam capacity at service conditions. This outcome is a concerning observation for moment connections, which are stiffer than simple connections, and the thermally induced forces and moments demands generated at the beam ends are expected to be even more significant relative to the respective member capacity potential leading to local failures and instabilities (rupture, buckling) within the member or the connection.

This thesis focused on investigating the structural behavior of floor beams with moment connections subjected to combined effect of bending moment and thermally induced axial force at elevated temperatures under an axial restraint through computational simulations. A member level study of typical floor beams (slender sections for compression) was conducted through finite element analysis to develop M-N-T interaction curves and compare these interaction curves against the M-N-T interaction curves developed using member strength equations provided in AISC Specification Appendix 4. Numerical investigations were conducted on flange bolted web connection (WUF-B) as a representative moment connection to develop moment-axial force-temperature (M-N-T) interaction curves for the connection at elevated temperatures using National Institute of Standards and Technology (NIST) [9] and the European Committee for Standardization (CEN) [10] material models. Finally, the M-N-T interaction curves for the moment connection were compared against the M-N-T interaction curves developed using the member strength equations given in AISC Specification Appendix 4 [11].

1.5 Research Goals and Objectives

The primary agenda of this research project was to investigate the behavior of WUF-B moment connection subjected to elevated temperatures representing fire through computational studies. The results obtained from these studies contribute to understanding the connection

under the events of fire hazards and the influence of different material models on the behavior of this connection. In addition, this research also studies the applicability of the AISC Appendix 4 equations [11] for determining the overall strength of moment connections. The research objectives are summarized in the following points:

1. To develop high fidelity finite element numerical models to study the structural behavior of beam-to-column moment connections.
2. To establish the relationship between axial force-bending moment-temperature (M-N-T) through numerical investigation by subjecting the members and connections to combined moment and axial forces at elevated temperatures.
3. To perform a comparative assessment on the influence of NIST and Eurocode 3 material models on the behavior of the WUF-B connection.
4. To study the applicability of the AISC Appendix 4 equations [11] and derive interaction curves for moment connections at elevated temperatures.

To accomplish the goals and objectives logically, the research project was divided into a series of following tasks:

- **TASK I – Literature Review of Prior Studies:** A thorough literature review on past research studies was conducted to study the effects of elevated temperatures on steel members and connections.
- **TASK II – Development of Benchmark Finite Element Models for Moment Connections:** A detailed three-dimensional (3D), nonlinear structural model was developed to predict the nonlinear inelastic behavior of steel moment connections using the finite element method implemented in commercially available programs such as Abaqus [12]. This model was developed to evaluate and benchmark the modeling

techniques by modeling the experimental beam-column assemblies by Yang et al. [13], which involves a moment connection, and by Al-Jabri et al. [14], [15], which consists of a flush-end plate using welded flange-bolted web type moment connection. The fidelity of the finite element models developed in Task I were further verified by comparing the load vs. displacement curves, moment vs. rotation curves, and failure modes with the experimental results by Yang et al. [13] and Al-Jabri et al. [14], [15]. These verified models were able to validate the modeling technique adequately.

- **TASK III – Analysis of Floor Beams at Elevated Temperature Conditions:** In this task, a member level study of typical floor beam sections (slender in compression) was conducted through finite element analysis. The study was conducted for elevated temperatures representing fire and involved assessment of 1) the compressive strength of the member (pure compression case), 2) the flexural strength of the members (pure bending case), and 3) the capacity of the members under combined axial loads and bending moments (M-N-T). The finite element results were then compared with the current member strength equations at elevated temperatures given in AISC Specification Appendix 4 [11].
- **TASK IV – Analysis of Moment Connections –** In this task, the fundamental behavior of beam-column moment connections, particularly the bolted shear tab and welded unreinforced flange-beam (WUF-B) connection type, subjected to pure axial, pure moment, and combined moment and axial force at elevated temperature (M-N-T relationship) was investigated. The influence of materials models such as NIST [9] and Eurocode 3 [10] was also studied. The M-N-T interaction curves obtained using the

NIST and Eurocode 3 material models were compared against the AISC Appendix 4 [11] member strength equations.

1.6 Thesis Outline

This thesis is divided into six chapters. Chapter 1 introduces this thesis, discusses research motivation and need, and provides an outline of the research's tasks. Chapter 2 provides a literature review and summary of previous work conducted on the analysis of beam-column connections subjected to fire. Chapter 3 presents the three-dimensional modeling technique and its benchmarking by comparing the results with past experimental studies. Chapter 4 presents an assessment of typical floor beams using finite element analysis and compares the M-N-T interaction results with the current AISC Appendix 4 [11] member strength equations. Chapter 5 discusses the behavior of a representative moment connection and the influence of the NIST [9] and Eurocode 3 [10] material mode on the behavior of this connection. This chapter also investigates the applicability of AISC Appendix 4 [11] equations in determining the capacity of typical moment connections. Chapter 6 summarizes the thesis with final conclusions and recommendations for future work.

2. LITERATURE REVIEW

2.1 Introduction

Limited studies conducted on both simple and moment resisting steel frame connections subjected to temperature histories representing fire loading have indicated that large axial forces (80-90% of squash load capacity) are generated in the horizontal elements of flooring systems (beams and girders). Due to the long spans used in steel construction, horizontal member design is generally governed by flexural demands, either due to the transverse loading resulting from gravitational loads or lateral loading. Thus, axial load consideration is not a part of horizontal steel member design or connections as the axial demands are typically less than 10% of the member's capacity and neglected during design.

When steel structures are subjected to fire, beams expand due to rising temperature exerting axial compressive forces at member ends and later contract when the structure cools down, causing the axial forces to reverse to tensile. Since these thermally induced axial forces are not considered in the design of horizontal members or beam-to-column connections, these members become susceptible to various limit states such as local failure, plastic hinging, and other instabilities that would be activated during a fire event. The expected joint behavior, at a minimum, is for the joint to have the capability of withstanding the service-loads during a fire event and redistribute the forces to adjacent bays without collapse of the frame. The effects of axial end-forces during fire hazard become an intriguing study because they represent the types of loading imposed on connections in a fire's heating and cooling phases, respectively. Emphasis is needed on understanding the influence of interaction between moment and thermally-induced axial load at elevated temperature since this is not considered in current

design standards, nor is any guidance provided. Note that this thesis only focuses on the heating phase and not the cooling phase.

Several experimental and numerical studies have been conducted on steel-concrete composite floor systems subjected to combined fire and mechanical loading, and this section highlights some of the relevant studies. Most of these studies investigated the connections of gravity frames (shear connections), and minimal experimental research was conducted on moment connections. The focus on simple connections, typically used in gravity frames, was due to the load combinations given in building codes combining fire with service level gravity loads and resulting in connections of the gravity load resisting members becoming the critical elements for the fire events [16]. Another reason for prior studies to primarily focus on gravity frames is credited to the nonexistence of interaction diagrams related to force-displacement-temperature or moment-rotation-temperature relationship.

2.2 Simple (Shear) Connection Subjected to Fire

This section presents some of the research conducted on simple connections highlighting the importance of frame behavior and considering a realistic fire application where most of the studies included a heating stage followed by a cooling stage.

2.2.1 Cedeno et al. (2009)

Cedeno et al. [17] conducted computational studies to investigate the structural behavior and interaction of composite floor systems with simple connections and moment-resisting connections in the perimeter bays subjected to realistic fire loading considering the cooling portion of the design fire. Detailed finite element model of a ten-story office building was designed according to current building codes and design specifications using IBC [18], ASCE-7 [19] , and AISC Specification [11] for moderate seismic zone requirements and was developed

and analyzed using Abaqus. The analysis of the fire behavior of the composite floor system was focused on the fifth floor because it was well above the ladder range of the firefighting department. The modeling techniques used in developing Abaqus models were validated against the behavior of steel columns from past standard fire tests. The analysis was conducted using two sequentially coupled nonlinear analysis steps: (i) heat transfer analysis and (ii) stress analysis. The studies evaluated the behavior of unprotected floor systems subjected to realistic design fires at the corner, exterior, and interior compartments.

One outcome from the study was that the primary and secondary beams undergo large structural deflections, which were proportional to their tributary areas but were affected by the horizontal end restraints. The studies indicated compressive fire-induced axial force in the early stages, reversing to tension during the decay phase. The computed axial tension force generated during the cooling phase was near the capacity of the connecting beam and significantly higher than the axial tension capacity of the connection. The tension capacities corresponding with the axial forces induced at the beam ends indicated that the shear connections will fracture under the applied realistic fire scenarios. This study was one of the first indications of problematic behavior expected in connections due to axial restraint.

2.2.2 Selamet and Garlock (2010)

Selamet and Garlock [20], [21] performed numerical investigations to evaluate the behavior of shear tab and all-bolted simple connections in the event of a fire and highlighted the importance of the connection details in the fire resistance of beam-column assemblies. The aim was to identify modifications that can be made to the single plate connections to evaluate their improved performance under fire and examine the effects of heating and cooling on the beam and connection requirements. The computational simulations were validated based on the

results obtained from system-level experimental frame studies with simple connections conducted at the Cardington tests [22]. Their research focused on the detailing practices that lessen the axial restraint by allowing expansion, contraction, and rotation of connections, resulting in reduced fire-imposed thermal loads.

The results from the parametric study indicated that the shear tab provides large rotational capacity developed during the heating phase changes into tensile strength in the cooling phase making it more susceptible to failure. Another outcome was the influence of the increasing gap between the beam and the connection member. This reduced the axial restraint, increased the tensile strength, and evenly distributed the tensile forces between the bolts. It allowed for more beam-end rotation without developing contact between the bottom flange and the connection member which eventually delayed the bearing connections failure by minutes of added fire resistance. It was observed that the failure mode of this type of connection is typically bolted shear.

In addition to the analysis of shear-tab connections, Selamet and Garlock [23] compared the behavior of single plate, single-angle, and double-angle connections under fire conditions using the finite element software Abaqus. Although the shear-tab connection models were validated using the results of a full-scale building fire test performed at Cardington, the single-angle and double-angle numerical models were not validated by experimental testing [23]. All the connections experienced local buckling in the beam lower flange in the heating phase, indicating the maximum compression in the beam and did not undergo fracture in the cooling phase.

2.2.3 Agarwal et al. (2011)

Agarwal et al. [16], [24], [25] conducted analytical investigations to study the structural response and collapse of steel buildings concerning fire location, fire intensity, and proximity of the fire to critical members in the structure. A ten-story office building was designed according to U.S. standards and codes [18]. The structural layout consisted of interior gravity frames and perimeter moment-resisting frames (MRFs). The high fidelity detailed finite element models were analyzed using nonlinear explicit dynamic analysis, which accounted for large deformations, temperature-dependent material, mechanical properties, and various complexities of structural behavior such as inelastic buckling of steel columns and yielding of steel beams. The analysis was conducted using the sequentially coupled thermal-structural analysis approach. The models developed in Abaqus were validated against the behavior of steel columns using the results from past standard fire tests.

The analytical results indicated the development of the negative bending moment in the connection region due to the thermal expansion and rotation of the beam at elevated temperatures, which led to the bottom flange of the beam to come in contact with the column even though the connections were designed only for vertical loads. This has reduced the positive moment demand at the mid-span and increased the resistance to fire, thereby delaying the time of failure. The analysis results further depicted the significant influence of inelastic buckling of interior gravity columns on the overall behavior of the complete building structure.

The parametric study observed that bolt shear was a standard failure mode of shear-tab connections during a fire. In some cases, yielding of the composite beam bottom flange and the column flanges of the gravity frames governed the failure mode. The rotation of the beam-ends at elevated temperatures led the bottom flange of the composite beams to come into contact

with the gravity columns causing large compressive forces in the bottom flange of the steel beams and large tensile forces in the bolts of the connections.

2.2.4 Selden et al. and Fischer et al. (2014-2015)

Selden et al. [26] and Fischer et al. [27] performed experimental and numerical studies on steel beams composite slabs to study the effects of the thermal and structural behavior on both member and connection response. The composite slabs were restrained against the effects of expansion and contraction. The experimental investigation consisted of large-scale composite beam tests with bolted simple shear connections subjected to constant gravity loading at the mid-span of the composite beam during the heating and cooling phase (see Figure 2-1). The numerical studies involved the development of 3D nonlinear finite element models of the experimental model using Abaqus. Further verification and benchmarking of modeling techniques were performed using experimental investigation data to determine the member capacity and predict similar thermal and structural behavior.

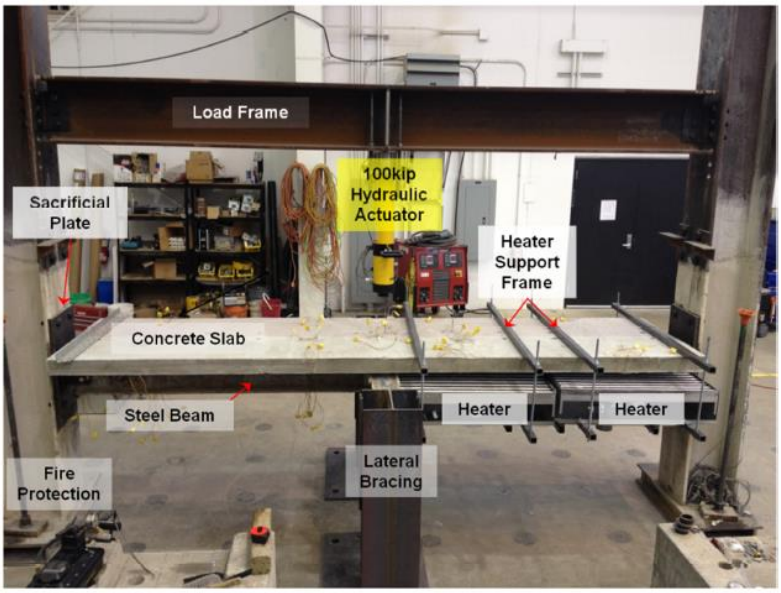

Figure 2-1 Composite Beam Experimental Test Setup Arrangement of Selden et al. [26]

The thermal response of the connection did not indicate a temperature gradient, but a temperature difference of about 200ºC was observed from the member bottom flange. Large deformations related to axial forces were observed at beam ends during the application of the fire loading, where local fracture, failure, and prying in the connections were observed. These thermally induced end forces were not measured during testing. However, follow-up computational studies simulating the testing observed that the member end forces imposed on the connections exceeded several connection limit states for the specimens that experienced failure during the tests [27].

2.2.5 NIST (National Fire Research Laboratory) (2020)

Large-scale experimental studies have recently been conducted on steel-concrete composite floor assemblies under realistic compartment fires and gravity loads at NIST's National Fire Research Laboratory [28]. Both member- and system-level tests have highlighted the importance of test configuration (see Figure 2-2) and failure modes that are typically overlooked or unnoticed during component testing. These structural-fire test specimens had simple (shear) connections and realistic end restraints. The study's primary purpose was to produce the practical and technical information essential for design for both development and validation of computational models and design tools used for performance-based design of structures in the event of a fire.

The observed failure modes were concentrated in the connection region, which underwent local buckling and bolt-weld fracture during the early fire stages. The steel beams exhibited local buckling near the connection due to restraint of thermal expansion being by end conditions. These observed experimental behaviors are expected to generate greater thermally

induced forces for stiffer connections (e.g., beam-column moment connections). They may cause severe damage,

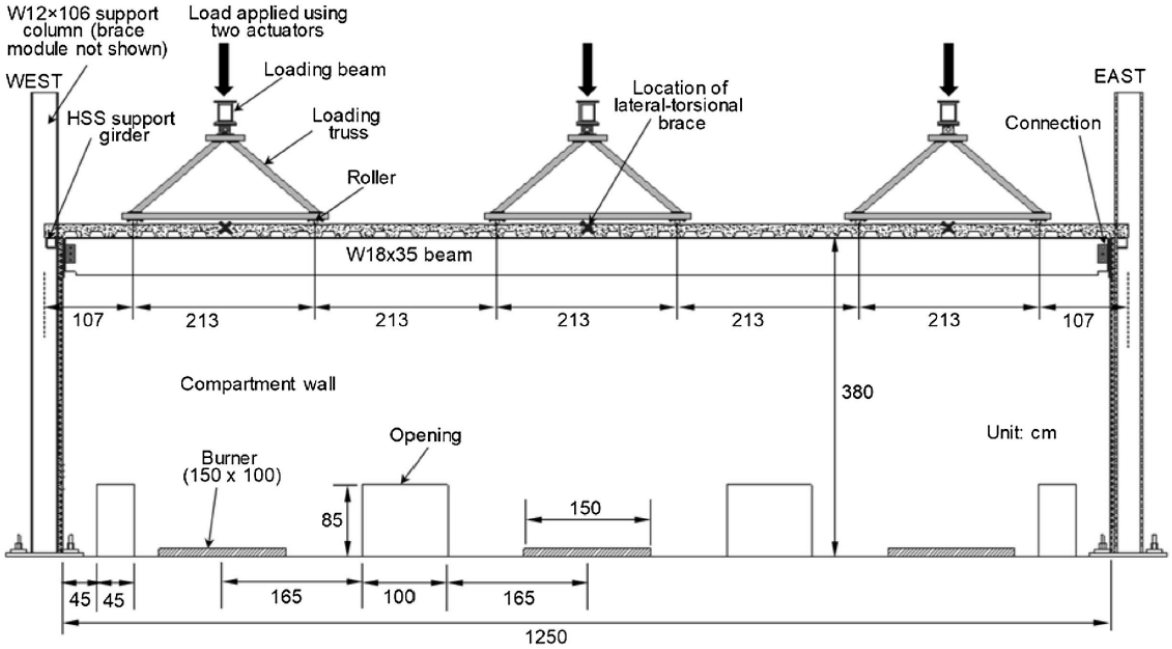

Figure 2-2 Front view Test Setup Arrangement of NIST et al. [28]

which can potentially lead to collapse and progressive structural failure. During these tests, the connection was covered with spray-type fire protection rated for 2-hours which caused the temperature measured near the connection to remain in a range of 300ºC to 500ºC.

2.3 Moment Connections Subjected to Fire

The limited research conducted to study the behavior of moment connections in fire conditions also focused on testing and analyzing isolated joints in various configurations. The studies summarized in this section investigated the flexural response of moment connections at elevated temperatures through testing isolated beam-column joints. The effects of frame continuity, thus the effect of thermally induced axial forces acting on the connections was neglected.

2.3.1 Al-Jabri et al. (2005)

The first experimental study on moment connections subjected to elevated temperature was conducted by Al-Jabri et al. [29], by testing twenty specimens with five different connection details. The specimen has a cruciform arrangement with cantilever beams connected to either side of a center column with two types of semi-rigid endplate connections on one end and free on the other end (see Figure 2-3). Two sets of the specimens had the composite deck to investigate the influence on the connection behavior. The testing was conducted by subjecting the connection to constant bending moment and linearly increasing the furnace temperature to 900ºC in 90 minutes.

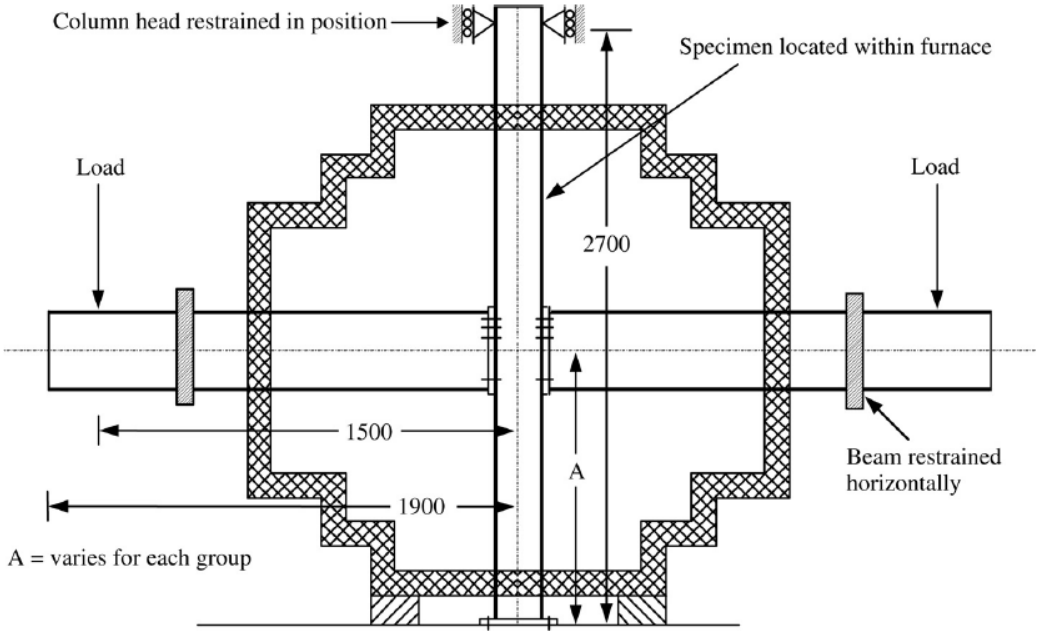

Figure 2-3 Cruciform Shape Specimen and Test Setup Arrangement of Al-Jabri et al. [29]

The experimental results were used to develop analytical models by curve-fitting to represent the moment-rotation-temperature response of endplate connections. The presence of the composite deck caused insulation and a heat sink effect that resulted in a thermal gradient in the steel beam with about a 30% difference between the top and bottom flanges but had an

insignificant effect on the connection capacity. The connections lost stiffness and strength with increasing temperature at different rates, but the temperature vs. rotation curves indicated a rapid increase in connection rotation beyond 500ºC. Analytical studies performed by other researchers based on these tests indicated a significant influence of axial load on initial rotational joint stiffness and presented interaction curves for the extended end plate configurations [30].

2.3.2 Yang et al. (2009)

Another experimental study on moment connections subjected to fire loading was conducted by Yang et al. [13] on sub-frames of a more commonly used moment connection in seismic areas to evaluate the fire performance of the steel beam-to-column moment connections and compute the complete structural response up to and beyond initial failure or local collapse (see Figure 2-4). The researchers completed four tests of welded unreinforced flange-bolted web (WUF-B) connections subjected to bending moments at elevated temperatures representing fire conditions. The performance beam-to-column specimens under fire load were examined by two different types of fire tests, namely: steady-state test and transient state test. In the steady-state tests, the specimens were heated to a specified temperature (550ºC - 650ºC) and gradually increased the load until the structure failed. In contrast, in the transient state tests, the constant service loads were applied to the steel columns and beams, followed by heating the specimen at the standard temperature-time heating rate until failure.

The experimental results from tests conducted at steady-state conditions indicated 60% stiffness reduction and 40% strength degradation at the applied joint temperature ranges. The deterioration of stiffness of the connection was observed to be more significant than the strength degradation as the temperature was higher than 500ºC. For the transient heating case, the

member deformation rate increased rapidly once the connection reached temperatures beyond 550ºC. The failure modes concentrated near the welded flanges, and the resistance provided by the web bolts degraded due to the loss of pre-tension and slippage. It was also observed that with a proper design of the fire-proofing material, the beam-to-column connection could retain its stability without significantly losing its strength and stiffness.

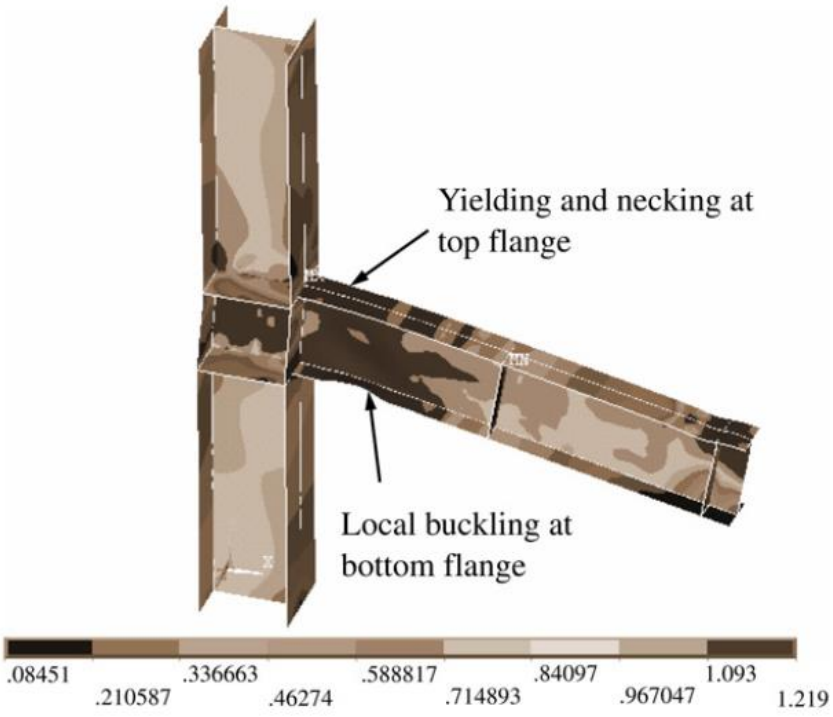

Figure 2-4 Sub-Frame Specimen and Failure Mode by Yang et al. [13]

2.3.3 Burgess et al. (2008)

This experimental study was similar to the study by Al-Jabri, where the flexural behavior of extended end plate moment connections was investigated by Burgess et al. [31] by testing cruciform shape specimens (see Figure 2-5) at elevated temperature to investigate the degradation of steel joints at elevated temperatures. Unlike the previous testing programs, this study was performed in two groups with and without axial restraint against the thermal

expansion of the beams. The beam axial restraint was simulated by applying constant end forces on the beam ends at 2.5% and 4% of the beam squash load capacity. A horizontally mounted jack provided the axial force at the ends of the beam sections, and two forked supporting systems were attached to prevent out-of-plane rotations of the beam ends. For the latter case, the lateral restraint system was attached to the portal frame to prevent lateral-torsional buckling and out-of-plane global buckling of the beam sections. The whole loading system consisted of a hydraulic jack to apply vertical loads at the top of the stub column.

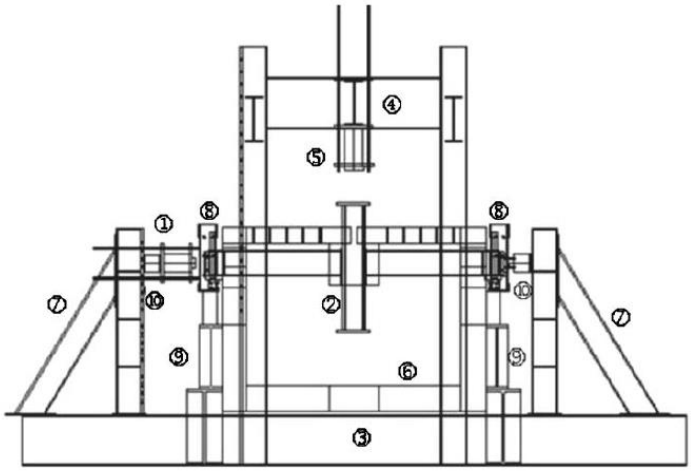

① Horizontal Hydraulic Jack; ② Cruciform Specimen;③ Support Beam; ④ Loading Portal Frame; ⑤ Vertical Hydraulic Jack;⑥ Heating Furnace;⑦ Reaction Frame;⑧ Fork Support System;⑨ Support;⑩ Restraint Beam.

Figure 2-5 Cruciform Test Setup Arrangement of Burgess et al. [31]

The experimental results were used to develop the moment-rotation-temperature characteristics for restrained and unrestrained steel beam-to-column joints. Although the applied axial load did not change with the applied temperature and remained at similar levels, a considerable difference between the unrestrained and restrained cases was observed in the flexural behavior and a substantial strength reduction of about 14%. It was observed that the

axial force significantly affects the structural connection behavior, primarily for moment connections. For the thermally unrestrained cruciform tests, beam web tension field action was developed near the column.

2.3.4 NIST Studies (2015)

Computational studies have also been performed on the behavior and response of frames with moment connections subjected to fire loading and various restraining conditions. NIST researchers [32] analyzed frames from two prototype buildings representing typical steel-composite construction in the United States [33], including the heating and cooling phases. The studies included analysis of two types of moment frames from each of the prototype buildings. The two moment frames included an intermediate moment frame with WUF-B connections and a special moment frame with reduced beam sections (RBS) connections. The frames considered in the study were portions of the prototype moment frames that consist of a beam supported on two columns and joined using the two moment connections (WUF-B and RBS). The joints of the analyzed frame assemblies included full-restraint, partial restraint, and unrestrained cases provided by the adjacent frames. The numerical investigation involved detailed finite element analyses, which were performed using explicit time integration in LS-DYNA for its ability to model sequential failure, including fracture. The assembly was subjected to a uniform gravity load along the beam applied along the centerline of the top flange, which was gradually applied over 0.5 seconds to avoid any dynamic implication.

The axial load measured at beam ends varied with the beam temperature, and its response was highly dependent on the restraint condition of the joint from the adjacent bay. Figures 2-6 and 2-7 depict the normalized axial load variation with applied temperature. These figures indicate that the computed axial load corresponded to 70-80 % of the axial load capacity

of the beam member, regardless of the restraint level at the joint, but were achieved at different temperature instances. The response of unrestrained and partially restrained specimens was significantly different from the fully restrained case as the former failed due to the bolts' shear rupture. The fully restrained beams failed due to local buckling followed by bolt shear rupture in the heating phase, with partial fracture of the flanges resulting from tensile forces developed in the cooling phase. The computational results indicated significant yielding and damage in the connections due to the temperature cycle representing fire at service-load condition.

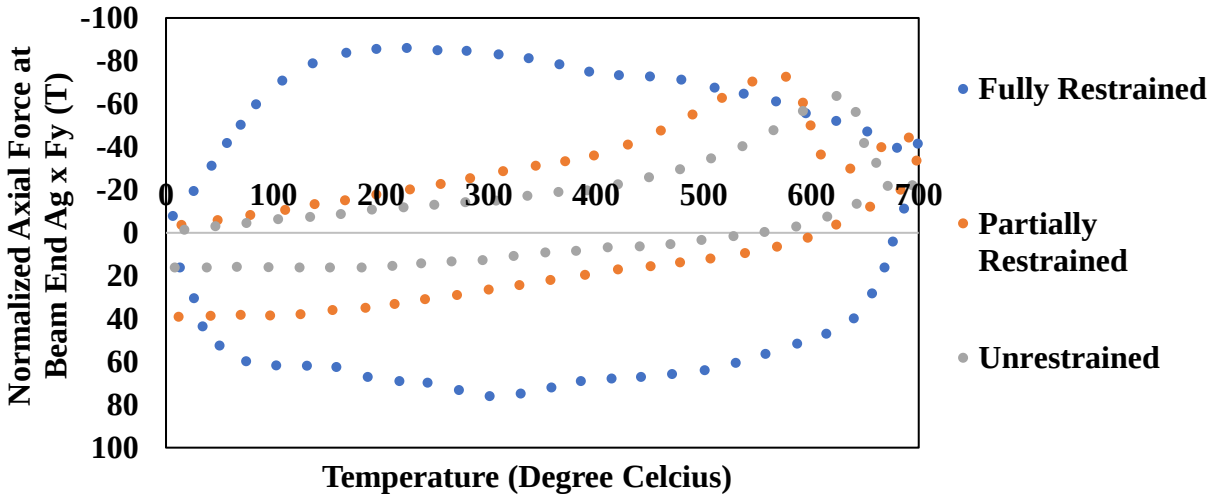

Figure 2-6 Normalized axial end force variation during fire cycle for W21x73 with WUF-B connection, reproduced from [32]

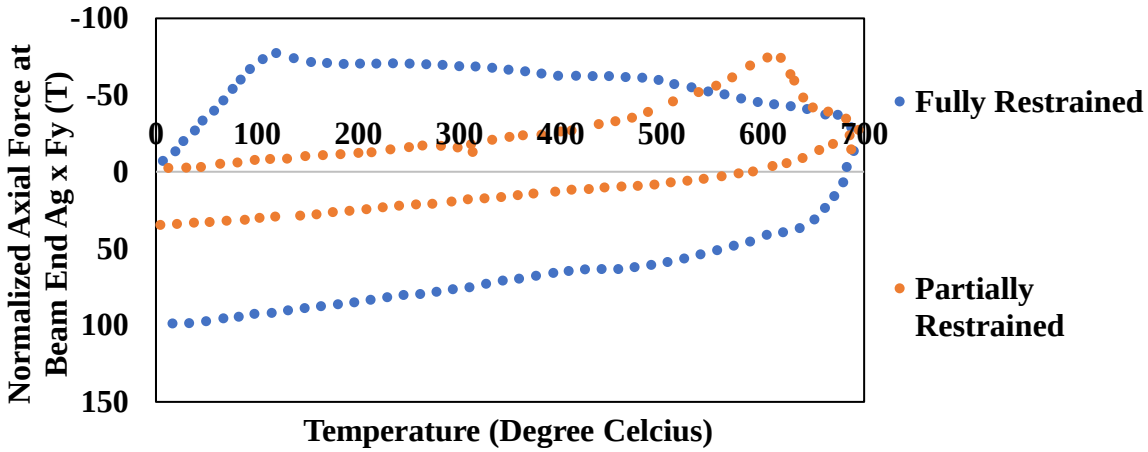

Figure 2-7 Normalized axial end force variation during fire cycle for W24x94 with RBS connection, reproduced from [32]

3. 3D FINITE ELEMENT MODELLING DEVELOPMENT

3.1 Introduction

Numerical investigation using finite element analysis plays a significant role in structural engineering research, especially when the corresponding large-scale experimental tests are costly, laborious and there are many complexities in scaling the prototype. Also, it is challenging to replicate realistic uncontrolled fires experimentally and obtain complex structural behavior. On the other hand, with the new advances in the computational field, computational simulation of structural systems has become highly convenient. Over the past thirty years, many researchers have used numerical tools to study the behavior of steel structures subjected to elevated temperatures. These developed models have given similar observations and results that authenticate the experimental testing and become a beneficial replacement in overcoming any experimental limitations.

The primary purpose of performing numerical analysis in this research is to study and develop a better understanding of the behavior of steel beam-to-column connections, their failure modes at elevated temperatures, and the influence of different material models on the connection behavior. This chapter focuses on the development of comprehensive 3D finite element models for efficiently predicting steel beam-to-column connections' structural behavior and performance at elevated temperatures. To test the fidelity of the modeling approach, these models were further evaluated by comparing the finite element results against the experiments described in the previous chapter through comparing load-displacement, moment-rotation curves, and failure modes.

3.2 Finite Element Modelling Overview

A detailed three-dimensional (3D), nonlinear, structural model was developed using the finite element method implemented commercial software Abaqus [12]. This finite element software was selected because it has the capability to include temperature-dependent material constitutive models and explicitly performs dynamic analysis to evaluate the structural behavior by accurately predicting all the failure modes, including local buckling at elevated temperatures. The analysis was conducted using a nonlinear explicit numerical solution technique and utilizing temperature-dependent material models for steel to predict the nonlinear inelastic behavior of steel moment connections and members subjected to mechanical loads.

In the finite element modeling approach, only a stress analysis model was developed. Heat transfer analysis was not conducted using finite thermal elements, as temperature-time histories were directly defined in the models by utilizing the predefined temperature fields. Temperature-dependent material properties were used, representing the material's degraded characteristics. These temperature-dependent material properties were incorporated using the methodology given in previous research [34], [35], which included defining nonlinear mechanical stress-strain-temperature (σ - ε - T) relationships for steel.

3.3 Material Models

The European Code (Eurocode) provides more guidance for structures subjected to fire [10] when compared with current U.S. design codes. During the investigations of the World Trade Center (WTC) collapse, NIST researchers established σ - ε - T relationships for seventeen different sheets of steel that were used in the WTC tower. Through the experimental work and extensive literature review, NIST researchers developed stress-strain curves at various temperatures for different steels commonly used in U.S. building construction [9]. Recently, the

NIST has published a guideline for structural fire resistance design of concrete and steel buildings [36] that recommends NIST-developed uniaxial σ - ε - T relationship for different types of steel including plates and bolts. The major limitation of Eurocode guidelines for temperature-dependent mechanical properties of steel is covering such relationship only for mild steel that are typically used for plates [36], [37]. The following subsection discusses the temperature-dependent material properties by NIST and Eurocode, and results from numerical studies with comparisons against experimental results of steel members and connections subjected to fire.

3.3.1 NIST Steel Material Model for Elevated Temperature

Past researchers have shown acceptable performance between the experimental results and FEM analyses in which NIST developed σ - ε - T relationship for steel was used [37], [38]. The NIST material models were obtained from NIST Technical Note [9]. The following equation (3.1) and (3.2) provide temperature-dependent expressions for the elastic modulus. In this expression, the constant term E_o was taken as 29000 ksi. The values for coefficients e_1 through e_4 are dependent on the type of steel used. In this study, hot rolled steel was assumed and the values of coefficients are considered as e_1 = 3.768, e_2 = 1.000, e_3 = 639ºC, and e_4 = 1650ºC. The modulus of elasticity is the same for bolts and structural steel. Thus, equation (3.1) below can be used for calculating temperature-dependent elastic modulus E.

$$E = E_0 \, exp\left(\left(-\frac{1}{2}\right)\left(\frac{\Delta T}{e_3}\right)^{e_1} - \left(\frac{1}{2}\right)\left(\frac{\Delta T}{e_4}\right)^{e_2}\right) \tag{3.1}$$

$$\text{where, } \Delta T = T - 20^{o}\text{C} \tag{3.2}$$

The following equation 3.3 provides temperature-dependent expressions for the yield

strength. This equation is limited to steels with nominal yield strength less than 65 ksi. In this expression, the constant term F_{yo} was taken as 50 ksi A 0.2 % offset for the yield strength is used by the model. The values for coefficients r_1 through r_4 are dependent on the type of steel used. For hot rolled steel, r_1 = 7.514, r_2 = 1.000, r_3 = 588ºC, r_4 = 676ºC, and r_5 = 0.090.

$$F_y(T) = F_{y0}\left[r_5 + (1 - r_5)\ \exp\left(\left(-\frac{1}{2}\right)\left(\frac{\Delta T}{r_3}\right)^{r_1} - \left(\frac{1}{2}\right)\left(\frac{\Delta T}{r_4}\right)^{r_2}\right)\right] \qquad (3.3)$$

The yield strength for A325 and A490 high-strength bolts can be calculated using the above equation (3.3), but the values for coefficients r_1 through r_5 used in the equations are different from those used for hot rolled steel. For bolts, r_1 = 4.967, r_2 = 1.000, r_3 = 456ºC, r_4 = 2040ºC, and r_5 = 0.000. Bolts can sustain large nominal strength with the increase of temperature until 400ºC, after which it starts reducing. Figure 3-1 depicts the degradation of the normalized yield strength with increasing temperature for ASTM A572 rolled steel and ASTM 490 bolts.

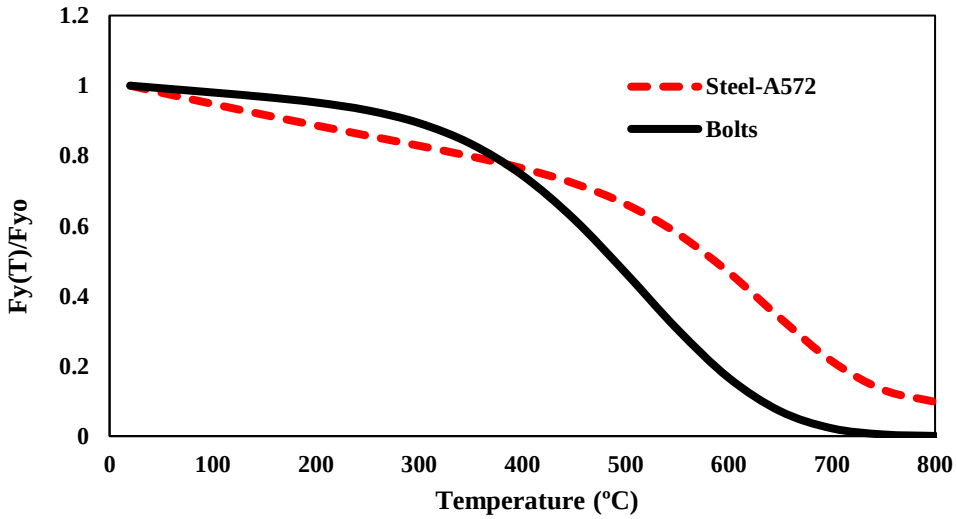

Figure 3-1 Normalized yield strength versus temperature for rolled structural steel and bolts [9]

Using the temperature-dependent expressions for the modulus of elasticity and yield

strength, the true stress σ as a function of true strain ε is given below in equation (3.4), which summarizes the true stress-strain relationship used in the FEM models. For members of Grade 50 steel, the constant term F_{yo} was taken as 50 ksi, and T is the temperature in ^oC. The strain hardening component n = 0.503 and values for coefficients k_1 through k_4 have the following values: k_1 = 7.820, k_2 = 540ºC, k_3 = 1006 MPa, and k_4 = 0.759 [9].

$$\sigma = \left[F_y(T) + (k_3 - k_4 F_{y0}) \, exp\left((-)\left(\frac{T}{k_2}\right)^{k_1} - \left(\frac{1}{2}\right)\left(\varepsilon - \varepsilon_y(T)\right)^n \right) \right] \tag{3.4}$$

$$\text{where, } \varepsilon_y = F_y(T) \,/\, E(T) \tag{3.5}$$

3.3.2 Eurocode Steel Material Model for Elevated Temperature

Eurocode 3, Part 1-2 [10] provides a stress-strain relationship at various temperatures for structural steel. The stress-strain relationship at elevated temperature depends on adequate yield strength ($f_{y,\theta}$), stress at the proportional limit ($f_{p,\theta}$), and slope of linear elastic range ($E_{a,\theta}$). The formulation was used for both compression and tension.

The equations prescribed for the uniaxial stress-strain-temperature relationship are divided into three different stages which are as follows: (i) elastic ($\varepsilon \leq \varepsilon_{p,\theta}$), (ii) transit elliptical ($\varepsilon \geq \varepsilon_{p,\theta,}$ and $\varepsilon \leq \varepsilon_{y,\theta}$), and (iii) plastic ($\varepsilon \geq \varepsilon_{y,\theta}$).

In the elastic stage, strain is less than or equal to the proportional limit ($\varepsilon \leq \varepsilon_{p,\theta}$). The stress σ is calculated using the tangent modulus, $E_{a,\theta}$ using equation 3.6.

$$\sigma = \varepsilon \, E_{a,\theta} \tag{3.6}$$

In the transit elliptical stage, the strain is between the proportional limit and the yield strain ($\varepsilon \geq \varepsilon_{p,\theta}$ and $\varepsilon \leq \varepsilon_{y,\theta}$). The stress σ is calculated using the below equation 3.7:

$$\sigma = f_{p,\theta} - c + \left(\frac{b}{a}\right)\left[a^2 - \left(\varepsilon_{y,\theta} - \varepsilon\right)^2\right]^{0.5} \quad (3.7)$$

where the values of a, b, and c are given by the following expressions:

$$a^2 = \left(\varepsilon_{y,\theta} - \varepsilon_{p,\theta}\right)\left(\varepsilon_{y,\theta} - \varepsilon_{p,\theta} + \frac{c}{E_{a,\theta}}\right) \quad (3.8)$$

$$b^2 = c\left(\varepsilon_{y,\theta} - \varepsilon_{p,\theta}\right) E_{a,\theta} + c^2 \quad (3.9)$$

$$c = \frac{\left(f_{y,\theta} - f_{p,\theta}\right)^2}{\left(\varepsilon_{y,\theta}, \varepsilon_{p,\theta}\right) E_{a,\theta} - 2\left(f_{y,\theta} - f_{p,\theta}\right)} \quad (3.10)$$

In the plastic stage, the strain exceeds the yield strain ($\varepsilon \geq \varepsilon_{y,\theta}$). Thus, the stress σ is equal to the effective yield stress using equation 3.11.

$$\sigma = f_{y,\theta} \quad (3.11)$$

Reduction factors are defined as proportions of values at elevated temperatures to those of ambient temperature. These depend on effective yield strength ($k_{y,\theta} = f_{y,\theta} / f_y$), proportional limit ($k_{p,\theta} = f_{p,\theta} / f_y$), slope of the linear elastic range ($k_{E,\theta} = E_{a,\theta} / E_a$) and the ultimate strength ($k_{u,\theta} = f_{u,\theta} / f_y$). These factors are given in increments of 100ºC. These reduction factors are required to be substituted in the equations defined in Eurocode 3 [10] to obtain the stress-strain curves at elevated temperatures. Figure 3-2 plots the reduction factors for the stress-strain relationship for carbon steel at elevated temperatures.

Eurocode 3 [10] considers rate-dependent effects such as creep while defining the stress-strain relationship at various temperatures. Figure 3-3 shows the Eurocode 3 [10] and NIST [9] for true σ - ε - T relationship at 200ºC, 400ºC, and 600ºC. Since NIST σ - ε - T relationship does not account for rate-dependent effects such as creep at elevated temperatures, it has higher yield stress and more post-yield strain-hardening than the corresponding Eurocode 3 σ - ε - T

relationship. Also, the reduction factors defined in NIST are calculated based on 0.2% offset strain, whereas Eurocode considers 2% offset strain. Eurocode does not distinguish between bolts and member material properties, whereas NIST differentiates the stress-strain plots based on the material strength and degradation with increasing temperature. The NIST σ - ε - T relationship was primarily incorporated in this research to define the mechanical properties of steel material at elevated temperature since rate-dependent effects like creep are not significant for the maximum temperature considered in the study.

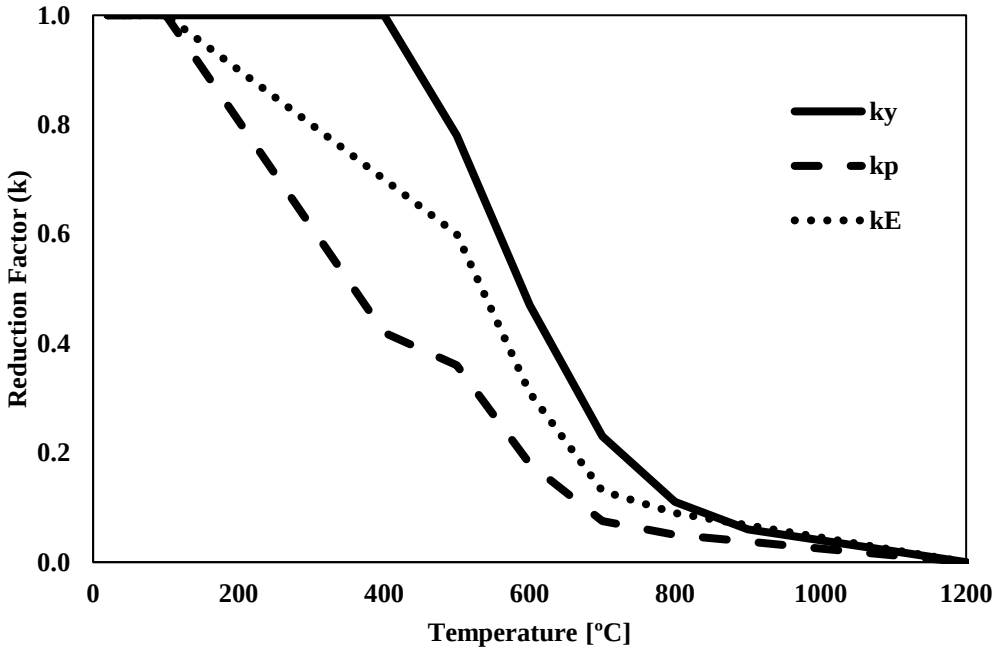

Figure 3-2 Reduction factors for the stress-strain relationship of carbon steel at elevated temperatures [10]

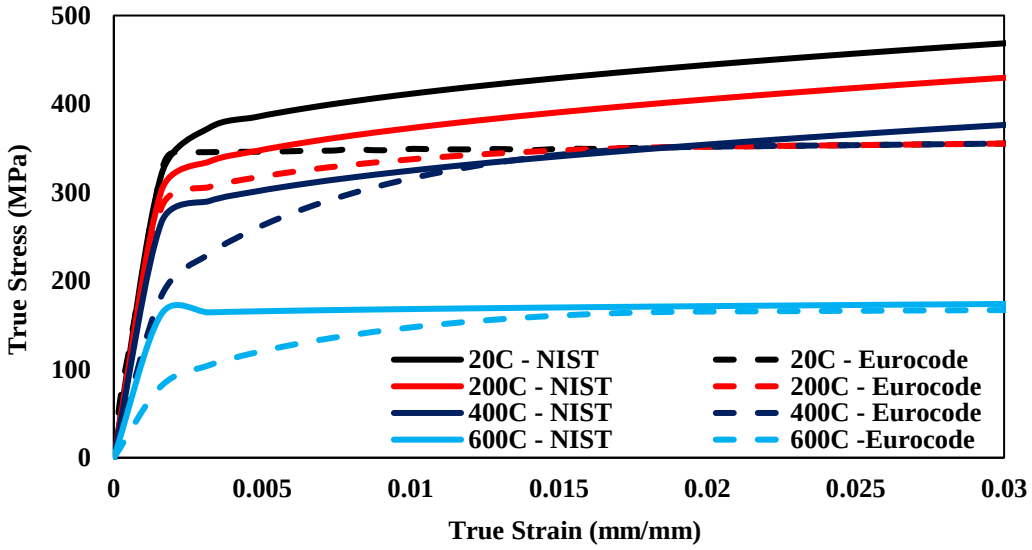

Figure 3-3 True stress-strain temperature relationship using NIST [9] and Eurocode [10]

3.4 Finite Element Modeling Technique

A typical three-dimensional finite element structural model used in this study consisted of the steel beam, steel column, and beam-column connection. These components were modeled using the first order 8-node linear brick element with reduced integration and hourglass control (C3D8R). This element has eight nodes with one node at each corner and allows only displacement degrees of freedom but no rotational degrees of freedom. For the connections with bolts, the bolt holes were considered 2 mm (~1/16 inch) larger than the bolt shank diameter and assumed to be unthreaded. The hexagonal bolt heads were modeled as cylinders by taking the washers' diameter into account, averaging the diameters [39]. The bolt nuts formed an integral component with the bolt shank instead of considering it as an individual part, reducing the number of contact planes and ramification of the model.

The bolts require a realistic representation of the contact interaction between the various components of the connections. For this purpose, the bolted connections were modeled using

surface-to-surface contact with a finite sliding option between the different surfaces of the connection. The contact formulation in Abaqus involves a master-slave type algorithm in which one surface which belongs to the body of more robust material is defined as master surface, and the other surface is defined as slave surface. The various contact areas involved in the bolted connection are the bolt shank-to-bolt holes, bolt head-to shear tab, bolt nut-to-beam web, and shear tab-to-beam web surface in which the contact surfaces of the bolt shank, bolt head, and bolt nut were always selected to be master surfaces. In contrast, the other contact surfaces were defined as slave surfaces. As the contact formulation identifies the surfaces in contact, penalty interactions replicate the bolt-bearing behavior on bolt holes throughout the test. The bolts were not pre-tensioned during the analysis. A friction coefficient of 0.3 was assigned for all the contact interaction surfaces. Based on a study by Al-Jabri [6], the composite slab on top of the beam does not change the failure modes of the beam and only enhances its overall capacity; therefore, the steel beams were modelled as bare steel without a slab on top. The welds used in the connection were represented using a tie constraint between the connecting elements instead of the weld metal itself. To achieve good accuracy for simulation of the contact interactions between the connection parts, fine meshing in the connection region and prolonged load application was practiced. Also, boundary conditions were assigned to achieve sensible behavior in the model. The shear tab was welded to the column, so the contact was defined using tie constraints as it was fixed on the edge.

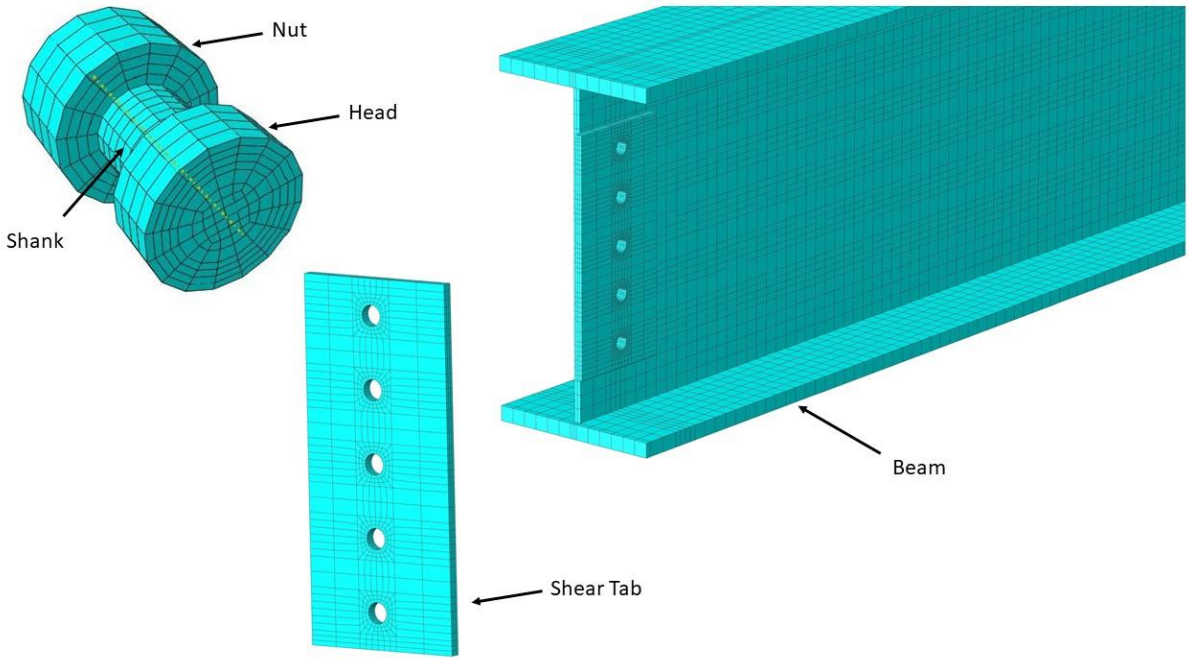

Figure 3-4 Mesh Pattern of Bolt, Shear Tab, and Beam

This study uses Abaqus/Explicit method for analysis; however, the Abaqus/Standard (Implicit) can also be used. The difference between the two methods that can be used is highlighted below, and the choice is based on its suitability. Abaqus/Standard is an equilibrium equation-based method that incorporates the Newton-Raphson approach for achieving a nonlinear solution. Also, the Arc-Length (Riks) approach used for buckling problems can be used for structures with non-continuous solutions involving contact problems. The contact problems are considered highly nonlinear problems and often comprise the solution convergence difficulties and frequent equilibrium checks. However, these convergence problems that emerge while using Abaqus/Standard can be avoided using the Abaqus/Explicit method because it is a non-equilibrium equation-based method.

Furthermore, Abaqus/Explicit method requests less storage capacity and time-length than the former method because it uses diagonal lumped-mass matrices, leaving the system to

be solved as uncoupled. The explicit method was developed to improve the problems related to high-speed dynamic events where large deformation occurs. This method may be used to obtain solutions for static problems, but many increments are needed. For obtaining good results, a minimum of 100,000 increments is required even though the solution may not be as accurate as the static solution of Abaqus/Standard [40].

3.5 Benchmarking the Finite Element Modeling Technique

Benchmarking the finite element model is critical before relying on the output produced through numerical analysis. Benchmarking is done by evaluating numerical analysis results against experimental results. The evaluation process of the finite element models is as follows; a) comparison of the moment connection models against load-displacement curves and moment-rotation curves, b) comparison of temperature vs. displacement curves for transient condition and c) comparison of various failure modes.

3.5.1 Verification of the FEM Model using Yang et al. (2009)

As mentioned in the previous chapter, Yang et al. [13] conducted the experimental and numerical investigation on a commonly used moment connection, i.e., welded flange-bolted web (WUF-B) and subjected to bending moments at elevated temperatures representing fire conditions. The testing program included four tests in which the load was monotonically applied under steady-state and transient state temperature conditions to examine reduction and strength degradation effects. The steady-state analysis was performed by heating the specimen to a specified temperature (550ºC or 650ºC) and gradually increasing the load until the structure failed. Whereas in the transient phase, the service loads applied to the steel column and beam of the specimen were kept constant, followed by heating the specimen to determine the fire resistance of the structure.

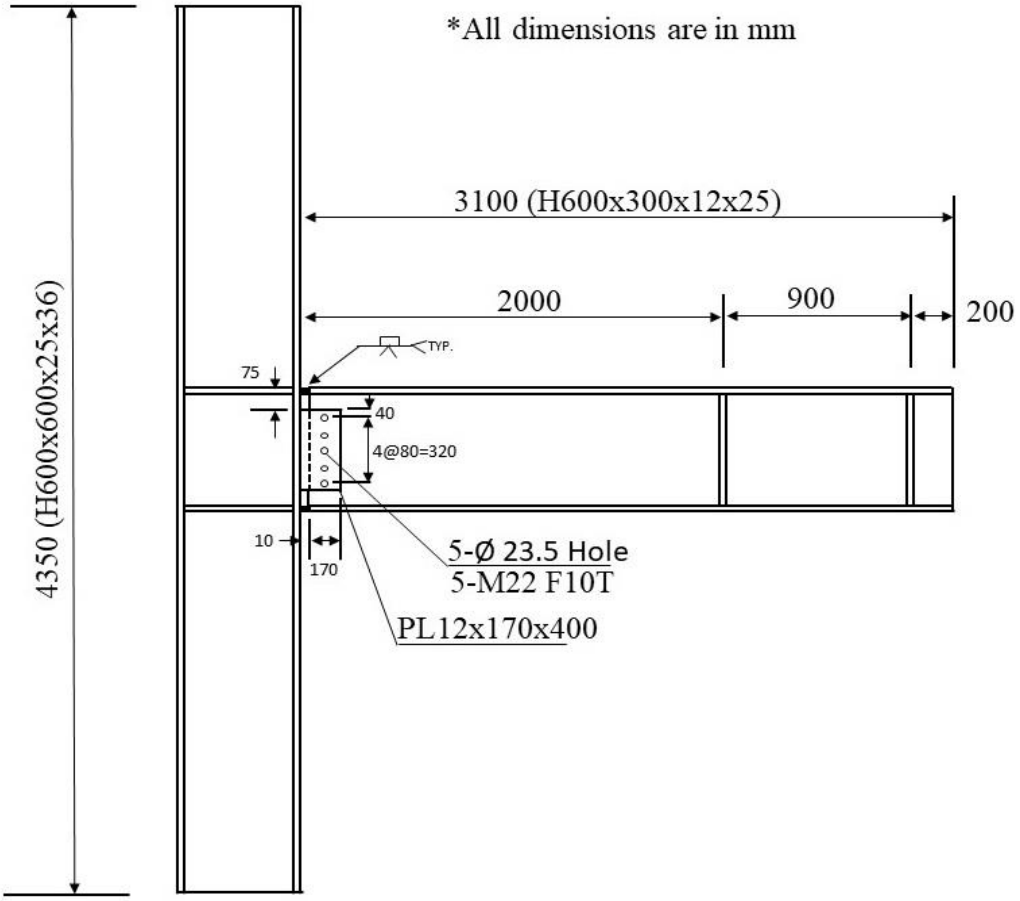

Figure 3-5 Dimensions and detailing of beam-to-column specimens by Yang et al. [13]

As shown in Figure 3-5, the experimental setup included an H600 x 300 x 12 x 25 mm beam and an H600 x 600 x 25 x 36 mm column with a height of 4350 mm. The beam measured 3100 mm in length, and the loading was applied at 2900 mm from the column flange. The lateral support was provided at 2000 mm from the column flange to prevent lateral-torsional buckling of the steel beam. The material properties of the steel section used in the analysis at temperatures 550ºC and 650ºC are based on the uniaxial tension test at various elevated temperatures [41]. As stated in Yang et al. [13], for steady-state analysis for 550ºC and 650ºC numerical models, the column was axially loaded with a compressive load of 0.3 x P_{nc} (5390 kN) and 0.25 x P_{nc} (3920 kN), respectively, where P_{nc} is the axial compressive strength of the

steel column. For the transient case, the column was axially loaded with a compressive load of 0.25 x P_{nc} and a beam load equivalent to 0.6 P_y was applied at the beam tip before the specimen was subjected to fire. Here P_y is the corresponding yield strength of the steel beam which was loaded at the beam tip.

3.5.1.1 Modeling Approach

The finite element model was developed using the procedure discussed in the structural modeling section (see section 3.4) above. The three-dimensional structural model consisted of the steel beam, steel column, and welded flange-bolted web connection (WUF-B). All the parts were modeled using the first order 8-node linear brick element with reduced integration and hourglass control (C3D8R) with only displacement degrees of freedom. The stress-strain relationship based on the uniaxial tension test [41], as shown in Figure 3-6, was used for defining the material model at elevated temperatures. The specimens were also modeled with and without a shear tab to understand their influence on the WUF-B moment connections. For the model with shear tab, only the beam top and bottom flanges were tied to the column flange, and for the model without shear tab, the whole beam cross section was tied to the column flange. Figure 3-7 shows the model with the shear tab, and Figure 3-8 shows the model without the shear tab. The column cross-section at the top was pinned, i.e., restrained along all three directions. However, the bottom was restrained along the two lateral directions, and axial column load was applied along the vertical direction. The beam was laterally braced at the end span near the beam tip where the load was applied.

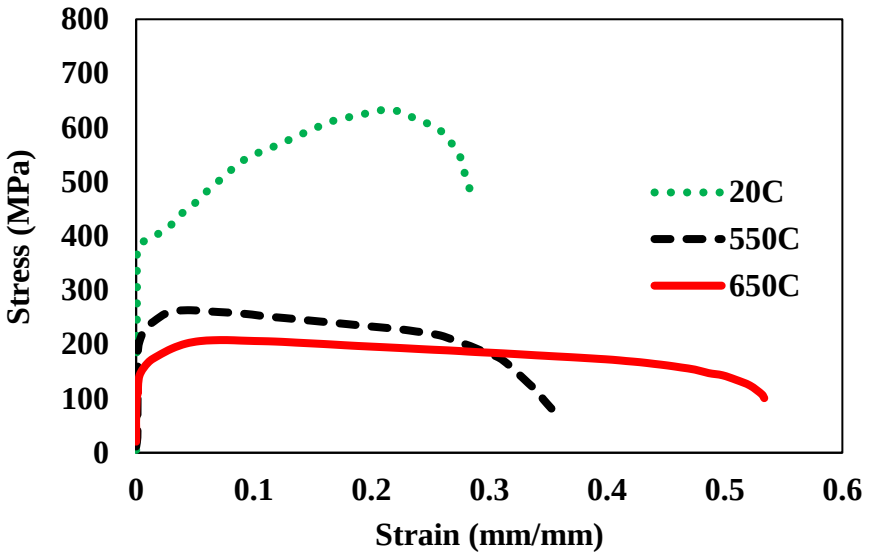

Figure 3-6 Stress-strain relation for steel (ASTM A572 Gr. 50) at various temperatures [41]

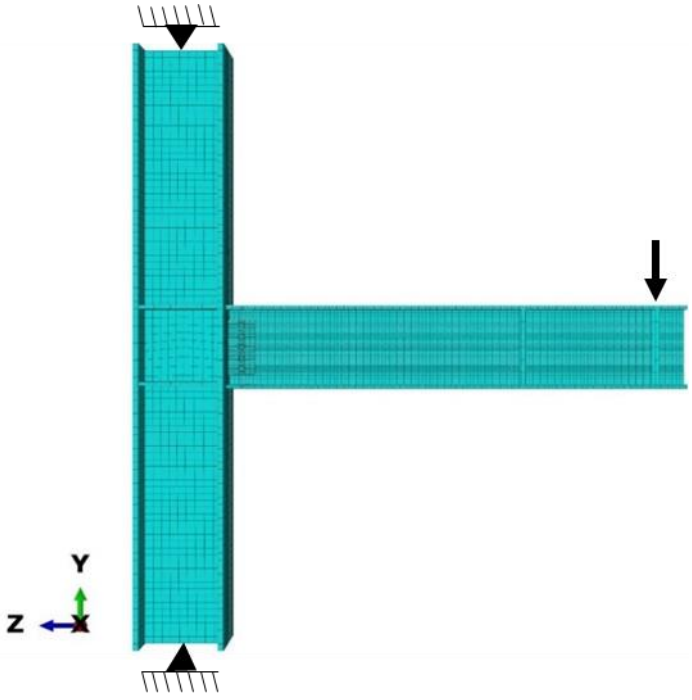

Figure 3-7 Finite Element Model with Shear Tab

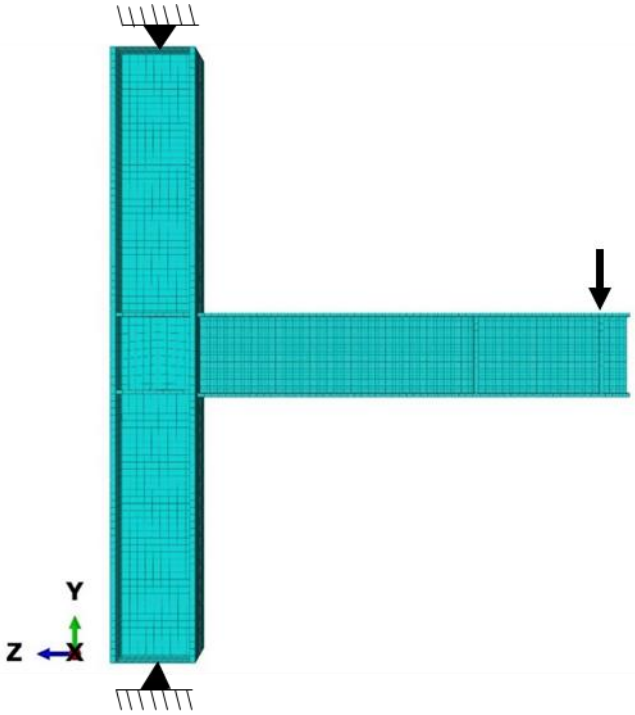

Figure 3-8 Finite Element Model without Shear Tab

3.5.1.2 Results and Comparison to test data

The results obtained from the numerical analysis using the stress-strain relationship based on the uniaxial tension test material properties [41], as shown in Figure 3-6, were compared against experimental results including the failure modes, to verify the modeling approach of steel beam-to-column WUF-B moment connection. Figure 3-9 and Figure 3-10 show the load vs. displacement curves between the Abaqus FEM results (with and without shear tab) and the results obtained through the experimental results and numerical analysis by Yang et al. [13] (also not considering shear tabs) for steady state analysis at 550ºC and 650ºC respectively.

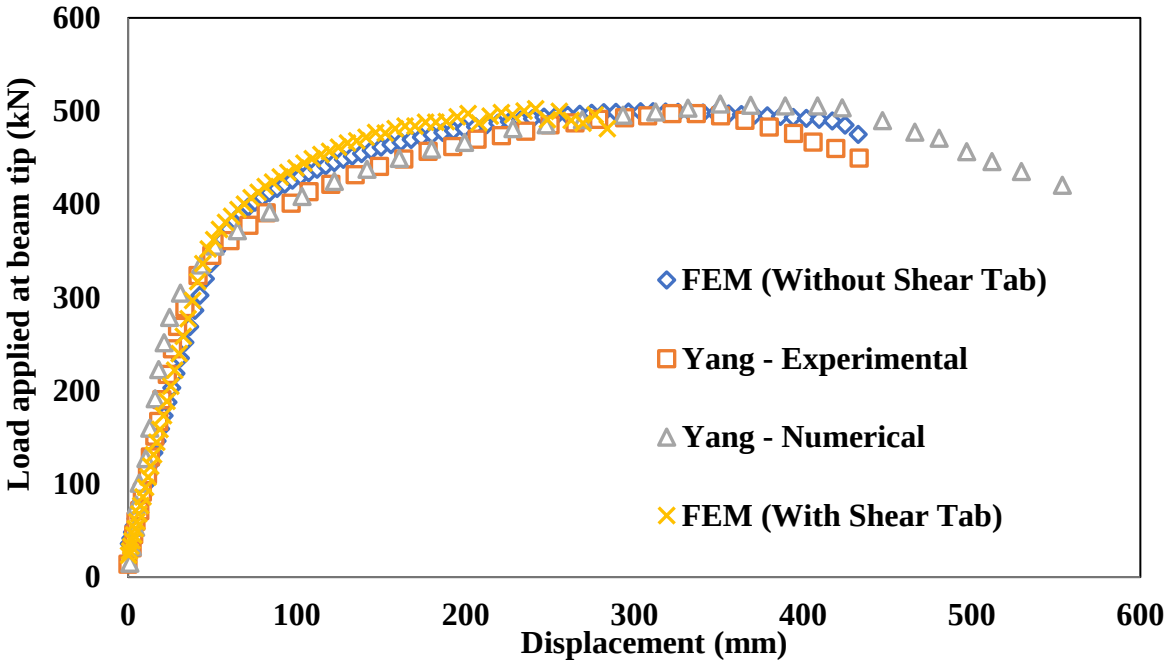

Figure 3-9 Load-Deflection Comparison between FEM results and Yang et al. [13] for 550°C temperature

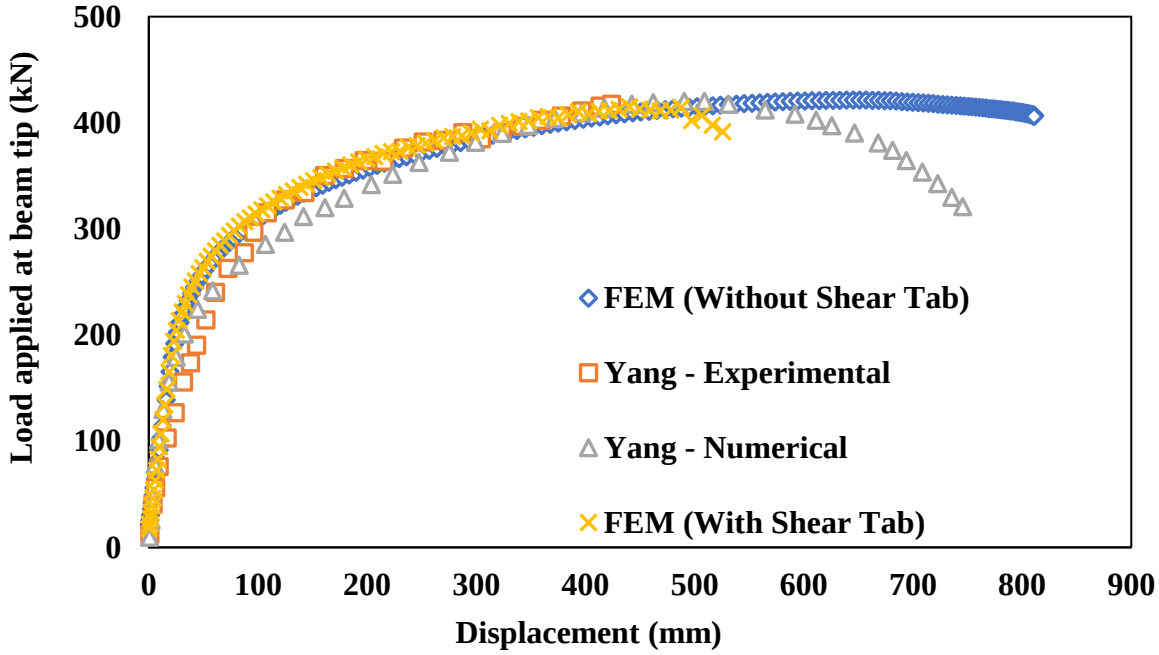

Figure 3-10 Load-Deflection Comparison between FEM results and Yang et al. [13] for 650°C temperature

As shown in the above Figures 3-9 and 3-10, the plot of load against displacement obtained from the FEM model agrees well with the experimental results shown by Yang et al. [13]. For specimens at 550ºC, the ultimate peak load for Yang's experimental and numerical results is about 508 kN. The peak load from the FEM analysis for both with and without shear tab case is determined to be about 502 kN. Similarly, for specimens at 650ºC, the peak load for Yang's experimental and numerical results is about 420 kN. The FEM analysis for both with and without shear tab case is determined to be about 422 kN. The transient case was also studied, where the beam was initially subjected to a concentrated force (0.6 P_y) on its free ends to produce the required moment about the connection. The temperature was then gradually increased until the beam failed. Figure 3-11 shows the comparison of the results for the transient case between experimental and finite element analysis, where the finite element results showed close agreement with the experimental results by Yang et al. The results at elastic and plastic stages of the curve align well with the experimental results. The overall response of the structure is predicted well by the FEM model at all moment levels.

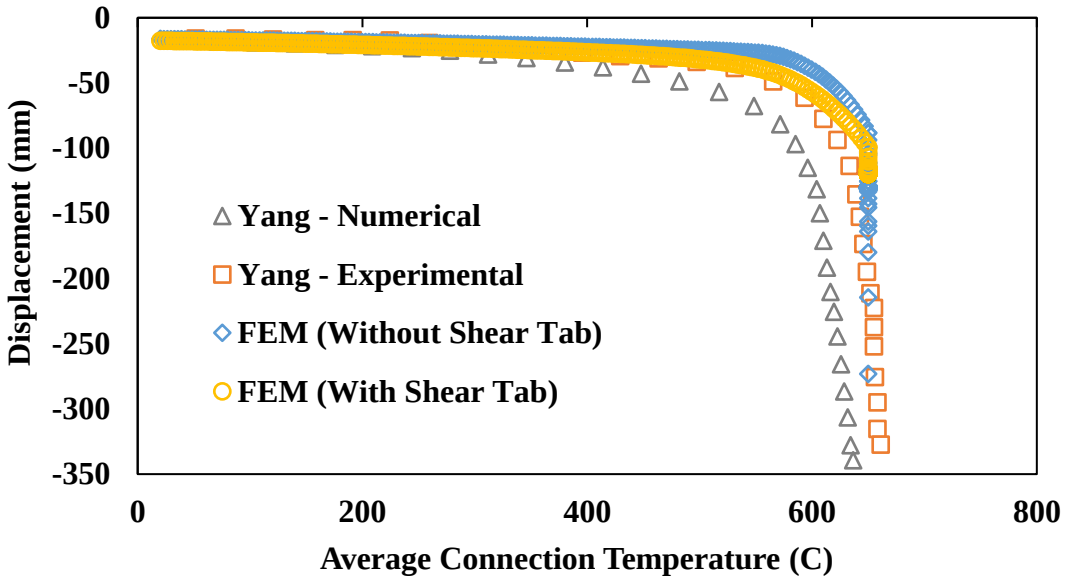

Figure 3-11 Average Temperature-Deflection Comparison between FEM results and Mao et al. test data [41] for transient state analysis

As per Figure 3-12, an observation between the damaged connection and the local buckling of the beam of the FEM results show good similarity against the experimental results by Yang et al. for specimen heated to 550ºC. Similarly, Figures 3-13 and 3-14 show reasonable accuracy between the FEM model and experimental data of Yang's test for the general beam deflection and the local buckling of beam for specimen heated to 650ºC. Based on these simulation results, it is found that the models can precisely predict the failure modes of steel beam-column connections. It is also observed that there is negligible difference in the results between the models with and without a shear tab. The overall stresses near the connection region are observed to be the same, and the local flange buckling of the beam was determined to be the limiting failure mode.

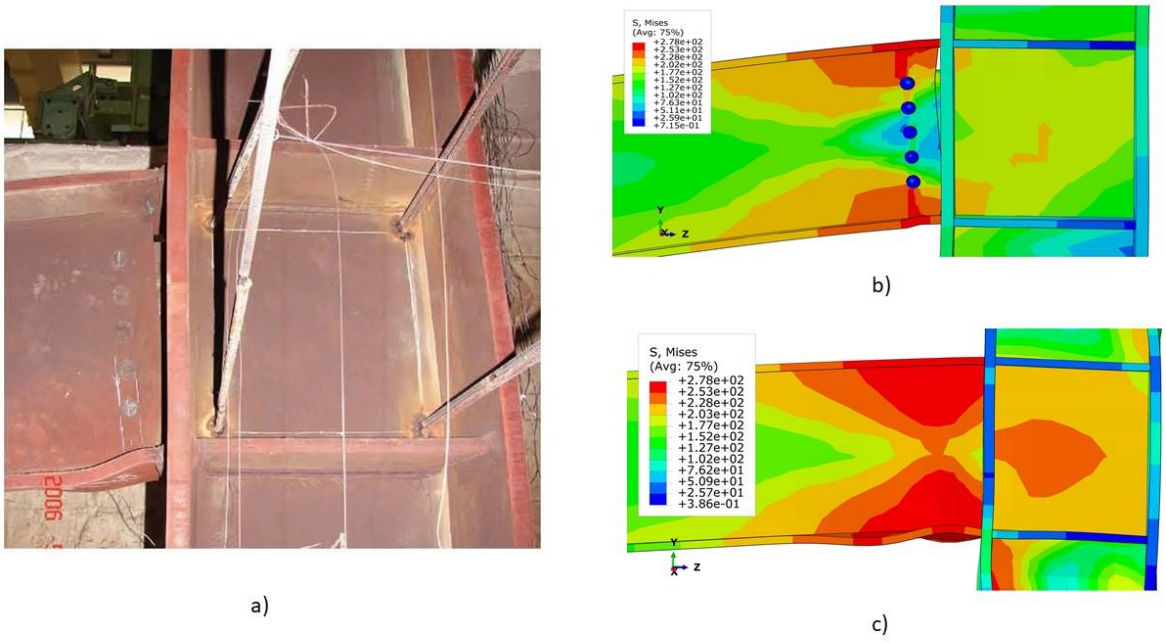

Figure 3-12 Comparison between Local Buckling at 550ºC; a) Experimental by Yang et al. [13], b) FEM Model with Shear Tab, and c) FEM Model without Shear Tab

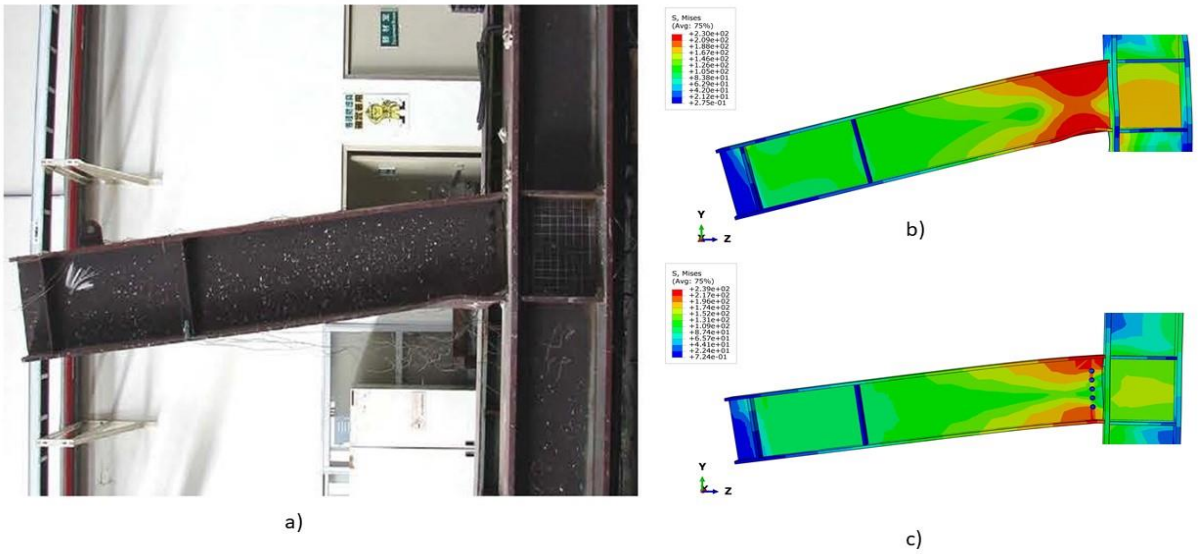

Figure 3-13 Comparison between Deflection at 650ºC; a) Experimental by Yang et al. [13], b) FEM Model with Shear Tab, and c) FEM Model without Shear Tab

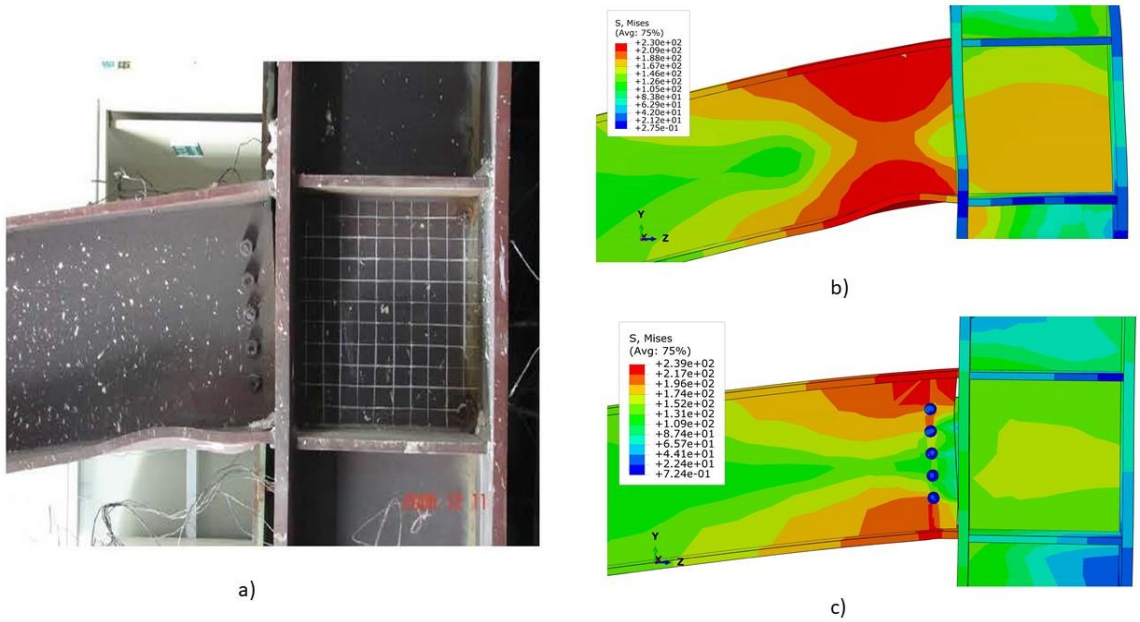

Figure 3-14 Comparison between Local Buckling at 650ºC; a) Experimental by Yang et al. [13], b) FEM Model with Shear Tab, and c) FEM Model without Shear Tab

To further investigate the influence of the NIST and Eurocode 3 temperature-dependent material models on the numerical results, the model was analyzed using both material relationships, and the results were compared with the experimental and numerical results by Yang et al. [13]. The results for the steady-state analysis at 550ºC and 650ºC are shown in Figures 3-15 and 3-16, respectively and the result for the transient analysis is shown in Figure 3-17.

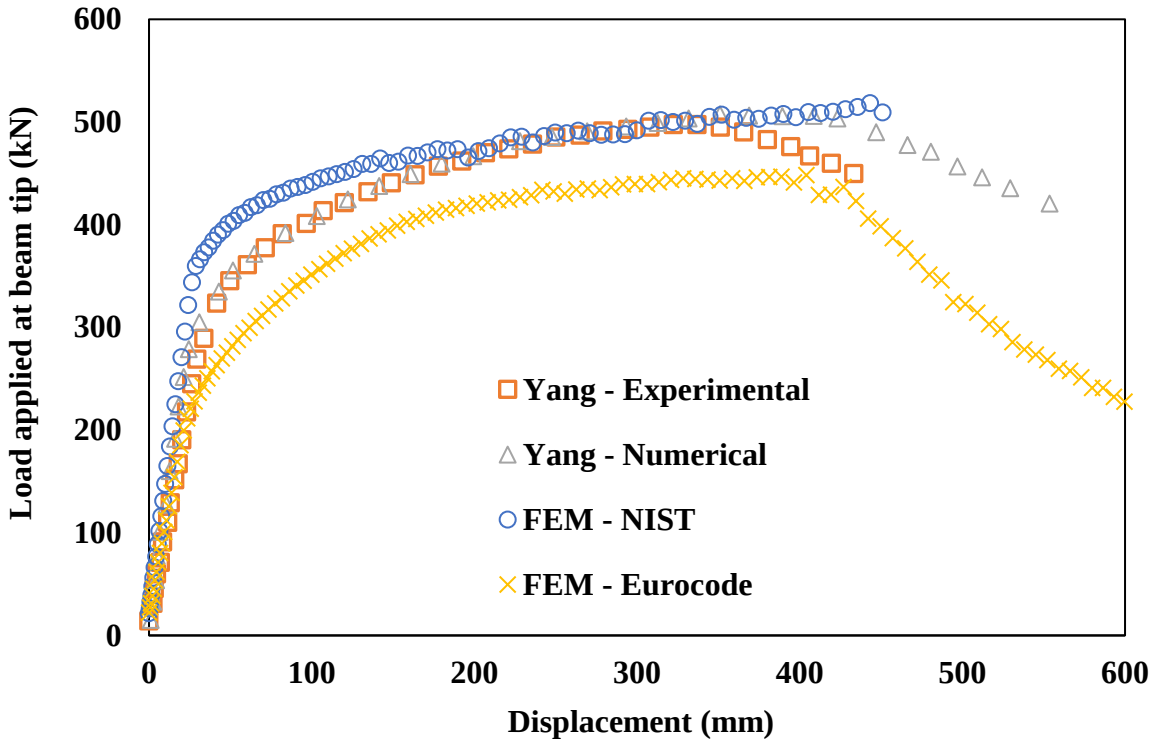

Figure 3-15 Load-Deflection Comparison between FEM results and Yang et al. [13] for 550ºC temperature using NIST and Eurocode 3 Material Models

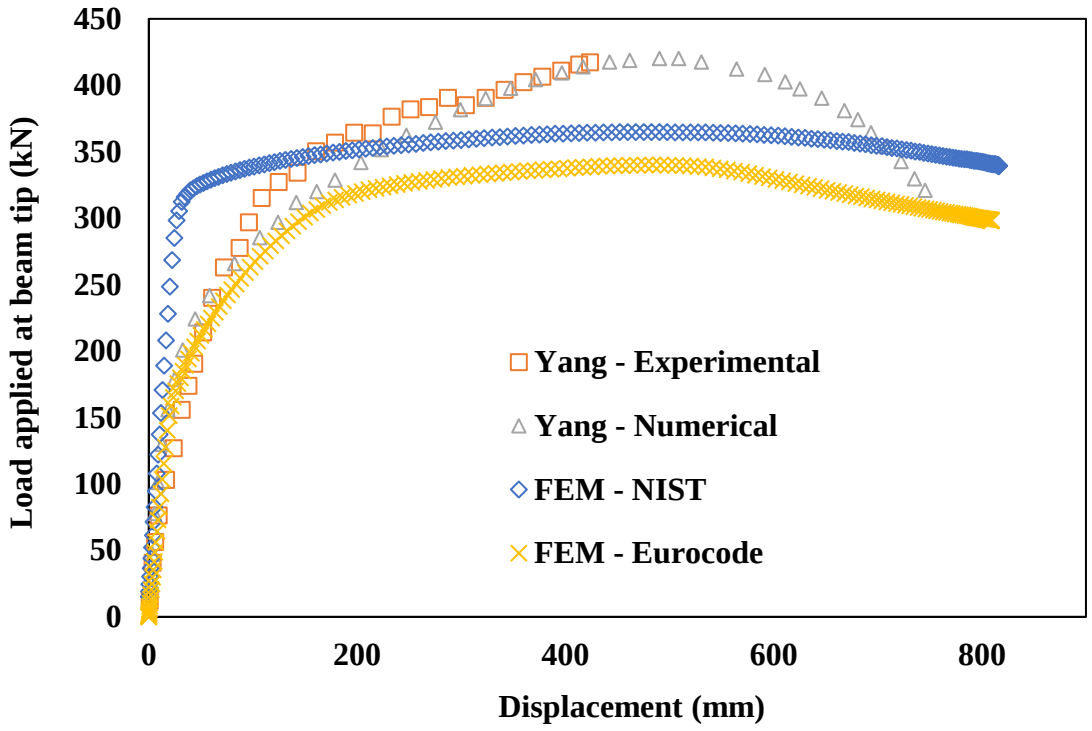

Figure 3-16 Load-Deflection Comparison between FEM results and Yang et al. [13] for 650°C temperature using NIST and Eurocode 3 Material Model

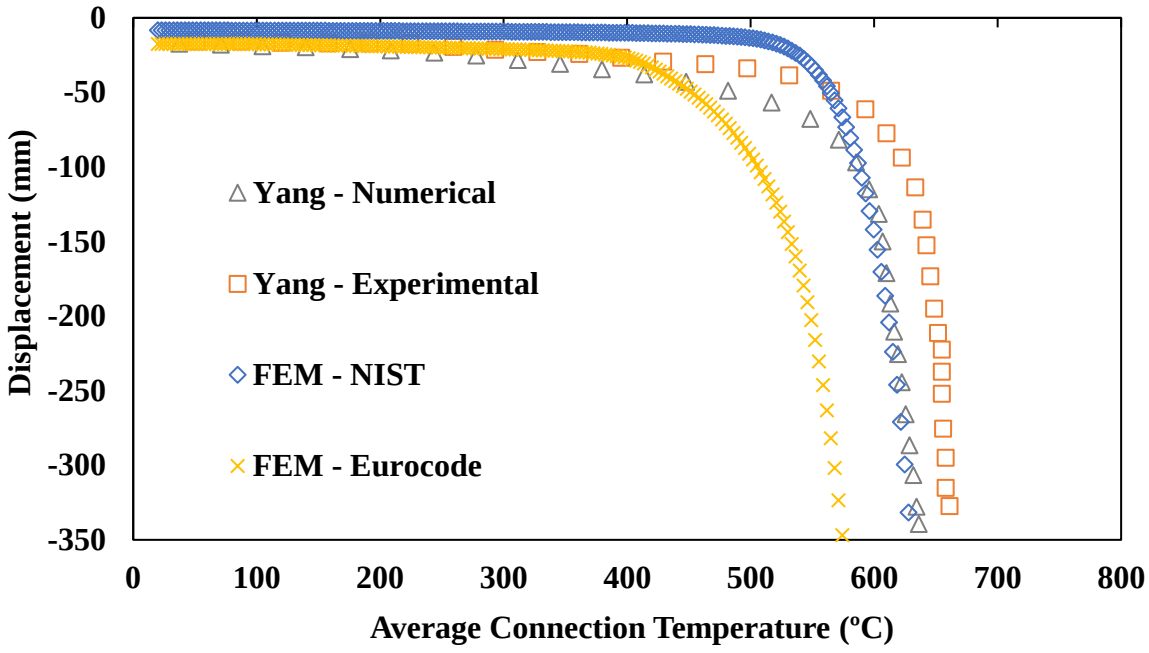

Figure 3-17 Average Temperature-Deflection Comparison between FEM results and Mao et al. test data [41] for transient state analysis using NIST and Eurocode 3 Material Model

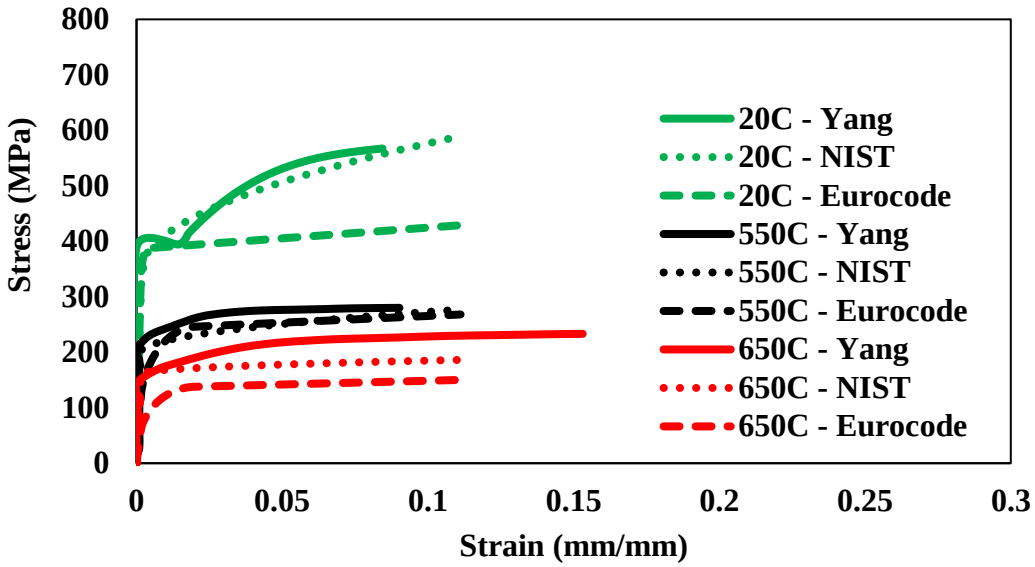

Figure 3-18 Comparison of True stress-strain curve between Yang et al. [13], NIST [9], Eurocode 3 [10] for 20ºC, 550ºC, and 650ºC

Figures 3-15, 3-16 and 3-17 show that the Eurocode 3 material model produced conservative results compared to the NIST and Yang's [13] experimental and numerical results. The Eurocode 3 material model had about 15% - 20% less capacity for the load vs. displacement results. On the other hand, the NIST material showed relatively good agreement with Yang's [13] experimental and numerical results. However, for the 650ºC steady-state temperature case, the results deviated especially in the earlier part of the response leading to the full plastification. The analysis results with the NIST and Eurocode model results showed a constant load plateau behavior after yielding in comparison to the experimental results, which showed strain hardening after yielding. This discrepancy might have been caused due to a more significant differences in the material models used by Yang et al. [13], NIST [9] and Eurocode 3 [10] at 650ºC as illustrated in the Figure 3-18. The shown comparisons verify that the Eurocode 3 material model produces relatively conservative results compared to the NIST material model.

3.5.2 Verification of the FEM Model against Studies by Al-Jabri et al. (2005)

Al-Jabri et al. [29] conducted experimental investigations on moment connections to provide moment-rotation-temperature data for various practical connections. The testing program included full-scale beam-to-column connections comprising of twenty specimens in five groups. The specimen had a symmetric cruciform arrangement with 1.9 m long cantilever beams connected to either side of a 2.7 m high center column. The testing was conducted by subjecting the specimen to constant bending moment and linearly increasing the furnace temperature to 900ºC in 90 minutes.

This experimental research provided additional data to evaluate the finite element modeling approach further. Group 1 and Group 2 specimens were modeled using the finite element approach out of the five groups. Their corresponding output in the form of a temperature-rotation graph and failure modes of the connection for the transient condition was compared against the experimental results. The test specimen of Group 1, as shown in Figure 3-19, were comprised of two 254 x 102UB22 (US equivalent of W10 x 15) beams connected to a 152 x 152UC23 column by 8 mm thick flush endplates, with six M126 Grade 8.8 bolts. Four tests were conducted at load levels in this group corresponding to connection moments of 4 kNm, 8 kNm, 13 kNm, and 17 kNm, representing 0.2, 0.4, 0.6, and 0.8 of the calculated moment capacities (M_{cc}) of the connection. In Group 2, as shown in Figure 3-20, the specimen comprised of a pair of 356 x 171UB51 beams connected to a 254 x 254UC89 (US equivalent of W14 x 34) column by 10mm thick flush endplates with eight M20 Grade 8.8 bolts. Similar to Group 1, four tests were conducted at load levels of 0.2, 0.4, 0.6, and 0.8 of the calculated moment capacities (M_{cc}) of the connection, which was 140 kNm. Table 1 shows the level of loading for each test under Group 1 and Group 2.

Table 1 Level of loading for Al-Jabri's connection tests [29]

Test		Moment Level	Applied Moment (kNm)
Group 1	FB11	$0.2M_{cc}$	4
	FB12	$0.4M_{cc}$	8
	FB13	$0.6M_{cc}$	13
	FB14	$0.8M_{cc}$	17
Group 2	FB21	$0.2M_{cc}$	27
	FB22	$0.4M_{cc}$	56
	FB23	$0.6M_{cc}$	82
	FB24	$0.8M_{cc}$	110

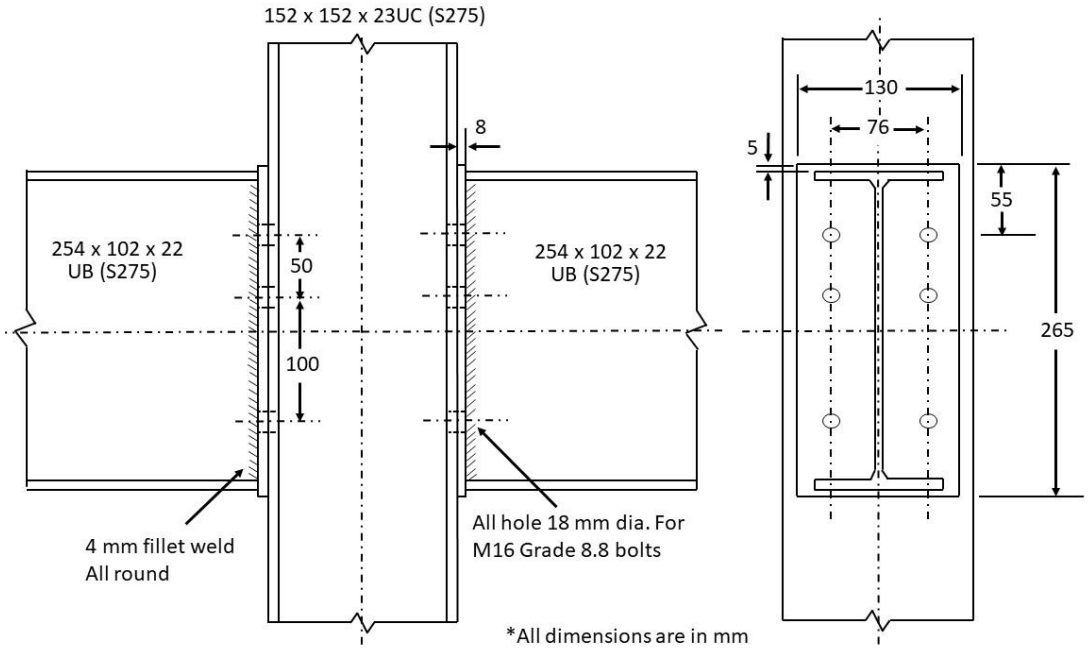

Figure 3-19 Group 1 connection detail by Al-Jabri et al. [29]

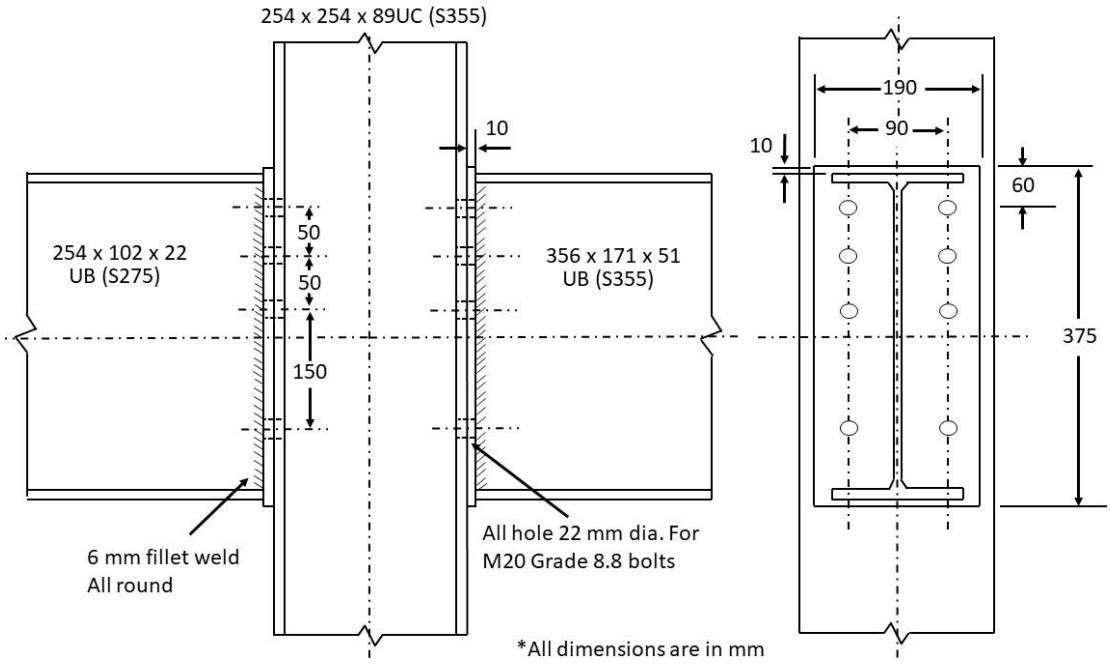

Figure 3-20 Group 2 connection detail by Al-Jabri et al. [29]

3.5.2.1 Modeling Approach

The finite element model was developed using the procedure discussed in the structural modeling (see section 3.4). The three-dimensional structural model consisted of the steel column, two steel beams, flush-end plate, and bolts (see Figure 3-4). The flush-end plate was bolted to the column. The beam cross-section was welded all-round to the flush-end plate, so the contact was defined using tie constraints as the connection was determined to be a fixed (rigid) connection. Also, for boundary conditions, the column was fixed at the top and bottom in both cases in this study.

As there was no information on the material model available for these assemblies, the NIST material model specified in Section 3.3.1 was utilized for the steel sections and bolts for the analysis. The beams located on either side of the column were initially subjected to a concentrated force on their free ends to produce the required moment about the connection. The

temperature was then gradually increased until it reached the desired level. Only the area near the connection was subjected to elevated temperatures (about 150 mm from the column). The other areas away from the column were subjected to ambient temperature to simulate the experimental testing conditions.

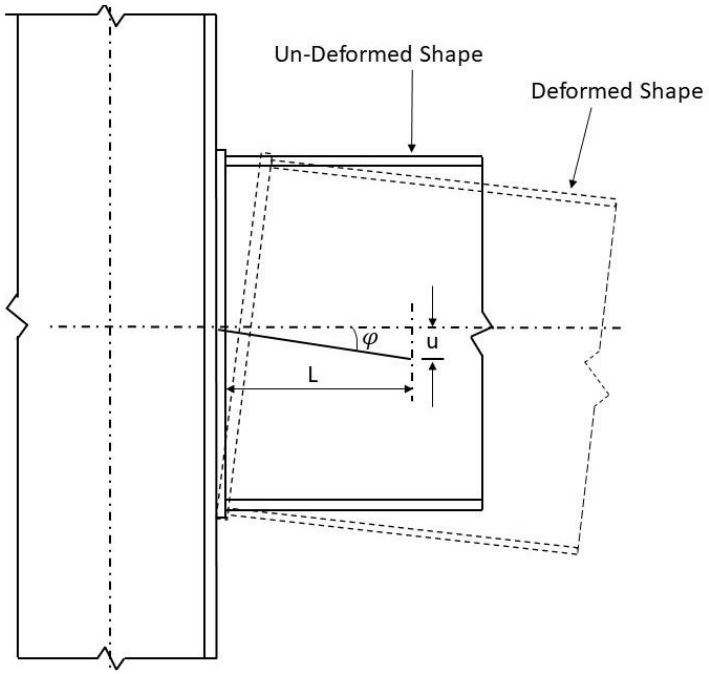

Figure 3-21 Rotation of the Connection [29]

As illustrated in Figure 3-21, the connection rotation at a particular point, relative to original beam orientation around the connection area was calculated using the following expression:

$$\varphi = \tan^{-1}(\frac{u}{L}) \tag{3.12}$$

Where u is the vertical deflection at the point of interest near the connection area and L is the distance along the connection centerline from the start of the connection to the load application point. Figure 3-22 provide an overview of the finite element model developed for Group 1 specimens.

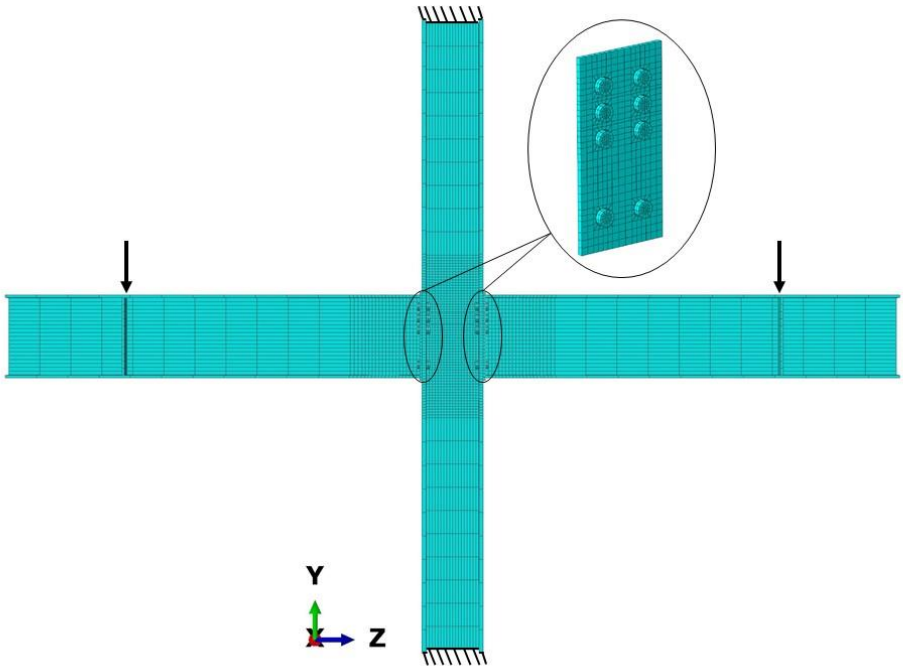

Figure 3-22 Finite Element Model of Al-Jabri et al. [29]

3.5.2.2 Results and Comparison to Group 1 test data

The output obtained from the finite element analysis from Group 1 specimens are compared against experimental results by Al-Jabri et al. [29] in Figure 3-23. The finite element results show close agreement with the experimental results by Al-Jabri et al. The results at elastic and plastic stages of the curve align well with the experimental results. The overall response of the structure is predicted well by the model at all temperature levels.

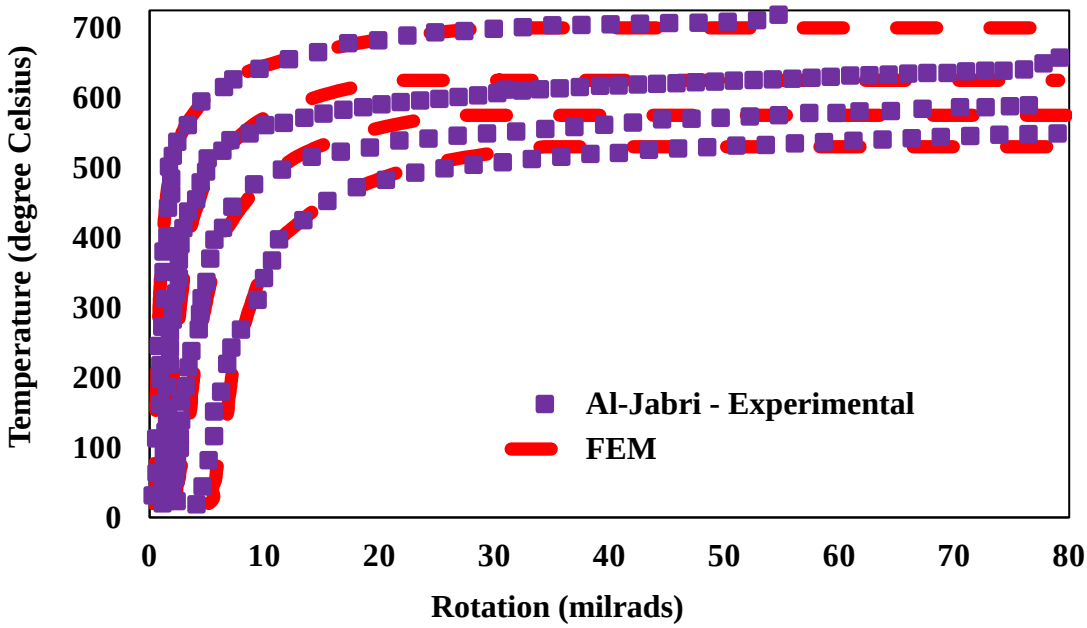

Figure 3-23 Temperature vs. Rotation Curve comparison between FEM results and Al-Jabri et al. test data [29] for Group 1 Specimen

3.5.2.3 Results and Comparison to Group 1 Failure Modes

Figure 3-24 visually compares the Group 1 failure mode between the experimental test by Al-Jabri et al. [29] and the finite element results. As shown, the connection simulated a negative moment case as the beam bottom flange is in compression and the top flange is in tension. The finite element analysis was able to predict the local deformation of the top plate due to high tensile stresses on the top bolts. The column flange also deformed due to the coupling action, and the analysis was able to predict the column local web buckling around the bottom compression region of the connection. The finite element results show good agreement with the experimental results.

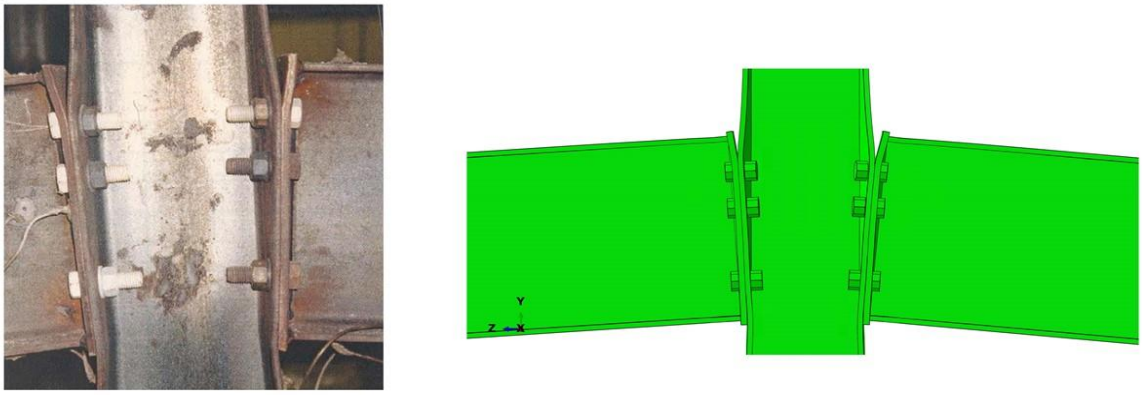

Figure 3-24 Comparison of Al-Jabri's [29] Experimental Failure Mode vs. Finite Element Failure Mode for Group 1 Assembly

3.5.2.4 Results and Comparison to Group 2 test data

The output obtained from the finite element analyses for Group 2 specimens are compared against experimental results. As shown in Figure 3-25, the finite element results show close agreement with the experimental results by Al-Jabri et al. The results at elastic and plastic stages of the curve align well with the experimental results. The overall response of the structure is predicted well by the model at all temperature levels. However, for Group 2, the finite element model predicted a stiffer rotational response than the experimental results.

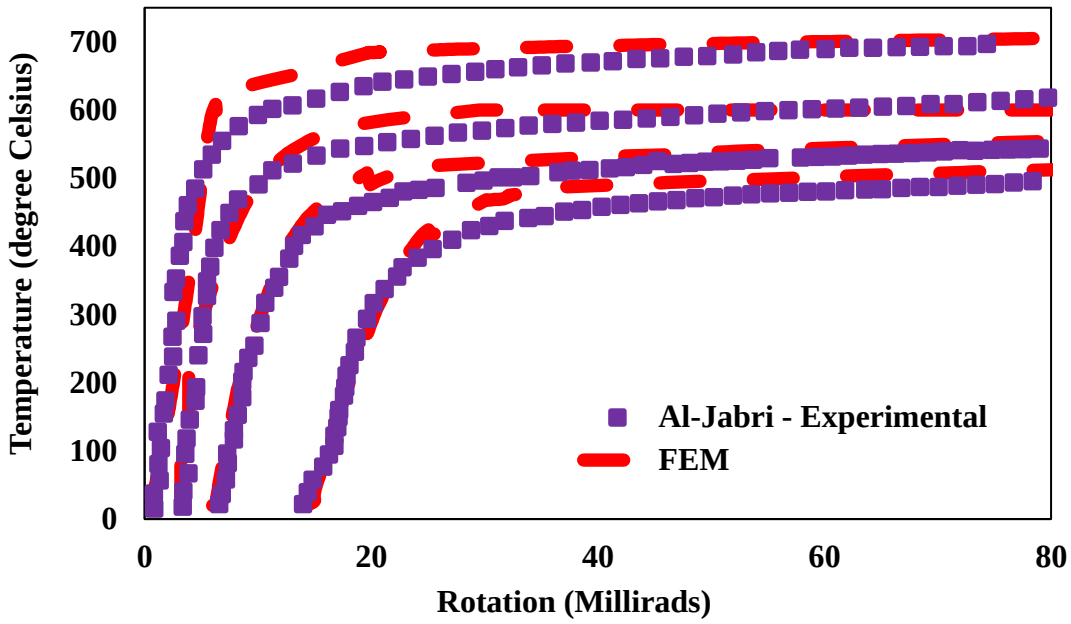

Figure 3-25 Temperature vs. Rotation Curve comparison between FEM results and Al-Jabri et al. test data [29] for Group 2 Specimen

3.5.2.5 Results and Comparison of Group 2 Failure Modes

Figure 3-26 compares the Group 2 failure mode between the experimental test by Al-Jabri et al. and the finite element results. The Group 2 flush endplate is stiffer than the Group 1 plate, and the Group 2 connection showed lesser deformation than the Group 1 connection. The column flange also deformed due to the coupling action, and the analysis was able to predict the column local web buckling around the bottom compression region of the connection. The finite element results show good agreement with the experimental results.

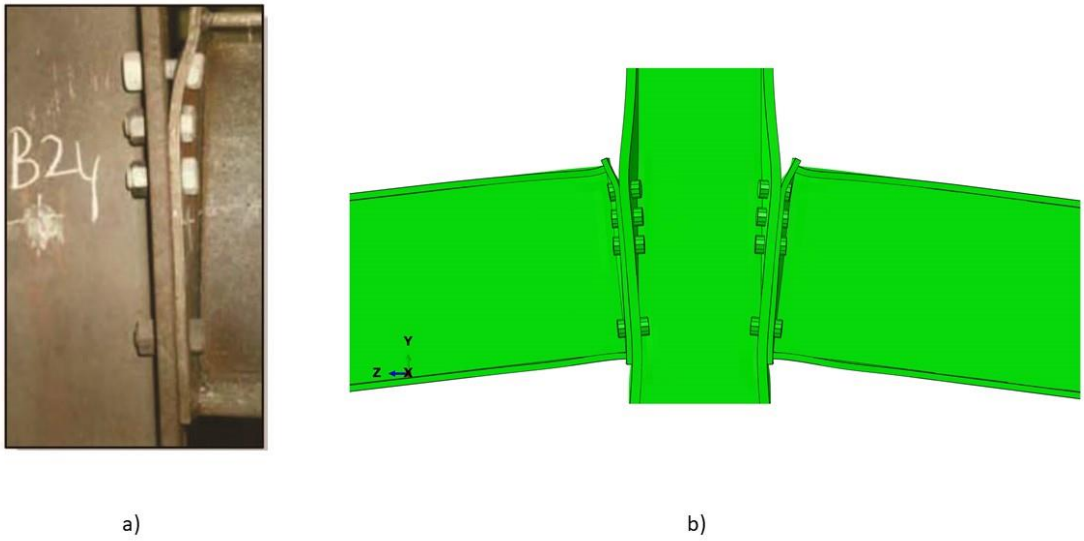

Figure 3-26 Comparison of Al-Jabri's [29] Experimental Failure Mode vs. Finite Element Failure Mode for Group 2 Assembly

3.6 Conclusions

This chapter presented the development and benchmarking of detailed 3D finite element models for predicting the behavior of steel beam-to-column moment connections subjected to fire. Two-moment connections, 1) welded flange bolted web (WUF-B) type moment connection tested type by Yang et al. [13] and 2) flush end plate-type moment connection by Al-Jabri et al. [29], were considered in the study. The connections were modeled in detail, including all the connecting elements. Also, the mechanical properties of the steel beam and connection elements were modeled using temperature-dependent properties. The contact interaction between the connection components such as beam flange and the column flange, shear tab, and the column flange was carefully established along with the contact between the bolt shank-to-bolt holes, bolt head-to shear tab, bolt nut-to-beam web, and shear tab-to-beam web surface. Thus, the

three-dimensional finite element models presented have simulated the bearing behavior of the moment connections.

The comparison focused on the load-displacement responses, moment-rotation curves, and observation of the connection failure modes. The comparison indicates that the developed numerical models could predict the observed behavior and failure modes accurately. It was also observed that C3D8R elements perform well, both in the elastic and inelastic regions, thereby undergoing large deformations. By comparing the finite element results with Yang et al. [13], it is also observed that the shear tab does not play a significant role in the WUF-B moment connection, as the comparison of the models with and without the shear, tab yielded the same results.

4. ANALYSIS OF INDIVIDUAL MEMBER STRENGTHS

4.1 Introduction

For fire protection, the thermal insulation requirements are considered to be adequate for structural fire resistance in building structures for certain durations during a fire event. This approach, however, falls short of providing alternative methods to establish structural performance calculations. There has been a remarkable development in the standards that provide structural fire resistance calculation similarly to how other strength limit states are calculated. For instance, the Eurocode 3 [10] includes detailed provisions to establish fire loads and evaluate their effects on steel structures using strength-based calculations. AISC [11] introduced Appendix 4, entitled “Structural Design for Fire Conditions”, which provides criteria for designing and evaluating structural steel components at elevated temperatures. Both Eurocode 3 and AISC provisions include an advanced or simple method to determine the strength of members under elevated temperatures, wherein the former method requires scrupulous structural and thermal simulations, and the latter method is based on member-based strength limit state equations. The AISC equations in Appendix 4 [11] vary from the strength equations at the ambient temperature given in the main specification. The equations in Appendix 4 of the specification were proposed by Takagi and Deierlein [42] and have the following limitations: a) developed for compact or near-compact sections, b) assume a uniform temperature distribution throughout the member cross-section, which may be unconservative for slender members where non-uniform temperatures can induce member deformation and rotation due to nonlinear thermal curvature.

The chapter describes the critical strength assessment of typical floor beams at elevated temperatures representing fire using finite element analysis. The assessment involved determining 1) the compressive strength of the steel section (pure compression case), 2) flexural strength of the laterally unsupported steel sections (pure bending case), and 3) the capacity of the steel sections under combined axial loads and bending moments at elevated temperature (M-N-T). The same beam sections selected for the study by Takagi and Deierlein; i.e., W14 x 90 and W14 x 22, were used in the analysis for comparing the results. In addition, a W21 x 73 section is also considered in the analysis to include a more commonly used beam size that was also evaluated in the connection studies described in Chapter 5. The W14 x 22 and W21 x 73 steel sections are compact in bending but are slender for compression loads. Conversely, the W14 x 90 steel section is compact in compression but non-compact in bending. The Eurocode material model was used for the original study and also used in performing finite element analysis in this study for comparison purposes. For the pure compression case, the maximum flexural buckling capacity is evaluated by applying a critical axial load to the steel section with pinned connections. For the pure bending case, the beam strengths are evaluated by applying bending moments about the major axis of the beam. The results obtained from the finite element analysis at elevated temperatures, such as, member compressive strength, flexural strength and combined axial force and bending moment strength (M-N-T) are compared against the nominal strength equations given in AISC Specification Appendix 4 [11] for member sections under pure compression, bending and combined axial and bending moments. This chapter aims to compare the finite element results with the AISC equations for W21 x 73 and revalidate the results obtained through this study with results obtained by Takagi and Deierlein [42] for W14 x 90 and W14 x 22 steel sections. The AISC Appendix 4 member strength equations for elevated

temperatures were initially developed for compact members, this study evaluates their applicability for slender members. Lastly, the results obtained through this study were used in Chapter 5 to determine the applicability of these AISC strength equations given in Appendix 4 [11] for deriving the capacity of moment connections at elevated temperatures.

4.2 AISC Appendix 4 Provisions

AISC Appendix 4 [11] imparts guidance and criteria for evaluating structural steel components for fire conditions. This provision further implies either performing the advanced analysis method by incorporating thermal and mechanical response to the design-basis fire or using the simple method, which involves calculating the member-based strength for compression and flexure.

4.2.1 AISC Column Strength Equations

The temperature-dependent nominal compressive strength (F_{cr}) for flexural buckling given in Equation (4.1) is dependent on yield stress at elevated temperature $F_y(T)$ and critical elastic buckling stress $F_e(T)$. $F_e(T)$ is obtained from Equation (4.2), which is a function of slenderness ratio (L/r) where L is the effective length which depends on boundary conditions, and r is the radius of gyration about the beam weak axis. The terms $F_y(T)$ and $E(T)$ are functions of temperatures that can be obtained using the coefficients provided in Figure 3-2.

$$F_{cr}(T) = \left[0.42^{\sqrt{\frac{F_y(T)}{F_e(T)}}}\right] F_y(T) \tag{4.1}$$

$$F_e(T) = \frac{\pi^2 E(T)}{\left(\frac{L_c}{r}\right)^2} \tag{4.2}$$

4.2.2 AISC Beam Strength Equations

The temperature-dependent nominal flexural strength (M_n) for lateral-torsional buckling of laterally unbraced doubly symmetric members are obtained using the provisions of AISC Appendix 4 [11], and it depends on the unbraced length (L_b). The below equations are functions of elevated temperature of steel (T).

When $L_b \leq L_r(T)$

$$M_n(T) = C_b \left\{ M_r(T) + \left[M_p(T) - M_r(T) \right] \left[1 - \frac{L_b}{L_r(T)} \right]^{c_x} \right\} \leq M_p(T) \tag{4.3}$$

When $L_b > L_r(T)$

$$M_n(T) = F_{cr}(T)\, S_x \leq M_p(T) \tag{4.4}$$

where,

$$F_{cr}(T) = \frac{C_b\, \pi^2\, E(T)}{\left(\frac{L_b}{r_{ts}}\right)^2} \sqrt{1 + 0.078 \frac{Jc}{S_x h_o} \left(\frac{L_b}{r_{ts}}\right)^2} \tag{4.5}$$

$$L_r(T) = 1.95\, r_{ts} \frac{E(T)}{F_L(T)} \sqrt{\frac{Jc}{S_x h_o} + \sqrt{\left(\frac{Jc}{S_x h_o}\right) + 6.76 \left(\frac{F_L(T)}{E(T)}\right)^2}} \tag{4.6}$$

$$M_r(T) = F_L(T)\, S_X \tag{4.7}$$

$$F_L(T) = F_y(k_p - 0.3\, k_y) \tag{4.8}$$

$$M_p(T) = F_y(T) Z_X \tag{4.9}$$

$$c_x = 0.53 + \frac{T}{450} \leq 3.0 \quad where\ T\ is\ in\ °\mathrm{F} \tag{4.10}$$

$$c_x = 0.6 + \frac{T}{250} \leq 3.0 \quad where\ T\ is\ in °\mathrm{C} \tag{4.11}$$

4.2.3 AISC Beam-Column Strength Equations

The temperature-dependent nominal strength for combinations of axial force and bending moment are obtained following the provisions of AISC Appendix 4 [11] using the steel properties at elevated temperatures (T). The provisions refer back to the combined axial and bending moments equations given in Chapter H of the AISC specification, with the exception that the individual strengths for axial load and moment capacities are obtained from the equations given in AISC Appendix 4 as presented in the previous sections. The interaction of flexure and axial load in doubly symmetric members is dependent on the ratio of required (P_r) and available axial strength (P_c) about the weak axis, which may be less than or greater than 0.2. The below equations (4.12) and (4.13) are also functions of required (M_{rx}) and available flexure strength (M_{cx}) about the major axis. This thesis only focuses on compressive (flexural buckling) strength about the minor axis and flexural strength about the major axis.

When $\frac{P_r}{P_c} \geq 0.2$

$$\frac{P_r}{P_c} + \frac{8}{9}\left(\frac{M_{rx}}{M_{cx}}\right) \leq 1.0 \tag{4.12}$$

When $\frac{P_r}{P_c} < 0.2$

$$\frac{P_r}{2P_c} + \left(\frac{M_{rx}}{M_{cx}}\right) \leq 1.0 \tag{4.13}$$

4.3 Finite Element Modeling

The detailed three-dimensional analyses of beam-columns using the finite element method are performed using Abaqus/Explicit analysis [12] to determine the accuracy of the AISC design

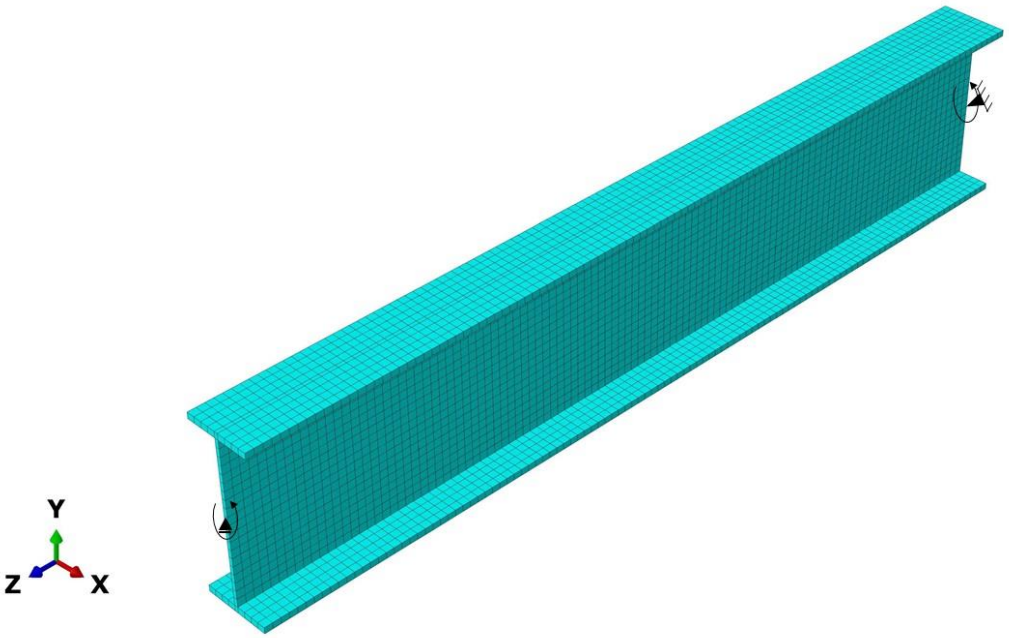

Figure 4-1 Finite Element Model and Boundary Condition for Strength Assessment

equations and check their applicability to slender members. Figure 4-1 shows the finite element model used in the analysis. The steel members are modeled using the first order 8-node linear brick element with reduced integration (C3D8R), and the rigid discrete endplate is modeled using the shell element. The model considered lateral-torsional buckling and buckling of elements such as flanges and web. The material model was taken from Eurocode 3 [10], which accounted for nonlinear stress-strain curves of steel at elevated temperatures, as explained in Section 3.3.2. The yield strength is assumed to be nominal specified values in AISC Appendix 4 [11] at ambient and elevated temperatures and kept consistent throughout the FEM analyses to provide a consistent comparison of the results with the AISC design equations. The temperature distribution is assumed to be uniform throughout the length and member cross-section. The loading in the models were applied using a load-controlled approach, and the peak load on the model is determined at various temperatures. To generate a uniform bending moment across the beam section, force couples were applied at beam ends wherein a compressive force was applied

on the top flange, and a tensile force was applied on the bottom flange. The contact formulation in Abaqus involves a master-slave type algorithm in which one surface which belongs to the body of more robust material is defined as master surface, and the other surface is defined as slave surface. The contact interaction involved in the endplate to flange and web surface in which the contact surfaces of the endplate are always selected to be master surfaces. A friction coefficient of 0.3 was assigned for all the contact interaction surfaces. Boundary conditions play a critical role as they have a significant influence in achieving practical member behavior and were considered the same as described by Takagi and Deierlein [42] as per the column or beam member strength assessment. The displacements of the web along the weak and strong axes and twisting rotation are restrained at both ends. The longitudinal displacements along the Z-axis are restrained at one end, and the rotational displacements about the weak and strong axes are free at both ends. While computing column axial strength analyses, the axial force is applied along the kinematically restrained endplate at one end of the member. For beam flexural strength analyses, a concentrated force couple is applied in the opposite direction on the top and bottom flange at each end to induce a uniform strong axis moment along the beams.

4.4 Results of Column Strength Assessment

The finite element results obtained through Abaqus for W14 x 90, W14 x 22, and W21 x 73 steel sections for pure compression cases are discussed in this section. As per AISC [11], Table 1-1, the W14 x 90 is a compact column section in compression; however, the W14 x 22 and W21 x 73 are beam sections and slender for compression. Thus, W14 x 22 and W21 x 73 are expected to be sensitive to local buckling at high compressive stresses. The compressive strength along the weak axis for these two sections is checked for various slenderness ratios ranging from 20 to 200. Figure 4-2 shows the comparison between the finite element results for the W14 x 22

section for pure compression at 500ºC temperature for varying slenderness ratios ranging from 20 to 200 with Takagi and Deierlein [42] and current AISC [11] equations. Figure 4-3 shows the comparison between the finite element results for the W21 x 73 section for pure compression at various temperatures such as 20ºC, 200ºC, 400ºC, and 600ºC with current AISC [11] equations for varying slenderness ratios. Note that the slenderness of L/r = 32.6 is selected as it is further used in chapter 5 to analyze the moment connection. Figure 4-4 also shows the contour plots of the flexural buckling for W14 x 22 and W21 x 73 sections for the slenderness of L/r = 20 and 60 at 500ºC.

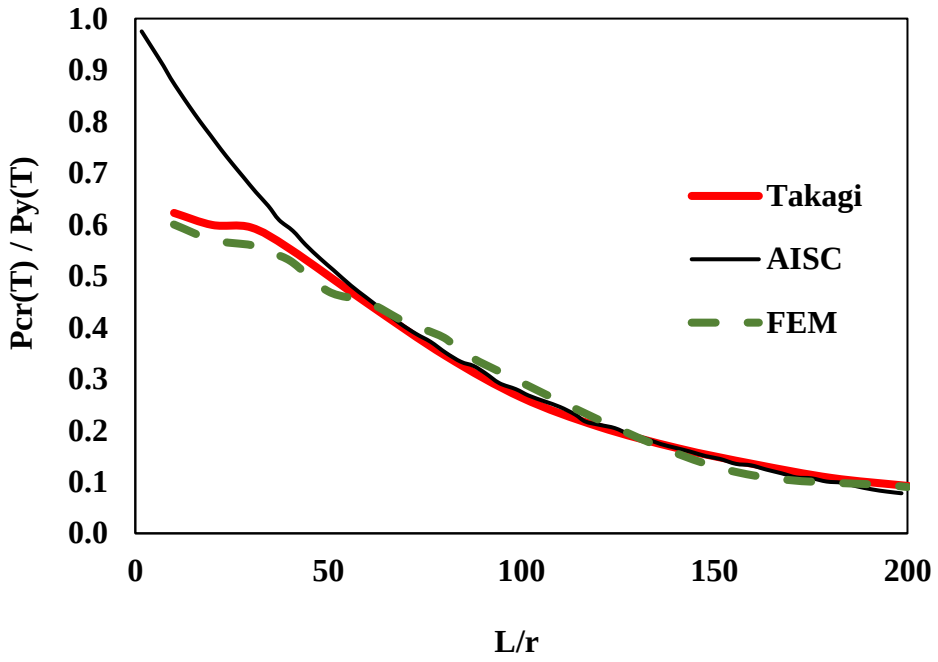

Figure 4-2 Comparison of Column Strength between Finite Element Results for W14 x 22 at 500ºC with Takagi and Deierlein [42] and AISC

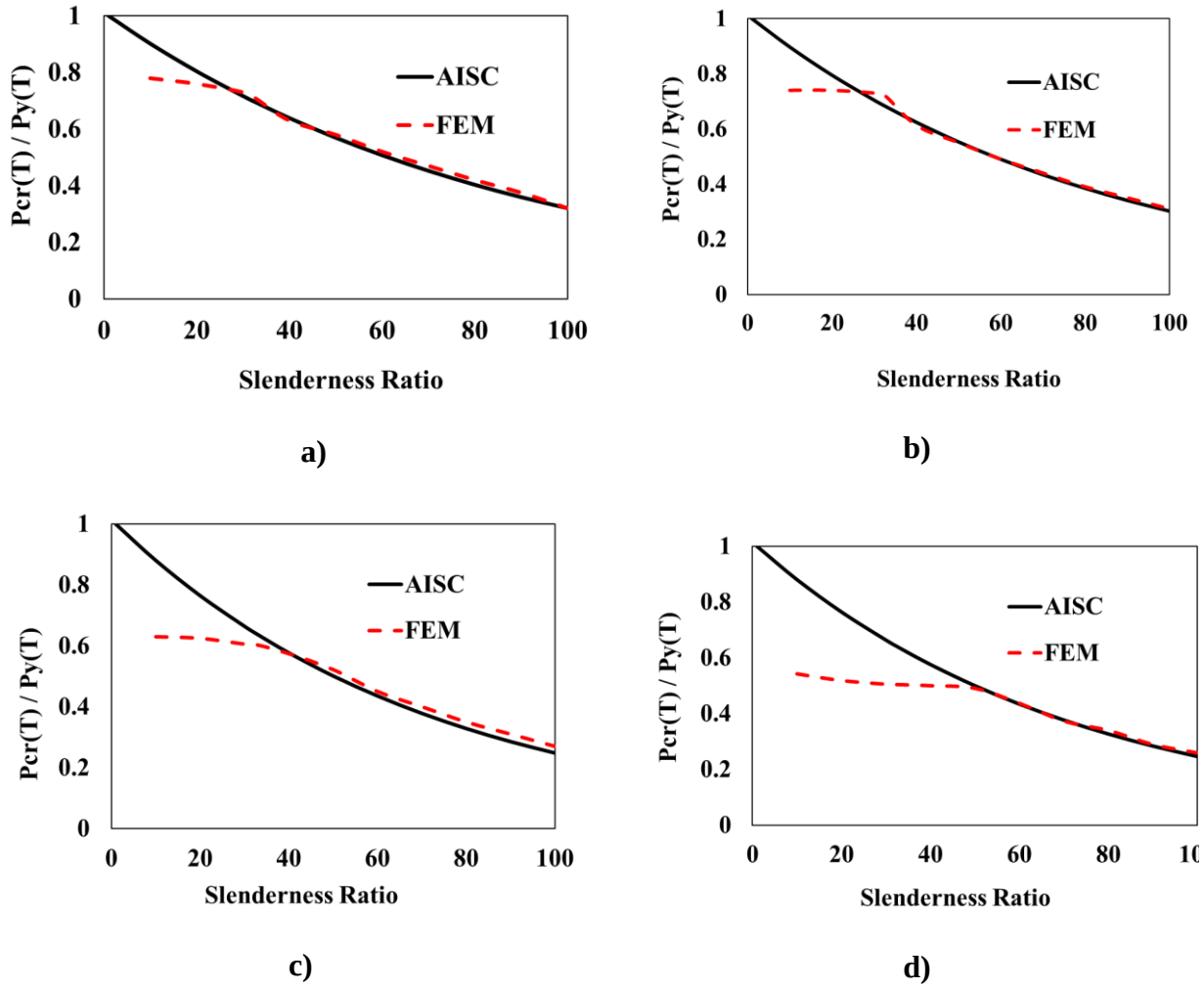

Figure 4-3 Comparison of Column Strength between Finite Element Results for W21 x 73 and AISC at a) 20°C, b) 200°C, c) 400°C, and d) 600°C

As shown in Figures 4-2 and 4-3, the compressive strength vs. slenderness plots generally agrees with the current AISC equations for slenderness ratios between 50 and 200. However, the finite element results deviate from the AISC equations for slenderness below 50. The effect of web slenderness is clearly seen at low slenderness (L/r < 50), as the failure is governed by local web buckling. This failure mode is not reflected in the current AISC column strength equations in Appendix 4 [11]. Thus, these equations provide unconservative results for low slenderness (L/r < 50) as they tend to predict compressive strength up to 40% more than the actual capacity.

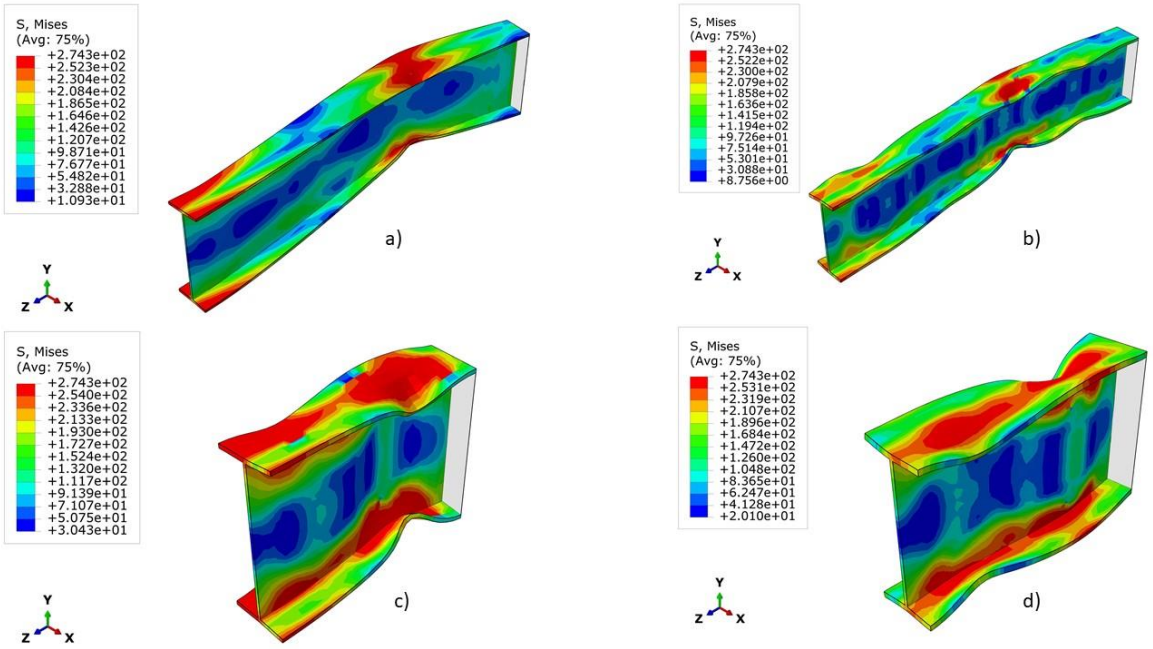

Figure 4-4 Flexural Buckling Results at 500ºC for; a) W14 x 22 with *L/r* = 60, b) W21 x 73 with *L/r* = 60, c) W14 x 22 with *L/r* = 20, and d) W21 x 73 with *L/r* = 20

4.5 Results of Beam Strength Assessment

The numerical results obtained from the finite element analyses for pure bending about the strong axis for W14 x 90, W14 x 22, and W21 x 73 steel sections are discussed in this section. Figures 4-5 and 4-6 show the bending moment capacities for steel sections W14 x 90 and W14 x 22 at various slenderness ratios ranging from 10 to 200 at elevated temperature of 500ºC respectively. These figures for 500ºC temperature were reproduced from Takagi and Deierlein [42] for W14 x 22 and W14 x 90 sections and showed good agreement with the current AISC Appendix 4 equations [11]. To verify the numerical modeling approach for the pure bending case, a slenderness ratio of *L/r* = 60 was chosen at a temperature of 500ºC and compared against results obtained by Takagi and Deierlein [42]. Figure 4-7 a) & b) show the finite element flexural strength results for W14 x 22 and W14 x 90 sections for pure bending: 1) laterally unbraced case with slenderness ratio of 60 and 2) beams with lateral bracing. As shown in Figure

4-7 a) & b), the normalized nominal flexural capacity of the beams for W14 x 22 and W14 x 90 for the slenderness of L/r = 60 at 500ºC temperature is 0.52 and 0.57, respectively. These results correspond well with Takagi and Deierlein's [42] and AISC results for the slenderness ratio of L/r = 60, showing in Figures 4-5 and 4-6. Figure 4-8 shows contour plots of the failure modes of W14 x 22 and W21 x 73 beams at slenderness of L/r = 60 at 500ºC temperature.

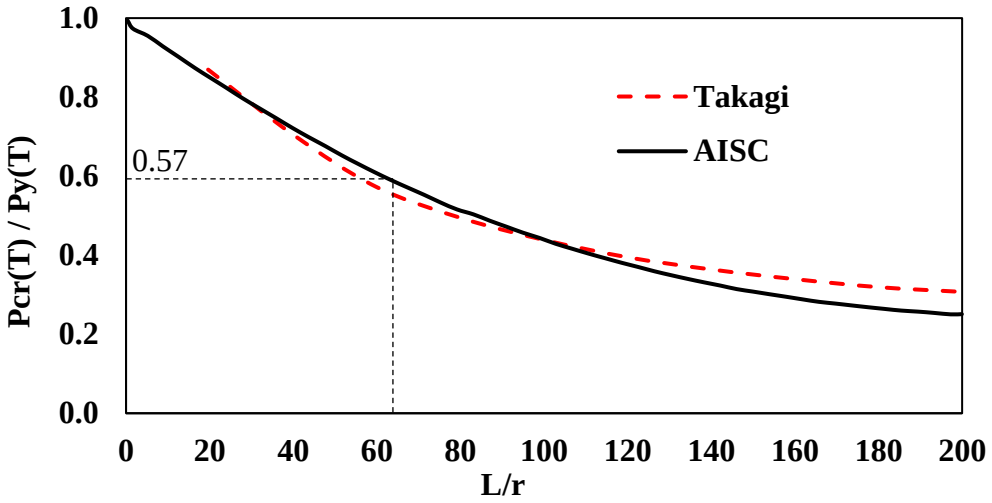

Figure 4-5 Comparison of Bending Moment Capacity between Takagi and Deierlein [42] and AISC for W14 x 90 Beam at 500ºC

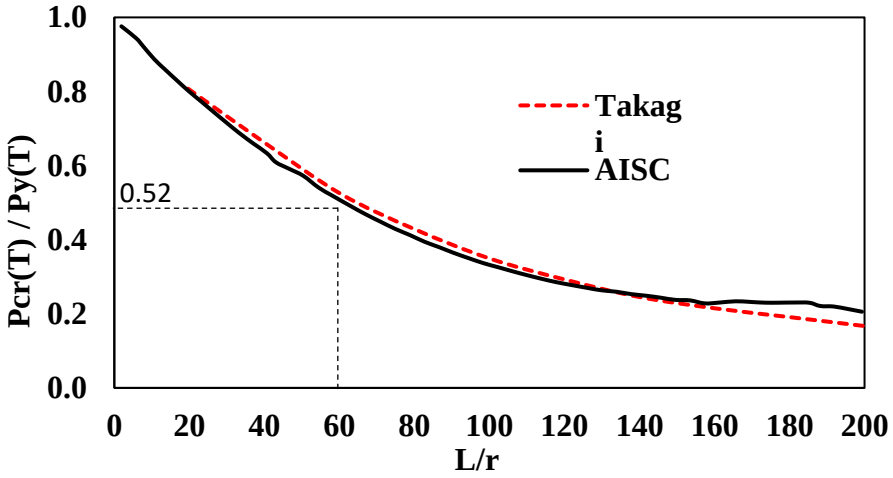

Figure 4-6 Comparison of Bending Moment Capacity between Takagi and Deierlein [42] and AISC for W14 x 22 Beam at 500ºC

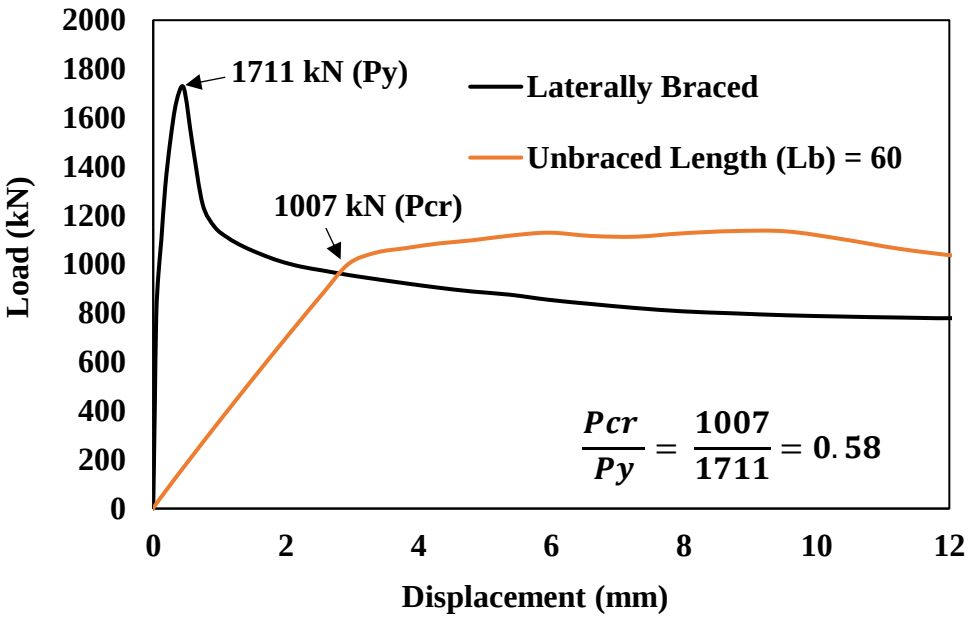

a)

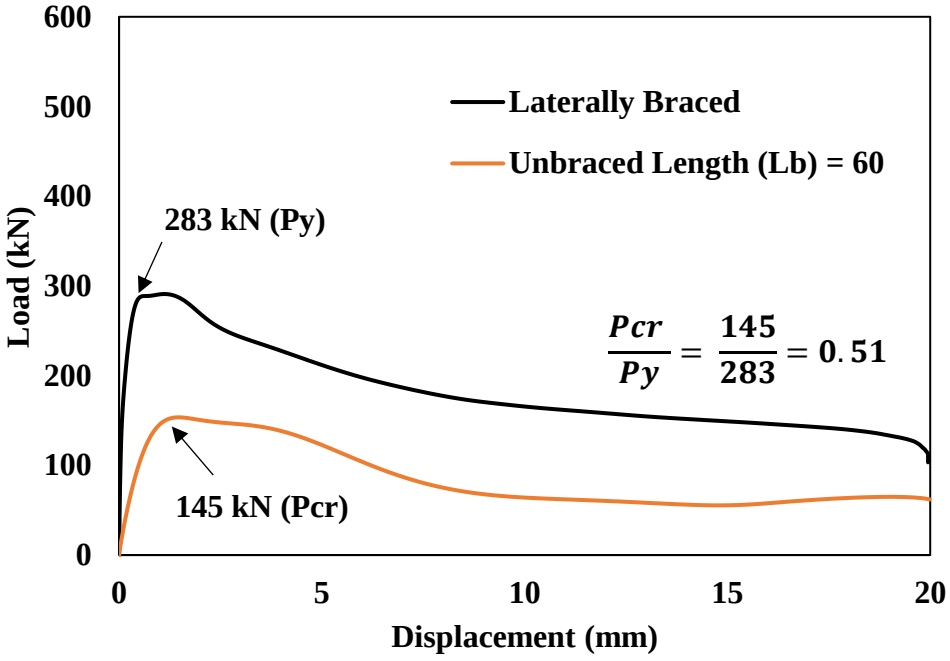

b)

Figure 4-7 Flexural Capacity for; a) W14 x 90 and b) W14 x 22

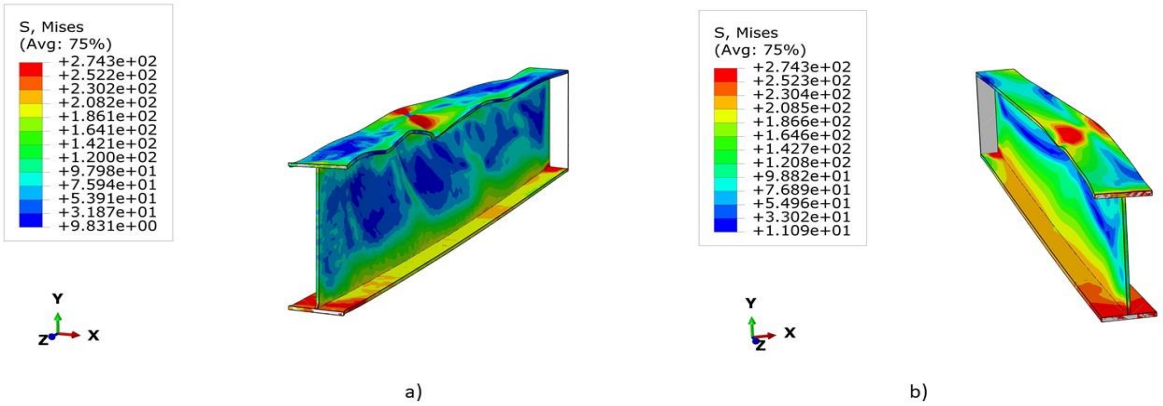

Figure 4-8 Pure Bending Results for the slenderness of L/r = 60 at 500ºC temperature for; a) W14 x 22 and 2) W21 x 73 sections

4.6 Results of Beam-Column Strength Assessment

The results obtained from the numerical analysis for combined compression and bending (M-N-T) for W14 x 90, W14 x 22, and W21 x 73 steel sections are discussed. For the analysis, the models were first subjected to compression, followed by bending moment. Figure 4-9 a) & b) compares the combined axial and bending moment, i.e., M-N-T interaction results with Takagi and Deierlein [42] and AISC for W14 x 90 and W14 x 22 sections at 500ºC temperature slenderness of L/r = 60. As per the AISC specification, the M_{rx} term in Equations 4.12 and 4.13 should include second-order effects, which is given through Equation 4.14, representing the second-order moment. For a pin-ended column subjected to uniform moment, this moment is calculated as follows [42]:

$$M_{x,end} = M_{rx}\,(1 - \frac{P_r}{P_c}) \qquad (4.14)$$

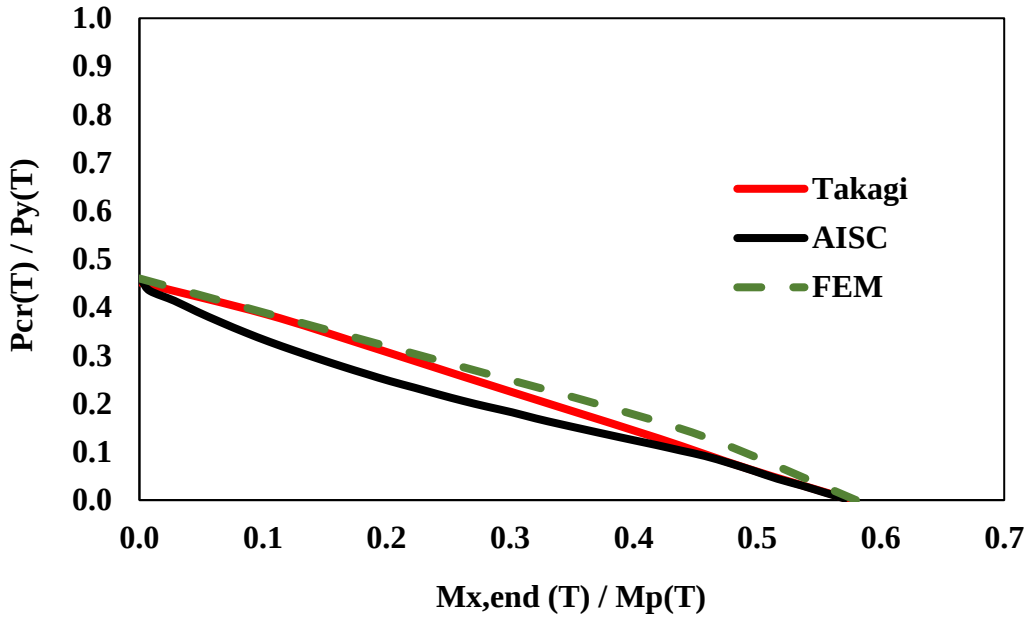

a) W14 x 90

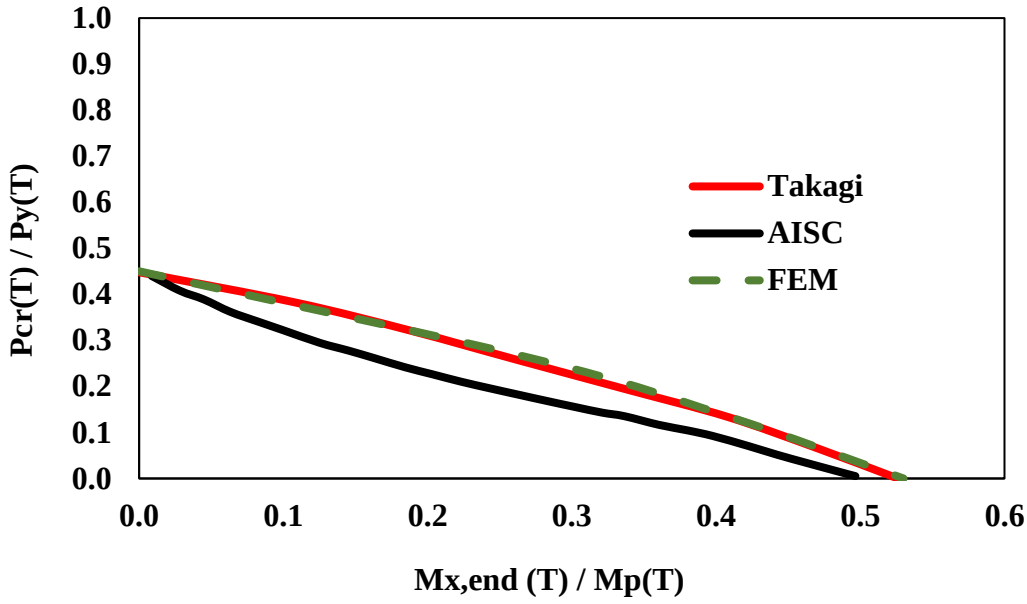

b) W14 x 22

Figure 4-9 Comparative assessment of beam-column at 500°C

Figure 4-10 shows the M-N-T interaction curve comparisons for the W21 x 73 section for temperatures 20ºC, 200ºC, 400ºC, and 600ºC with current AISC [11] equations for a slenderness ratio of L/r = 32.6. Note that L/r = 32.6 is selected as this slenderness ratio was used in chapter 5 to analyze the moment connection. The M-N-T interaction curves show good agreement with the current AISC equations 20ºC, 200ºC, 400ºC, however, the results deviate from each other for the temperature of 600ºC when the moment is very small and there is high compression. This was expected as the results for pure compression, which is discussed in Section 4.4, showed discrepancy in the results as the AISC equations do not take into consideration the local web buckling of the beam web. The M-N-T interaction curve comparison of W21 x 73 section for temperatures 20ºC, 200ºC, 400ºC, and 600ºC with current AISC [11] equations for a slenderness ratio of L/r = 20 was also plotted, as shown in Figure 4-11 to understand the impact of lower slenderness ratio on the M-N-T curves. As shown in Figure 4-11, the M-N-T interaction curves showed higher discrepancy in the results when compared against M-N-T interaction curves plotted using AISC equations, particularly for temperatures 400ºC, and 600ºC where the difference between the two results was even higher. It is observed that M-N-T interaction curves plotted using the AISC equations are unconservative, particularly below slenderness ratio of 60 at higher elevated temperatures.

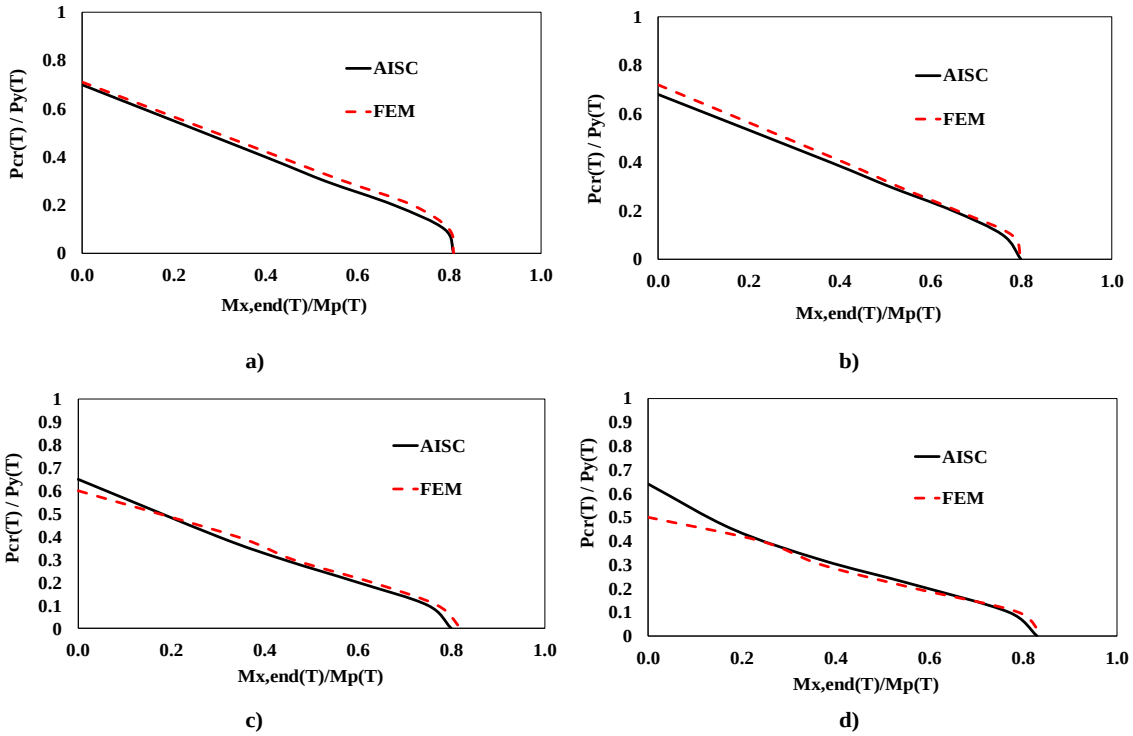

Figure 4-10 Comparative assessment of beam-column strength for W21 x 73 section for slenderness of *L/r* = 32.6 at a) 20°C, b) 200°C, c) 400°C, d) 600°C

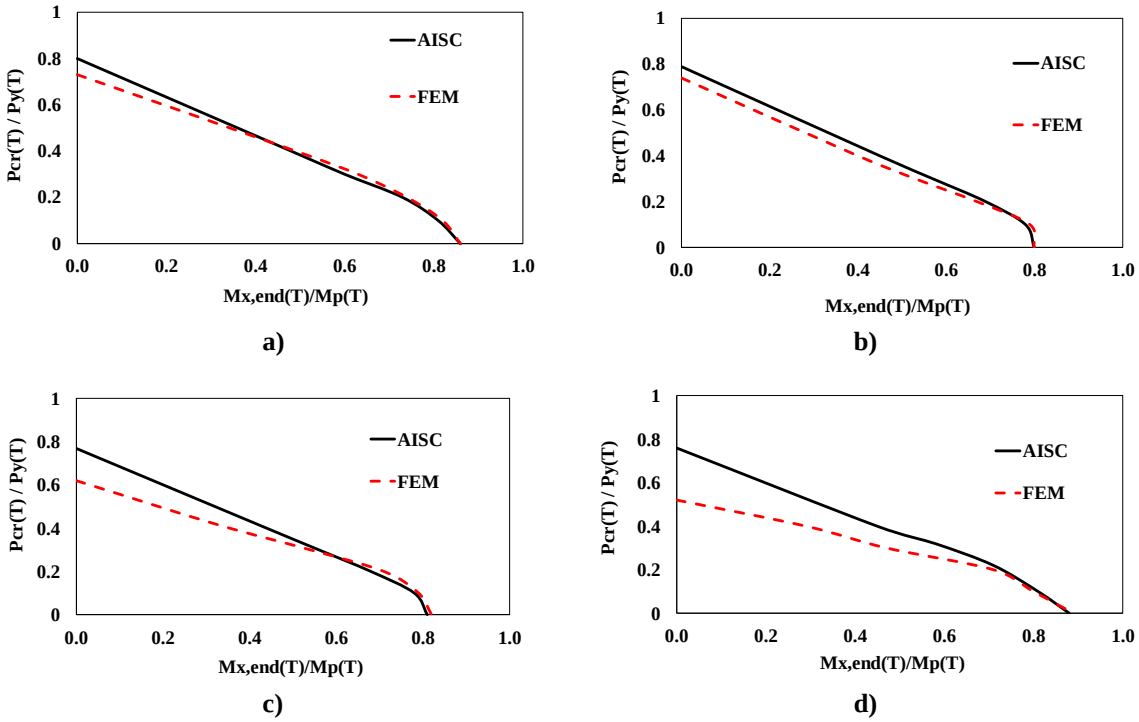

Figure 4-11 Comparative assessment of beam-column strength for W21 x 73 section for slenderness of *L/r* = 20 at a) 20°C, b) 200°C, c) 400°C, d) 600°C

4.7 Summary and Conclusion

The chapter describes the critical assessment of the member strength equations for elevated temperatures provided in the AISC Specification that were initially developed for compact members, and their applicability to slender members through detailed finite element simulation. Member sections W14 x 90, W14 x 22 and W21 x 73 section was used in the analysis, wherein, W14 x 22 and W21 x 73 are slender in compression. The finite element model was developed utilizing solid 3D elements in Abaqus, which captures the effects of local and overall buckling failure modes. The studies involved assessment of these members at elevated temperatures to determine 1) the nominal compressive strength of the members (pure compression case), 2) nominal flexural strength of the laterally unsupported members (pure bending case), and 3) nominal capacity of the members under combined axial loads and bending moments (M-N-T). The comparison of the finite element results with AISC Appendix 4 member strength design equations found that for the pure compression case, the results showed good agreement with AISC equations for compact W14 x 90 steel section; however, the AISC equations are unconservative in predicting the nominal compressive strength of slender W14 x 22 and W21 x 73 sections for low slenderness ratios ($L/r_y < 60$). This discrepancy is because the AISC equations for compressive strength at elevated temperatures do not consider the local buckling failure for slender elements of the steel section. This was also reflected in the M-N-T interaction curves, wherein, for lower slenderness ratios, particularly at higher elevated temperatures, the M-N-T interaction curves overpredicted the results when compared against the FEM results. Therefore, it is concluded that the AISC equations for combined axial and bending strength show good agreement for slenderness ratio of 60 and above. For slenderness ratio below 60, the M-N-T curves are unconservative, particularly at higher elevated temperatures.

5. ANALYSIS OF WUF-B CONNECTION

5.1 Introduction

Moment frames act as lateral force resisting systems, which are widely used in steel structures. They offer superior ductility and energy dissipation capacity [43]. Their ductile behavior is realized through flexural yielding of the beam and shear yielding of the panel zone. During the event of severe earthquakes, the member and the connection joint of the moment frame must undergo a significant amount of plastic deformation. Many experimental tests in the 1960s and 1970s were carried out, which demonstrated that the moment frames were an effective lateral force resisting systems [44].

Fully welded connections were the most used moment connections in the earthquake-prone areas of the United States before the Northridge earthquake [43] because they were considered to provide the optimum combination of strength, stiffness, and ductility. Investigations in the wake of the Northridge earthquake uncovered unexpected brittle failures of moment frames and connections in the form of brittle weld fractures with little evidence of inelastic action. As such, the hinge that formed in the beam close to the connection has very little rotational ductility [45]. The WUF-B connection was prequalified for seismic applications in the 1998 Uniform Building Code [46] and later adopted into the AISC “Seismic Provisions for Structural Steel Buildings: (AISC 1992) based on the nonstandard laboratory testing carried out during the 1970s and 1980s [47]. However, these results, accompanied with other laboratory results of WUF-B connections preceding the Northridge earthquake, revealed that the performance of WUF-B connections showed immense inconsistency [48] and was given nonchalant treatment by building code officials and structural engineers. With substantial research (FEMA 2000b) [49], several improvements and appropriate quality assurance were

carried out to these connections to ensure reliable performance. FEMA 355D [49] provides comprehensive information on the testing and performance of the WUF-B connections. Some of the improvements that were carried out over the typical pre-Northridge connections involved; 1) using weld metal with appropriate toughness, 2) removing weld backing from bottom-beam-flange-to-column-flange welds, 3) back gouging and addition of a reinforcing fillet weld, 4) using improved weld access hole shape and finish 5) and applying better weld quality control and quality assurance [33].

At the NIST, Lew et al. [33] worked with a panel of practicing structural engineers across the U.S. to develop prototype 10-story building designs to study the vulnerability of structures to disproportionate collapse and improve guidance to reduce such vulnerability. The buildings were designed and referenced material standards according to the American Society of Civil Engineers 7-02 standard (ASCE) [50], including the AISC "Load and Resistance Factor Design Specification for Structural Steel Buildings" (AISC 1999) [51] and AISC "Seismic Provisions for Structural Steel Buildings: (AISC 2002) [52]. These prototype buildings are considered representative of typical construction in the U.S. The moment frame used in their analysis included an intermediate moment frame (IMF) with WUF-B connections. WUF-B moment connection is one of the prequalified steel connections listed in FEMA 350 (FEMA 2000a) [53].

The WUF-B connection modeled in this research project as a representative moment connection is shown in Figure 5-1. As seen in Figure 5-1, the assembly consists of a 1.5-meter-long single cantilevered W21 x 73 beam attached to a W18 x 119 column which is 4128 mm in height using a WUF-B connection. The moment connection consists of a shear tab bolted to the beam web on one end using three 25 mm diameter, high strength bolts and welded to the column flange on the other end using an 8 mm fillet weld on both sides of the shear tab. The size of the

shear tab is 13mm x 305mm x 152mm (0.5 in x 12 in x 6 in). The bolt holes are standard holes with an edge distance (between the center of the hole to the edge of the shear tab) of 70 mm. The beam flanges are joined to the column flange using complete joint penetration (CJP) groove welds. Continuity plates are provided for columns, as shown in Figure 5-1. ASTM A992 structural steel was for the beams and columns with an ambient temperature nominal specified yield strength of F_{yo} = 345 MPa (50 ksi). ASTM A36 steel with F_{yo} = 250 MPa (36 ksi) was used for the shear tabs and continuity plates at the beam-column connections. Bolts were used to connect the shear tab to the column web, which was ASTM A490 with F_{yo} = 896 MPa (130 ksi). The column was artificially stiffened by increasing the column stiffness (i.e., modulus of elasticity) 1.5 times to suppress any unintended column failure modes. The beam was loaded on its free end, and two web stiffener plates were also used at the beam's free end.

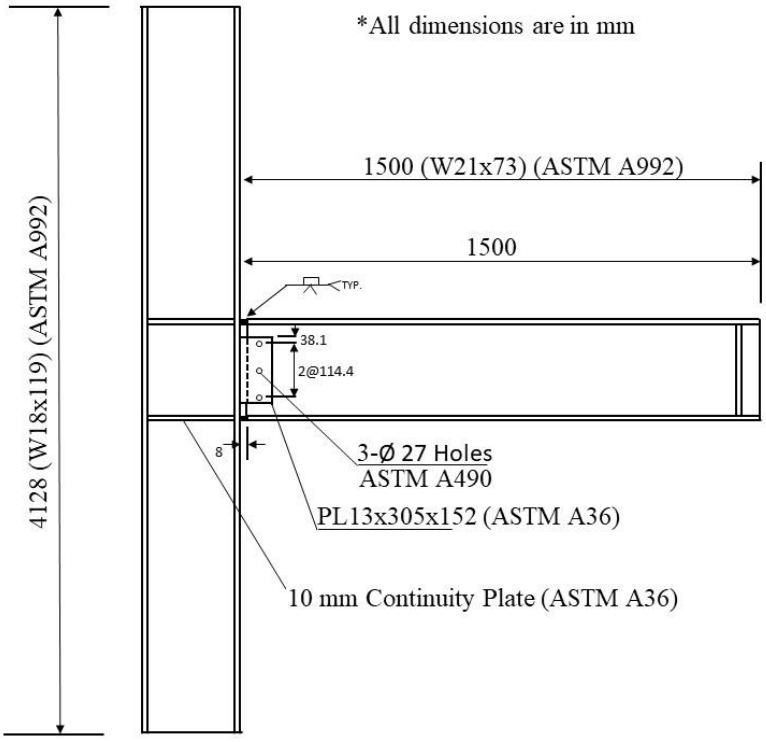

Figure 5-1 Beam-Column Assembly and WUF-B Connection Details [32]

5.2 Objectives

The primary objective of the work described in this chapter is to investigate the behavior of a representative moment connection subjected to elevated temperatures of 20ºC, 200ºC, 400ºC, and 600ºC representing fire through computational studies. The response of the connection at elevated temperatures when subjected to; 1) pure axial load, 2) pure bending moment, and 3) combined axial and bending (M-N-T) was studied. In addition, the influence of NIST [9] and Eurocode [10] material models on the response of these connections was also studied, along with the influence of fracture damage property in Abaqus. The results obtained from these studies contribute to understanding the connection under the events of fire hazards and the influence of different material models on the behavior of this connection. Ultimately, the M-N-T interaction curves obtained in this study for moment connections was compared against the M-N-T interaction curves using AISC Appendix 4 [11] for the strength of members at elevated temperatures and the applicability of the AISC equations in Appendix 4 [11] for deriving the capacity the moment connection will be determined. The research objectives are summarized in the following points:

1. To establish the relationship between axial force-bending moment-temperature (M-N-T) through numerical investigation by subjecting the model to combined moment and axial force at elevated temperatures.
2. To perform a comparative assessment on the influence of NIST and Eurocode 3 material models on the behavior of the moment connection and understand the impact of fracture.
3. To conduct a comparative evaluation of the M-N-T interaction plots for the moment connections obtained through finite element analysis against AISC Appendix 4 member strength equations.

5.3 Modeling Approach

The same modeling approach described in Section 3.4 was used for modeling the assembly in Abaqus. Figure 5-2 shows the finite element model for the assembly. The beam, columns, shear tab, stiffeners, and bolts were modeled in a consistent manner as the benchmark numerical models described in Chapter 3. Figure 3-4 provides a screen view of the modeled assembly. The complete joint penetration weld between the beam flange and column was assumed to be a rigid connection, and there, the beam was directly tied to the column using the tie command. The shear tab was welded to the column, so the contact was defined using tie constraints as it was fixed on the edge. For the boundary conditions, the column end was fixed at the top and bottom. The column was restrained along its flange end to prevent lateral movement, whereas the beam was laterally braced at its end span at the location of the load.

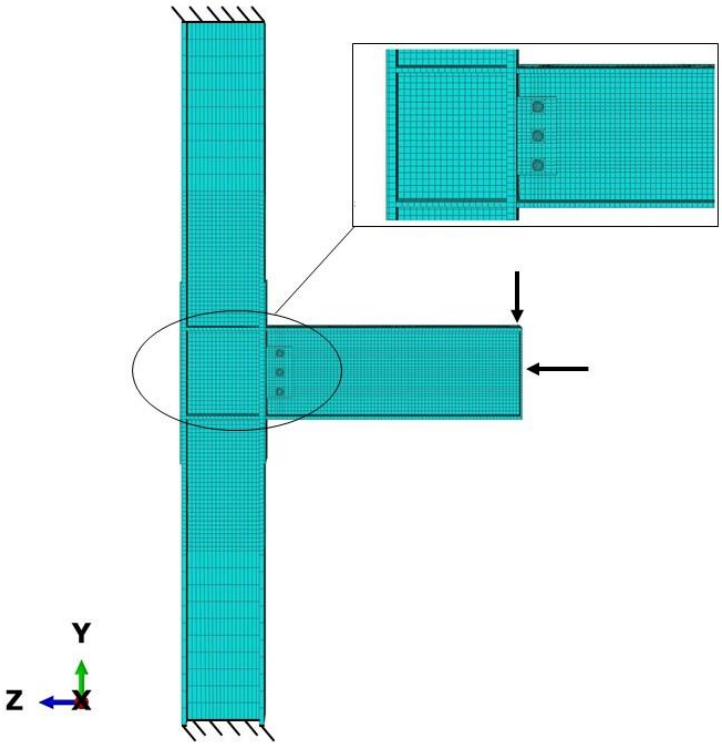

Figure 5-2 Finite Element Model of the Assembly

A rigid plate was tied at the end of the beam member in the models. The axial load was applied to this rigid plate to distribute the load to the beam cross-section evenly. Next, a concentrated vertical load was applied at the beam end to generate a bending moment on the connection. Thus, the combined axial-bending case was run in two steps, wherein the first step involved applying axial load at the beam end until the axial load reached a target value. Finally, in step two, the bending moment was applied until failure.

5.4 Results using NIST Material Model

The NIST stress-strain model [9] described in Section 3.3.1 is used for performing finite element analysis. The material model, up to 10 % strain, was considered in the analysis. The model was analyzed for elevated temperatures of 20ºC, 200ºC, 400ºC, and 600ºC. This section will study the influence of the NIST stress-strain model on the response of the connection at elevated temperatures when subjected to; 1) pure axial load, 2) pure bending moment, and 3) combined axial load and bending moment. The results in the form of load vs. displacement and moment vs. rotation are plotted. The rotation of the beam is calculated using the methodology discussed in Section 3.5.2.1.

5.4.1 Pure Axial Results

Figure 5-3 shows the load plotted against the displacement for the pure axial case at various temperatures such as 20ºC, 200ºC, 400ºC, and 600ºC using the NIST stress-strain model [9]. The horizontal lines in the Figure 5-3 indicate the theoretical axial capacities at elevated temperature for the beam. Figure 5-4 shows the typical failure mode at the connection location due to axial compression.

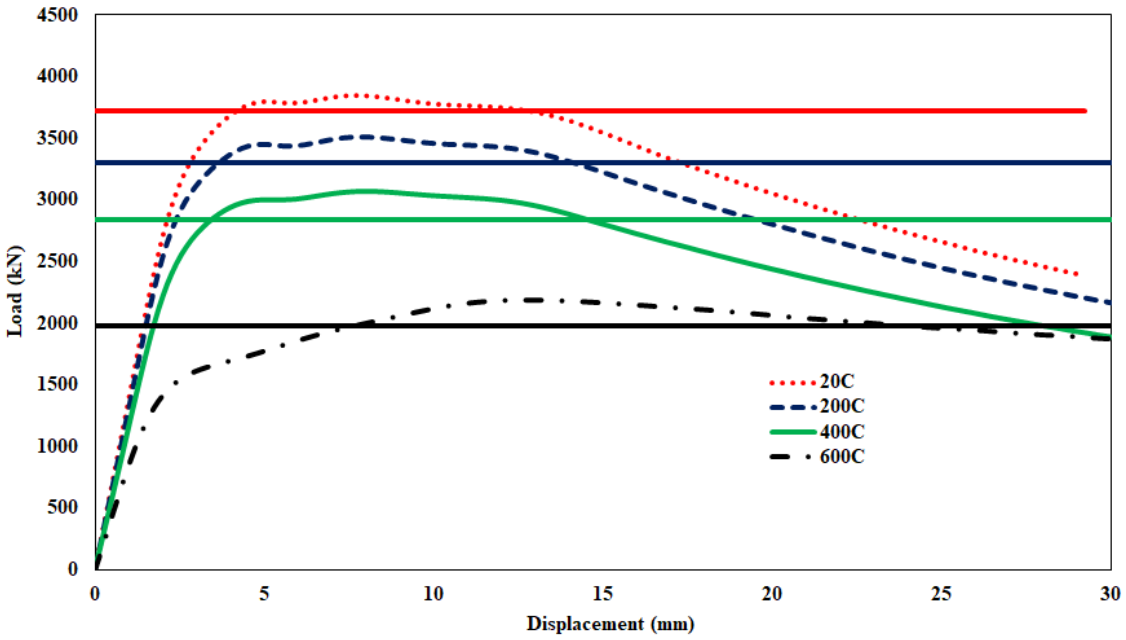

Figure 5-3 Load vs. Displacement Curve for Pure Axial Cases using NIST Material Model

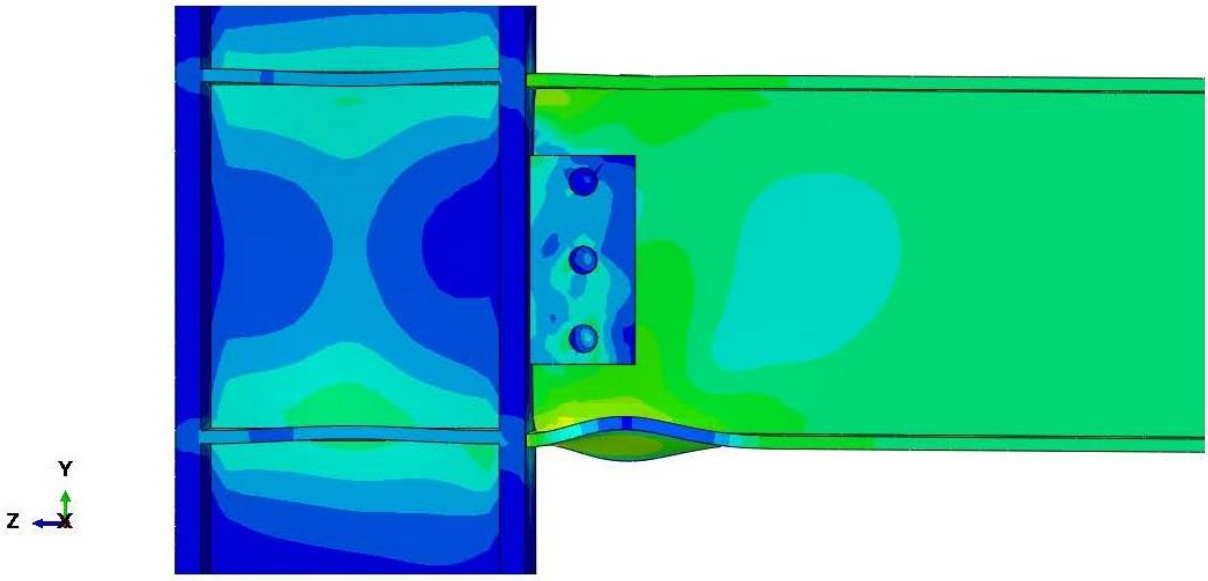

Figure 5-4 Local Buckling of Flange due to Pure Axial Compression

5.4.2 Pure Bending Results

The results for a pure bending case using the NIST stress-strain model at various temperatures such as 20ºC, 200ºC, 400ºC, and 600ºC are presented in this section. The models

were also analyzed incorporating fracture in the FE model and compared against no fracture case. For the fracture case, the ductile damage option in Abaqus was used to model the ductile fracture of steel material after reaching an ultimate strain threshold that corresponds to damage initiation. Based on previous literature review and stress vs strain curve, the damage initiation strain was specified as 5% and the triaxiality for uniaxial loading was specified to be 1/3 [54]. The element deletion option was enforced at ultimate strain of 10 %. Figures 5-5 and 5-6 show the load vs. displacement and moment vs. rotation curves considering fracture and no fracture cases. For the fracture model, the failure was observed in the shear tab. The shear tab fractured after reaching its fracture strain and the simulation stopped. Also, the horizontal lines in the figures indicate the theoretical flexural capacities at elevated temperature for the beam. The horizontal lines indicate the nominal flexural capacity of the beams at elevated temperatures (Z_x x $F_y[T]$). Figure 5-7 shows the typical failure mode at the connection due to pure bending moment. Table 2 below shows the comparison of the results using model with and without fracture. As shown in the table, there was a minor strength reduction between the two models with a difference in the peak load between the two models was observed to be 16.34 %. The model without fracture damage was determined to be more ductile as the maximum difference in the peak displacement and rotation was determined to be 77.64 % and 72.15 % respectively. However, it should be noted that very stringent damage properties were defined for the fracture case and the overall results obtained using fracture model are very conservative.

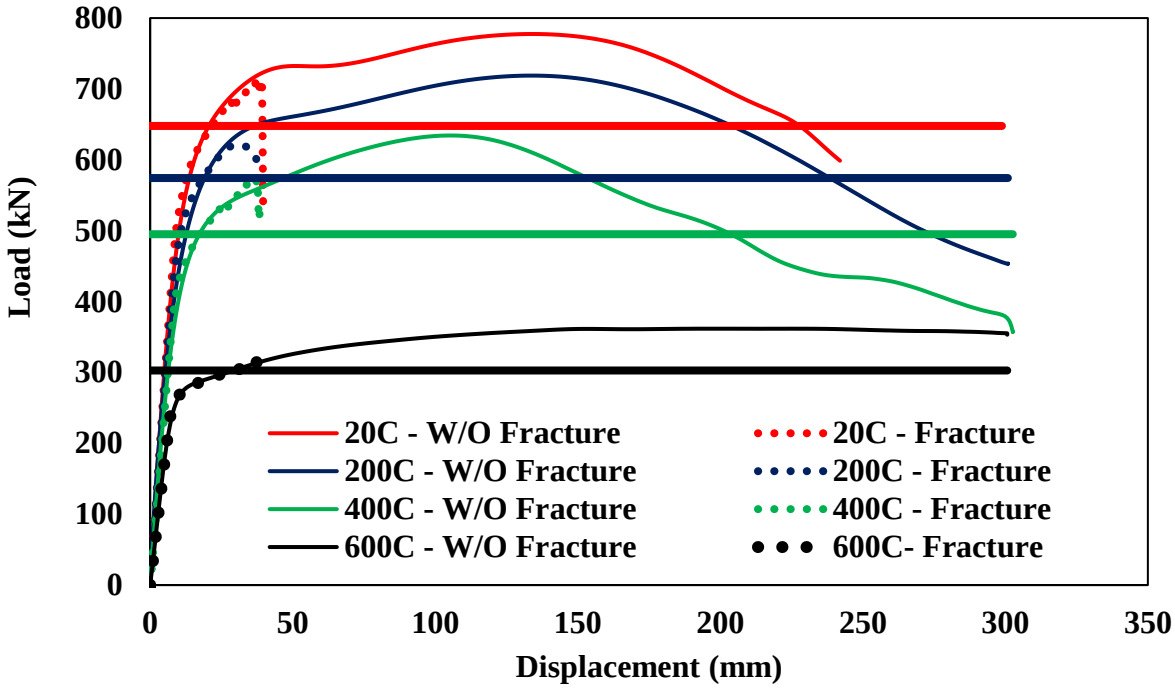

Figure 5-5 Load vs. Displacement Curves for Pure Bending Cases using NIST Material Model with and without Fracture

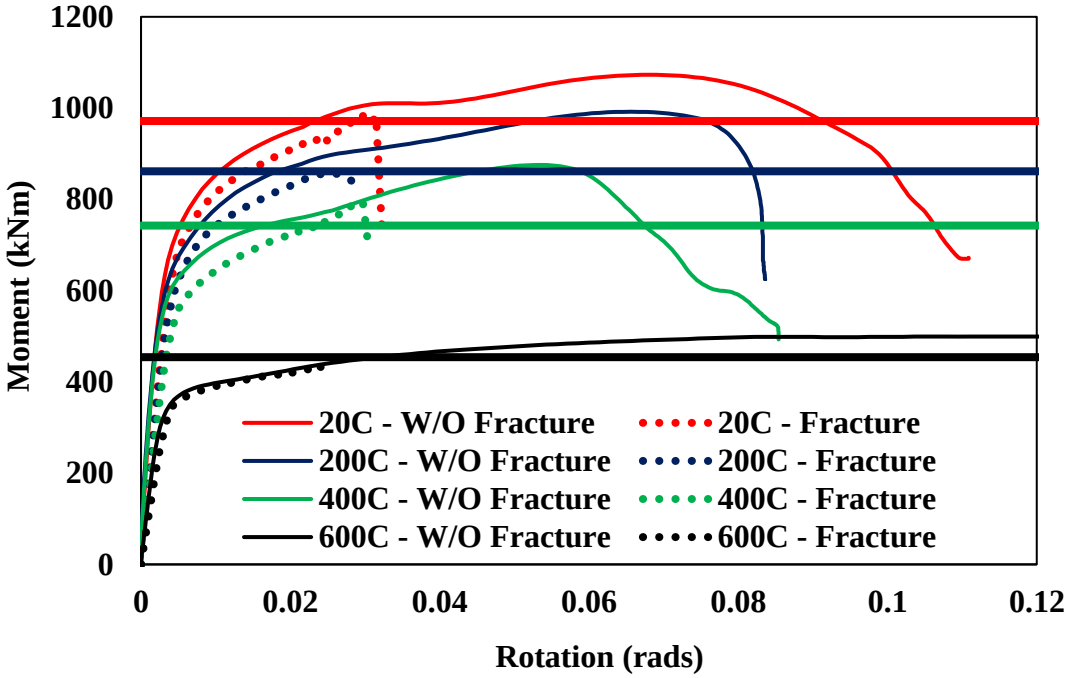

Figure 5-6 Moment vs. Rotation Curves for Pure Bending Cases using NIST Material Model with and without Fracture

Table 2 Comparison of Results using Fracture and Non-Fracture

Temp (ºC)	Analysis Type	Load (kN)	Displacement (mm)	Rotation (rads)
20	Without Fracture	774.00	146.00	0.07
	With Fracture	704.00	38.00	0.03
	%Reduction	**9.04**	**73.97**	**57.53**
200	Without Fracture	716.00	142.00	0.07
	With Fracture	618.00	35.00	0.05
	%Reduction	**13.69**	**75.35**	**36.26**
400	Without Fracture	634.00	106.00	0.05
	With Fracture	567.00	38.00	0.03
	%Reduction	**10.57**	**64.15**	**42.00**
600	Without Fracture	361.00	161.00	0.08
	With Fracture	302.00	36.00	0.02
	%Reduction	**16.34**	**77.64**	**72.15**

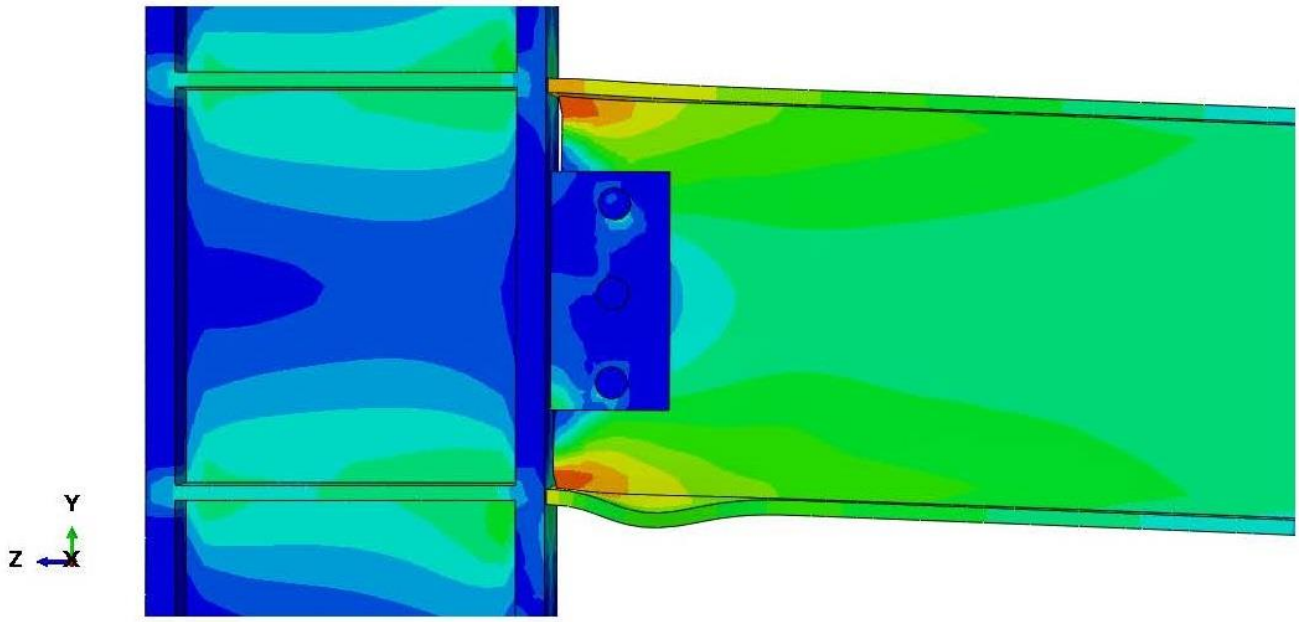

Figure 5-7 Local Buckling of Flange due to Pure Bending Moment

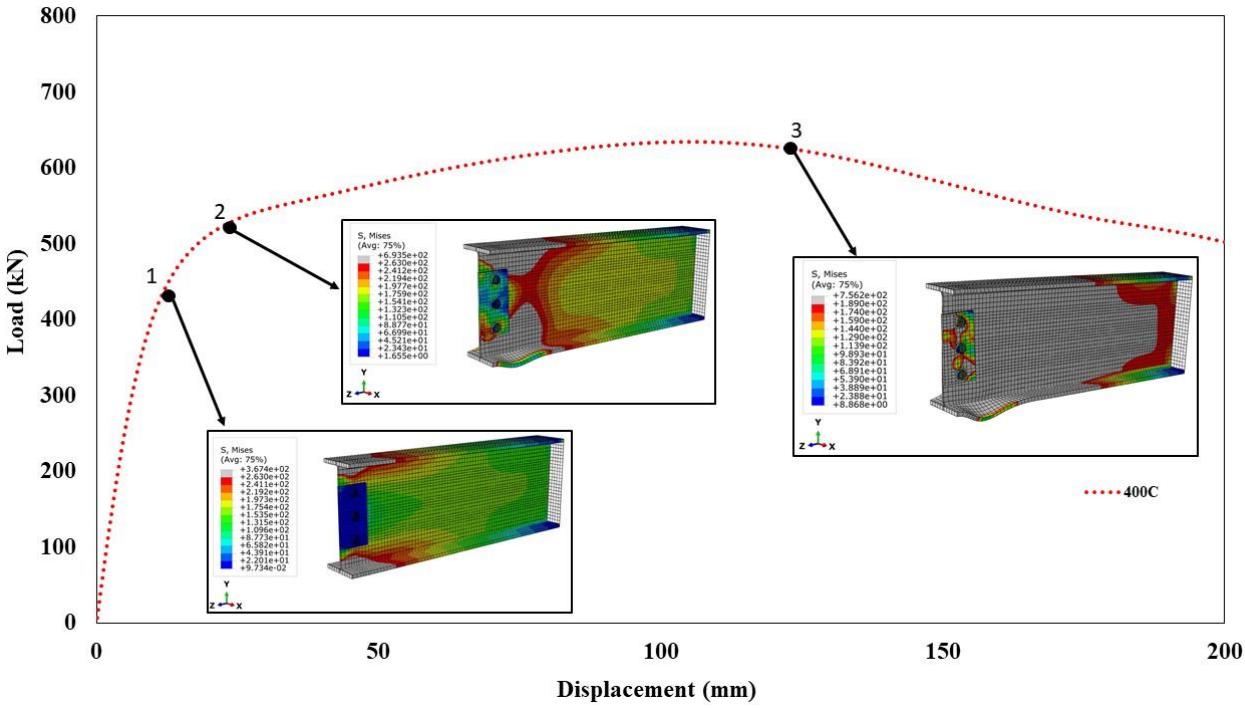

Figure 5-8 Deformation and Progression of Yielding in Moment Connection at 400ºC

Figure 5-8 shows a load vs. displacement curve and a visual representation of the failure mode at the connection region for non-fracture model at different points along the curve for 400ºC. As shown Figure 5-8, at point 1, the beam top and bottom flanges yielded first, and no significant stress was observed on the shear tab and the bolts. At point 2, before the curve started to plateau, significant portion of the beam cross section has yielded and the beam bottom compression flange has undergone local buckling, however, the shear tab or bolts did not reach its yield capacity. Finally, at point 3, the whole member failed after the shear tab and bolts failed. Note that the point 3 would not occur in fracture model as the shear tab would fail somewhere close to point 2 in the curve due to fracture. The FE models made a steady prediction that the overall failure mode of the assembly is governed by the member's failure and not the connection. It was also observed that the failure at the connection region was governed by the local buckling of the bottom compression flange. As shown in the Figure 5-8, the shear tab and

the bolts did not have any significant contribution towards the overall strength of the connection. This was also observed during the benchmarking process in Chapter 3, wherein, Yang's [13] test specimen with and without shear tab and bolts showed no significant change in results (see Figure 3-9, 3-10 and 3-11 in Chapter 3).

5.5 Comparison of Results using NIST and Eurocode Material Model

The Eurocode 3 stress-strain model described in Section 3.3.2 is used in the finite element analysis of the moment connection. Similarly, the model was analyzed for elevated temperatures of 20ºC, 200ºC, 400ºC, and 600ºC. This section compares the results obtained using the NIST and Eurocode 3 stress-strain models for temperatures 20ºC, 200ºC, 400ºC, and 600ºC. Figure 5-9 shows the comparison between the two-material model response for pure axial cases. Similarly, Figures 5-10 and 5-11 compare the load vs. displacement and moment vs. rotation response for the pure bending cases.

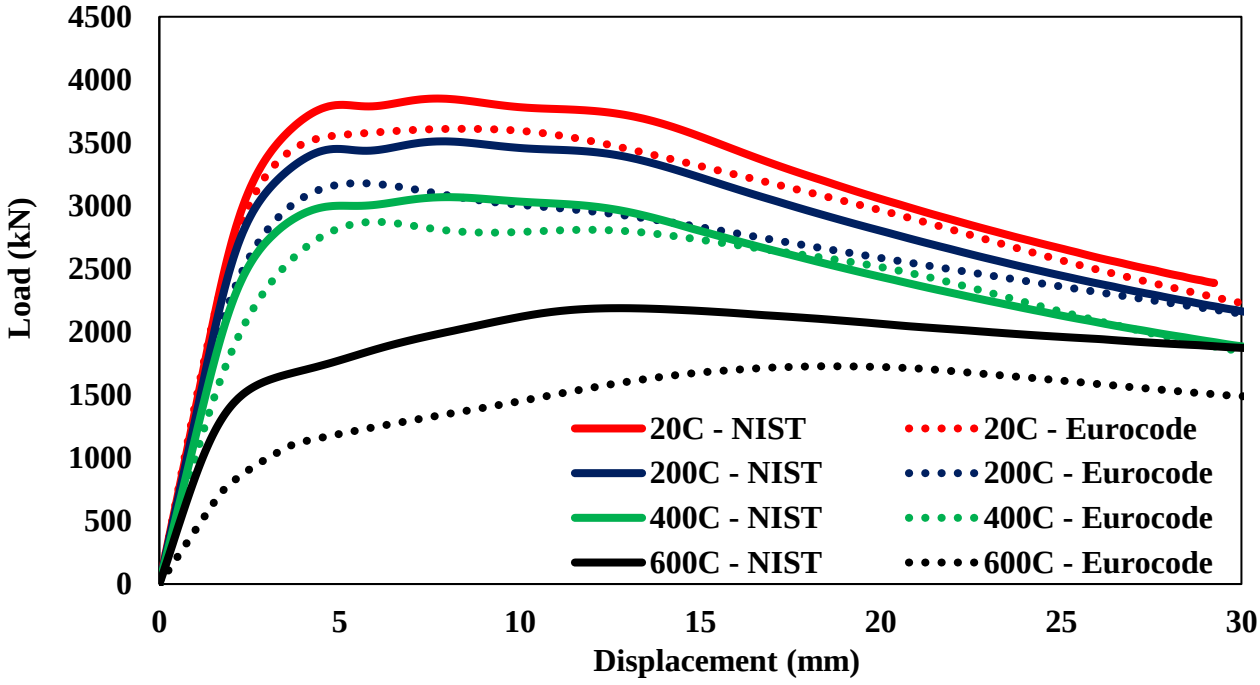

Figure 5-9 Comparison of Results between NIST and Eurocode 3 stress-strain models for Pure Axial Cases at Elevated Temperatures

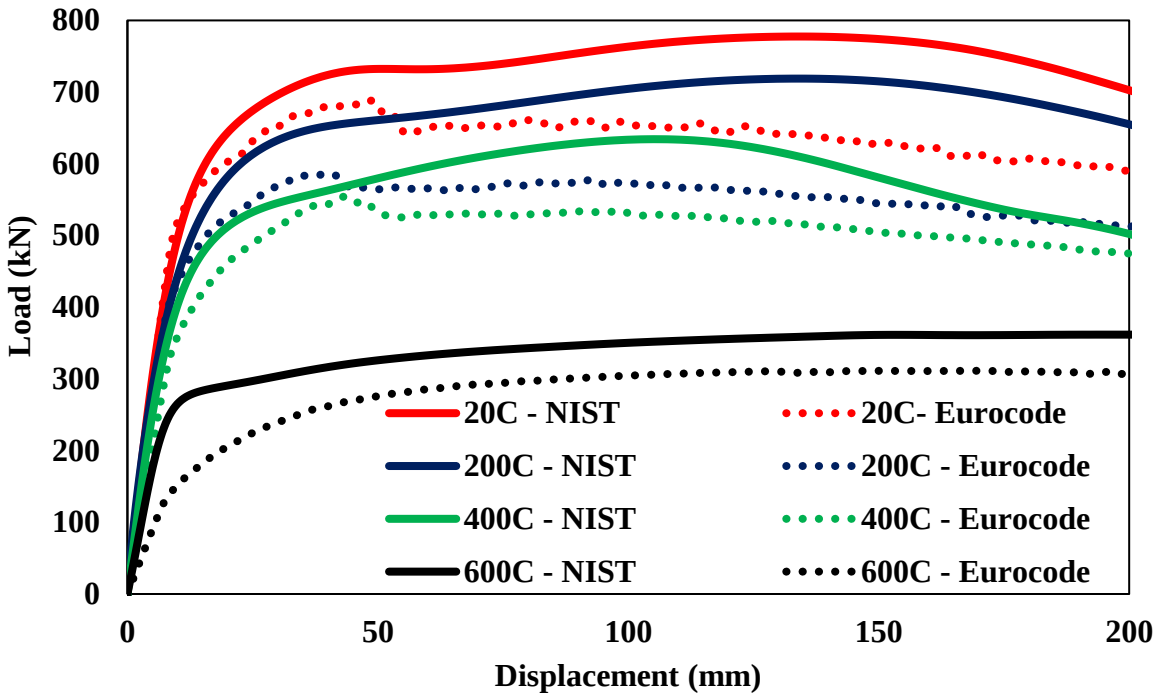

Figure 5-10 Comparison of Load vs. Displacement Curves using NIST and Eurocode 3 Material Model for Pure Bending Cases at Elevated Temperatures

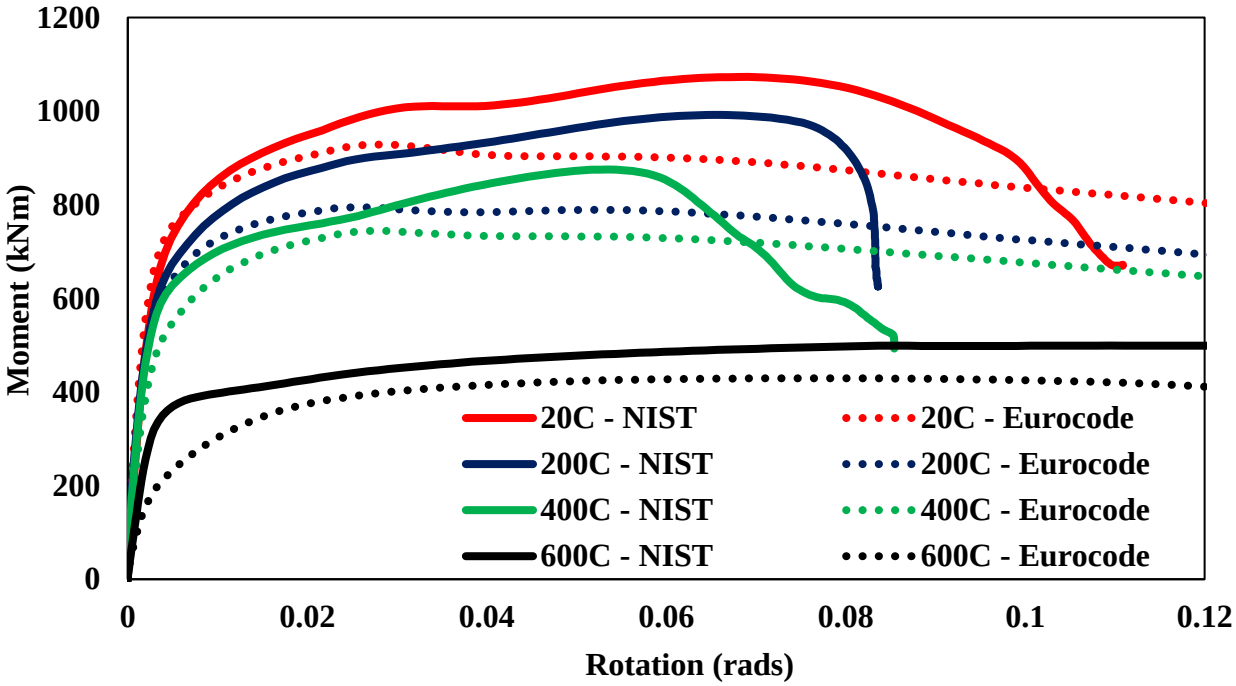

Figure 5-11 Comparison of Moment vs. Rotation Curves using NIST and Eurocode 3 Material Model for Pure Bending Cases at Elevated Temperatures

The above Figures 5-9 to 5-11 show that the finite element models analyzed using Eurocode stress-strain model indicate a smaller load-resisting capacity than the NIST material model. The analysis indicated that the FE model analyzed using Eurocode 3 material model, in general, showed at an average 10-15 % lesser capacity than the NIST material model up to temperatures of 400ºC. However, at elevated temperatures beyond 400ºC, the Eurocode 3 model predicted a significant drop in stiffness and capacity. This discrepancy is speculated as a result of the elastic behavior conservatively predicted by the Eurocode 3 stress-strain model. Eurocode 3 [10] considers rate-dependent effects such as thermal creep while defining the stress-strain relationship at various temperatures. Since NIST σ - ε - T relationship does not account for rate-dependent effects like a creep at elevated temperatures, it has higher yield stress and more prevalent post-yield strain-hardening than the corresponding Eurocode σ - ε - T relationship. Also, the reduction factors defined in NIST are calculated based on 0.2% offset strain, whereas Eurocode considers 2% offset strain. The modulus of elasticity of the Eurocode 3 and NIST material model starts to drop at temperatures above 100ºC (see Figure 3-2). At an elevated temperature of 600ºC, the Eurocode 3 elastic modulus is about 52 % of the NIST elastic modulus. The beam failure mode is governed by the local buckling of the compression flange and it is observed that the Eurocode 3 model provides conservative prediction of the beam capacity due to its inherent material characteristics, which shows a significant drop in the modulus of elasticity at 600ºC. Choe et al. [55] made similar observations in their study while comparing NIST and Eurocode 3 material models for column strength, wherein, the Eurocode 3 made conservative predictions on the flexural buckling behavior due to its retained elastic moduli are smaller than those of the NIST material model at elevated temperature. In addition, similar results were observed in Chapter 3 while benchmarking Yang's [13] specimen using

NIST and Eurocode 3 material models, wherein, the Eurocode material showed lower strength capacity in comparison with NIST material model and the experimental results (see Figures 3-15, 16 and 17).

5.6 Comparison of Axial Load and Moment Interaction Curves using NIST and Eurocode 3 Material model and AISC equations

This section compares the moment and axial load interaction curves at elevated temperature (M-N-T) generated using the NIST [9] and Eurocode 3 [10] stress-strain models through the FE analysis at various temperatures such as 20ºC, 200ºC, 400ºC, and 600ºC. Figure 5-12 shows the comparison of M-N-T interaction curves plotted using the NIST and Eurocode 3 material models and AISC Appendix 4 beam-column member strength estimations.

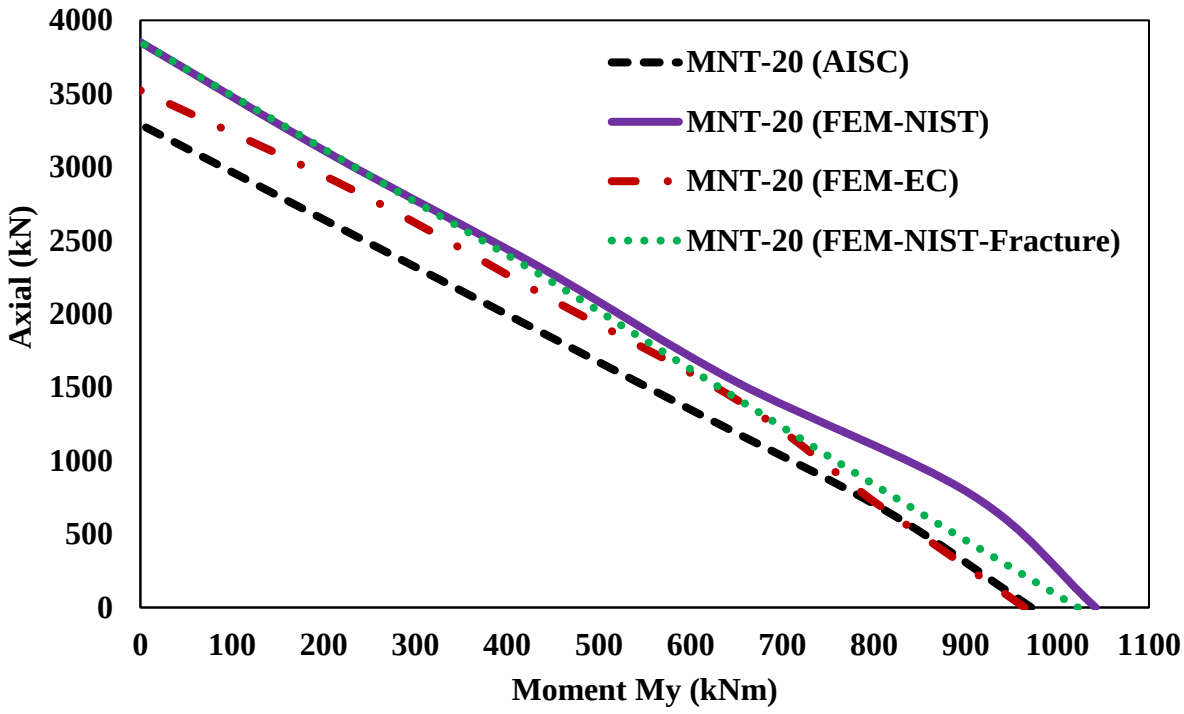

a)

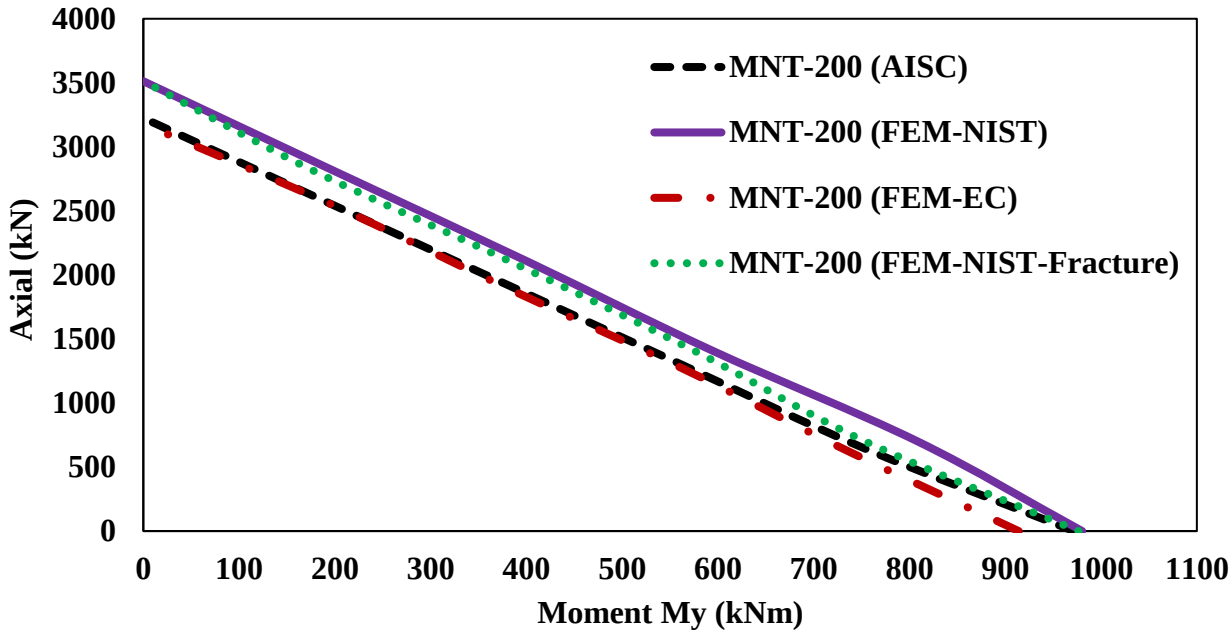
4000
3500
3000
2500
2000
1500
1000
500
0
Axial (kN)
0
100
200
300
400
500
600
700
800
900
1000
1100
Moment My (kNm)
MNT-200 (AISC)
MNT-200 (FEM-NIST)
MNT-200 (FEM-EC)
MNT-200 (FEM-NIST-Fracture)

b)

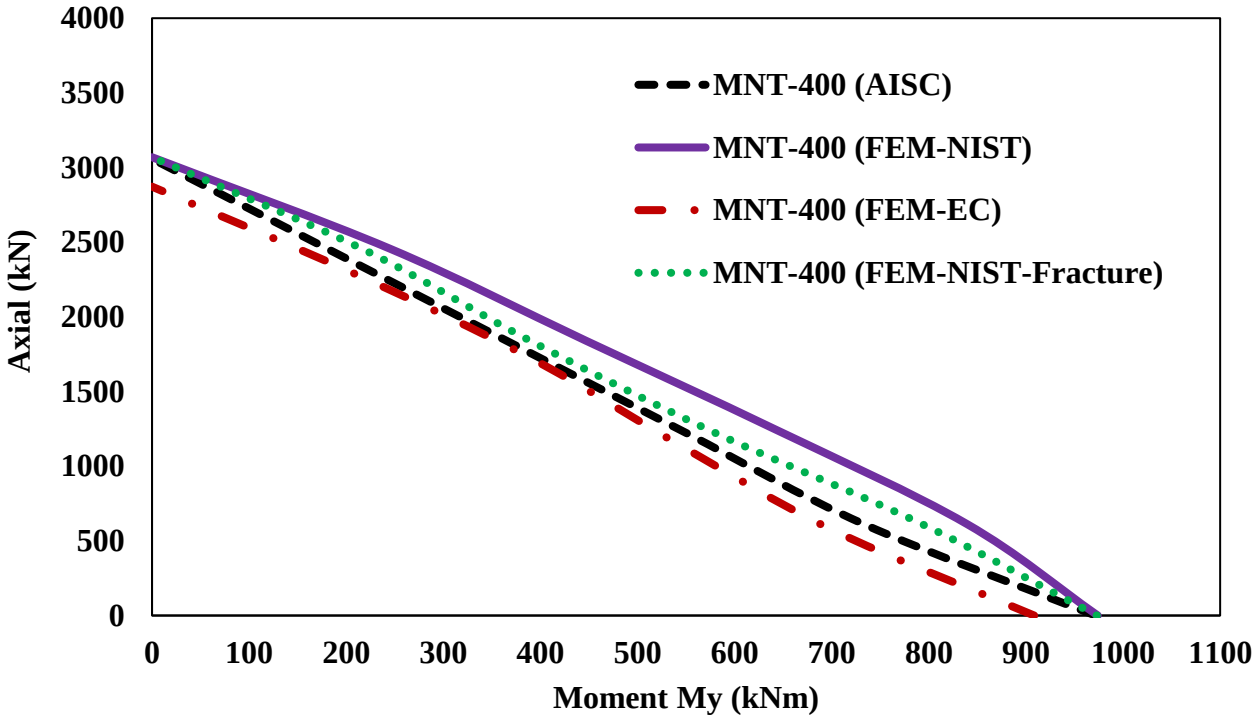
4000
3500
3000
2500
2000
1500
1000
500
0
Axial (kN)
0
100
200
300
400
500
600
700
800
900
1000
1100
Moment My (kNm)
MNT-400 (AISC)
MNT-400 (FEM-NIST)
MNT-400 (FEM-EC)
MNT-400 (FEM-NIST-Fracture)

c)

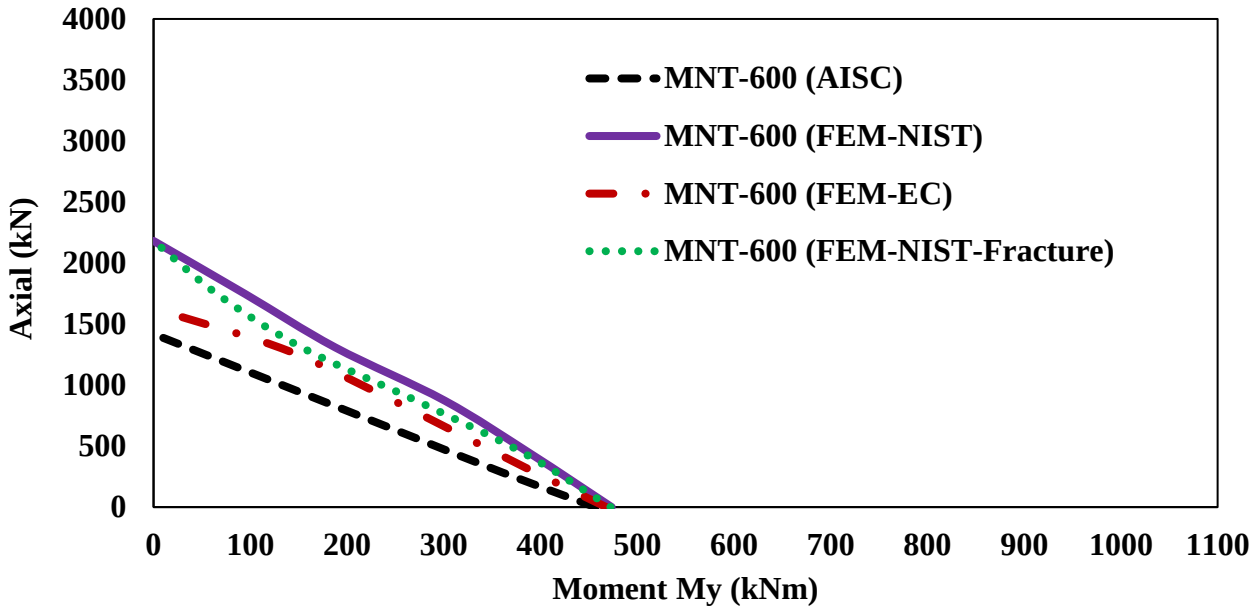

d)

Figure 5-12 Comparison of the M-N-T Interaction Curves between NIST, Eurocode 3, and AISC for elevated temperatures of; a) 20ºC, b) 200ºC, c) 400ºC, and d) 600ºC

The results above show the comparison of the M-N-T interaction curves between NIST, Eurocode, and AISC for the moment connection. The same AISC equations used in Section 4.2 were used to derive the AISC curves. The results obtained due to NIST and Eurocode 3 show good agreement between the curves generated by the AISC beam-column member strengths. Up to temperatures of 400ºC, the AISC curves do not show a significant change in their moment capacities, but only slight change in the compressive strength. This is expected as the yield strength proportionality limit was derived from Eurocode 3, and the proportionality limit does not change up to 400ºC. However, at 600ºC, the capacities drop significantly due to the significant drop in the proportionality limits.

The AISC equations, although initially developed to be only used for member strength equations, show good agreement with the M-N-T interaction curves for moment connections.

Additionally, as these equations were derived by Takagi and Deierlein [42], these equations apply to only members with compact or near compact shapes. However, the W21 x 73 member used in this study is a slender member for compression, and based on the above results, the M-N-T interaction curves for the moment connection show good agreement with the M-N-T interaction curves using AISC equations for member sections. Therefore, this phenomenon is thought of as the failure mode for the moment connection governed by the member failure (local flange buckling) and not the connection itself, according to the modeling approach used in this study.

6. SUMMARY, CONCLUSIONS, AND RECOMMENDATIONS

6.1 Research Summary

Fire is a hazardous event that subjects the structure to a distinctive set of demands during its performance to resist significant forces and excessive deflections and rotations that may lead to extensive damage. U.S. codes and standards provide a prescriptive design approach, wherein, the structural floor beams and connections of moment frames are designed against flexural demands that relies on sets of load combinations comprising of service loads such as structural gravity loads and lateral loads, and thermally induced axial loads are often not part of the design approach. Past research on steel connections subjected to elevated temperature simulating fire events have indicated that these thermally-induced loads are primarily dependent on the temperature change and connection type. Moment (rigid) connections are expected to be subjected to significant stresses due to their high rotational and translational stiffness, thus become particularly susceptible to various failure modes due to the combined effect of bending moment and axial loads during a fire event. Therefore, it is imperative to quantify the behavior of moment frame members such as steel beams and moment connections due to the combined axial force-bending moment interaction during a fire event (M-N-T) while considering thermal restraint.

3D finite element numerical models were developed for evaluating the structural response of floor beams and moment connections by accounting for temperature-dependent material properties recommended by Eurocode and NIST. To verify the modeling approach, benchmark numerical models were developed by comparing against past experimental results. The analysis results accurately predicted the results and failure modes at different temperatures

when compared against the past experimental results. After establishing the benchmark finite element modeling approach, the thesis focused on assessing the member capacities of typical floor beams (slender in compression) under pure axial, pure moment, and combined moment and axial forces at elevated temperatures. The analysis results were also compared against the member strength equations given in AISC Appendix 4 [11] at elevated temperatures. The results indicated that the AISC equations for pure compression cases are unconservative for slender members with relatively low slenderness ratios (less than 60), and this was also reflected in the combined axial force and bending moment cases. The next phase of the research evaluated a representative beam-to-column moment connection to obtain the fundamental connection response under pure axial, pure bending and combined axial force-bending moment at different temperature levels under realistic thermal restraint representing adjacent bays. The moment connection behavior was primarily governed by the failure mode exhibited at the end of the connecting floor beams, therefore the axial load and moment interaction relationships (M-N-T) developed for member strengths using AISC Appendix 4 [11] equations showed good agreement with the M-N-T interaction curves for the moment connection. Thus, the final recommendation is to also use the AISC Appendix 4 [11] equations for estimating strength estimates for moment connections for slenderness ratios of 60 and above.

6.2 Conclusions

The key objectives of this research have been achieved successfully. Based on the numerical investigations conducted using three-dimensional finite element analysis, the following conclusions are drawn:

1) The developed numerical models were capable of capturing the behavior and response of both beams and connection elements of typical moment frames. The primary influence on

the analysis results were the variations in the temperature material models. Incorporating damage evolution and failure criteria in the material model had relatively minor impact on the overall moment connection strength.

2) The Eurocode 3 material properties, which are also used for defining steel mechanical properties at elevated temperature in the AISC specification, result in more conservative capacity estimates in comparison to the NIST material model. This is mainly because the Eurocode 3 elastic modulus and yield strength is considerably smaller than that of the NIST model at elevated temperatures, particularly for temperatures beyond 400ºC.
3) The analysis results indicated more accurate comparisons when NIST-developed temperature dependent material properties were used compared to the Eurocode properties. The improvement in the results were credited partly due to the NIST models accounting for types of steel such as plates and bolts. Therefore, the NIST material models are recommended for detailed analysis of steel members at elevated temperature.
4) Failure modes observed for connections of moment frames with slender beam members were typically governed by the flange and web local buckling of beam members occurring near the connection.
5) The AISC Appendix 4 equations for columns (pure compression cases) given in Appendix 4 are unconservative for slender beam elements due to not taking of the strength reduction from local buckling into account. Similarly, the beam-column equations used for estimating the strength of floor beams and moment connections subjected to combined axial and moment cases also provided unconservative results for beams with slenderness ratios below 60. Therefore, the applicability of AISC equations can be extended towards predicting the capacity of moment connections with connecting beam members that

typically include slender webs for compression design for slenderness ratios of 60 and above only.

6.1 Suggestions for Future Work

The research presented in this thesis focused on the structural behavior of members in moment frames at elevated temperatures. Some pertinent issues have not been addressed during this research which could lead to additional guidance by improving understanding of behavior. These suggestions are proposed below for future work:

1) Further investigation of the connection behavior under reversing axial loads (from compression to tension) that represent the cooling phase in the post-fire stage are recommended.
2) This research project studied the WUF-B connection behavior as a generic moment connection type and used W21 x 73 as a typical steel beam section. Additional studies on the connection behavior for different moment connection types and beam sections are recommended.
3) The effects of thermal stresses and expansion on the moment connection response should be investigated for more controlled thermal restraint levels.
4) This thesis assumes uniform temperature distribution throughout the member cross-section, which may not be conservative for some members where non-uniform temperatures can induce member curvature that can cause more prevalent geometric non-linear effects.
5) The studies only consisted of bare steel members without composite slab. Additional investigations are recommended to include the effects of steel beams with concrete topping.

6) This research did not explicitly model the welds physically present in moment connections between the beam and column flanges. Future studies can incorporate weld models with associated damage and failure models to investigate the effects on the overall response.

LIST OF REFERENCES

[1] R. Latter, "The European Market for Constructional Steelwork," *New Steel Construction,* vol. 2, 1995.

[2] S. Desai, "Future Eurocodes and Structural Fire Design," *The Structural Engineer,* vol. 68, pp. 451-453, 1990.

[3] G. Cooke, "Practical Fire Engineering- The Context," *National Structural Steel Conference, London,* 1984.

[4] D. A. Nethercot, "Towards a Standardisation of the Design and Detailing of Connections," *Journal of Constructional Steel Research,* vol. 46, pp. 3-4, 1998.

[5] J. Davison and D. Nethercot, "Overview of Connection Behavior," *In the Structural Connection-Stability and Strength,* pp. 1-22, 1989.

[6] K. Al-Jabri, "The Behavior of Steel and Composite Beam-to-Column Connections in Fire," *PhD. Thesis, Department of Civil and Structural Engineering, University of Sheffield,* 1999.

[7] J. Robinson, "New Thinking on Multi-storey Building Fires: The Cardington Fire Test Programme- Initial Conclusions," *Fire Safety Engineering,* vol. 4, pp. 25-26, 1997.

[8] "Investigation of Broadgate Phase 8 Fire, Structural Fire Engineering," *Steel Construction Institute,* 1991.

[9] M. Seif, J. Main, J. Weigand, F. Sadek, L. Choe, C. Zhang, J. Gross, W. Luecke and D. MeColskey, "Temperature-Dependent Material Modeling for Structural Steels: Formulation and Application," U.S. Department of Commerce, 2016.

[10] "European Committee for Standardizartion (CEN)," *Eurocode 3: Design of Steel Structures, Part 1.2: General Rules-Structural Fire Design,* 2005.

[11] American Institute of Steel Construction, Inc., Chicago, IL: AISC, 2010.

[12] "Abaqus/Standard Version 6.19 User's Manual," Providence, RI, 2019.

[13] K.-C. Yang, S.-J. Chen and M.-C. Ho, "Behavior of beam-to-column moment connections under fire load," *Journal of Constructional Steel Research,* vol. 6, pp. 1520-1527, 2009.

[14] K. Al-Jabri, A. Seibi and A. Karrech, "Modelling of unstiffened flush end-plate bolted connections in fire," *Journal of Constructional Steel Research,* vol. 62, pp. 151-159, 2006.

[15] K. S. Al-Jabri and F. Al-Jahwari, "Advances Finite Element Modelling of Flexible End-Plate Beam-to-Column Joints in fire," *Advances in Structural Engineering,* vol. 1, no. 3, pp.

311-324, 2012.

[16] A. Agarwal and A. Varma, "Fire induced progressive collapse of steel building structires: The role of interior gravity columns," *Engineering Structures,* vol. 58, pp. 129-140, 2014.

[17] G. Cedeno, A. H. Varma and A. Agarwal, "Behavior of Floor Systems under Realistic Fire Loading," *Structural Congress,* 2009.

[18] IBC, International Building Code, Washington D.C.: International Code Council, 2012.

[19] ASCE, Minimum Design Loads for Buildings and Other Structures (ASCE 7-10), Reston, VA: American Institute of Steel Construction , 2010.

[20] S. Selamet and M. E. Garlock, "Robust fire design of single plate shear connections," *Engineering Structures,* vol. 32, pp. 2367-2378, 2010.

[21] S. Selamet and M. Garlock, "Modelling and Behavior of Steel Plate Connections subject to various fire scenarios," *Journal of Structural Engineering,* pp. 897-906, 2010.

[22] M. Gillie, A. Usmani and J. Rotter, "A structural analysis of the first Cardington test," *Journal of Constructional Steel Research,* vol. 57, pp. 581-601, 2001.

[23] S. Selamet and M. Garlock, "A Comparison between the Single Plate and Angle Shear Connections Performance Under Fire," in *ASCE Structures Congress*, Las Vegas, NV, 2011.

[24] A. Agarwal, A. H. Varma and G. Cedeno, "Stability Behavior of Steel Building Structures with Perimeter MRFs under Fire Loading Effects," *Structures 2009,* pp. 687-696, 2009.

[25] A. Agarwal, K. Selden and A. Varma, "Stability Behavior of Steel Building Structures in Fire Conditions: Role of Composite Floor Systems with Shear-Tab Connections," *Journal of Structural Fire Engineeering,* vol. 5, no. 2, pp. 77-96, 2014.

[26] K. L. Selden, E. C. Fischer and A. Varma, "Experimental Investigation of Composite Beams with Shear Connections Subjected to Fire Loading," *J. Struct. Eng.,* no. 142(2): 04015118, 2016.

[27] E. C. Fischer and A. H. Varma, "Fire behavior of composite beams with simple connections: Benchmarking of numerical models," *Journal of Constructional Steel Research,* vol. 111, pp. 112-125, 2015.

[28] L. Choe, S. Ramesh, W. Grosshandler, M. Hoehler, M. Seif, J. Gross and M. Bundy, "Behavior and Limit States of Long-Span Composite Floor Beams with Simple Shear Connections Subject to Compartment Fires: Experimental Evaluation," *J. Struct. Eng.,* no. 146(6): 04020088, 2020.

[29] K. Al-Jabri, I. Burgess, T. Lennon and R. Plank, "Moment-rotation-temparture curves for

semi-rigid joints," *Hournal of Constructional Steel Research,* vol. 61, pp. 281-303, 2005.

[30] N. Ramli-Sulong, A. Elghazouli and B. Izzuddin, "Behavior and design of beam-to-column connections under fire conditions," *Fire Safety Journal,* vol. 42, pp. 437-451, 2007.

[31] Z. Qian, K. Tan and I. Burgess, "Behavior of Steel Beam-to-Column Joints at Elevated Temperature: Experimental Investigation," *Journal of Structural Engineering,* vol. 134, no. 5, pp. 713-726, 2008.

[32] M. S. Seif, J. A. Main and F. H. Sadek, "Behavior of structural steel moment connections under fire loading," in *Proceedings of teh Annual Stability Conference Structural Stability Research Council,* Nashville, Tennessee, 2015.

[33] H. Lew, J. A. Main, S. D. Robert, F. Sadek and V. Chiarito, "Performance of steel moment connections under a column removal scenario T; Experiments," *Journal of Structural Engineering, ASCE,* vol. 139, no. 1, pp. 98-107, 2013.

[34] ASCE, "Standard Calculation Methods for Structural Fire Protections (ASCE/SEI/SFPE 29-05)," in *American Society of Civil Engineers, Society of Fire Prevention Engineers*, Reston, VA, 2007.

[35] L. Leston-Jones, I. Burgess, J. Davison and R. Plank, "Finite element modelling of steel fin plate connections in fire," *Fire Safety Journal,* vol. 42, pp. 408-415, 2007.

[36] L. Phan, J. Gross and T. McAllister, Best Practice Guidlines for Structural Fire Resistance of Concrete and Steel Buildings (NIST-TN-1681), Gaitherburg, MD: National Institute of Standards and Technology, 2010.

[37] L. Choe, W. Luecke and J. Gross, "A Comparison of two temperature-dependent stress-strain models for structural steel under transient heating condition," in *8th International Structures in Fire Conference*, Shangai, China, 2014.

[38] K. L. Selden, "Structural Behavior and Design of Composite Beams Subjected to Fire," Purdue University, West Lafayette, IN, 2014.

[39] I. T., "Design of composite structures containing bolt holes and open holes," Department of Aeronautics, Royal Institute of Technology, Sweden, 1999.

[40] K. Barth, J. Orbison and a. R. Nukala, "Behavior of steel tension members subjected to uniaxial loading," *J. Construct. Steel Reserach,* vol. 58, pp. 1103-1120, 2002.

[41] C. Mao, Y. Chiou, P. Hsiao and M. Ho, "Fire response of steel semi-rigid beam-column moment connections," *Journal of Constructional Steel Research ,* no. 65, pp. 1290-1303, 2009.

[42] J. Takagi and G. G. Deierlein, "Strength design criertia for steel members at elevated

temperatures," *Journal of Constructional Steel Research,* pp. 1036-1050, 2007.

[43] M. Bruneau, C. Uang and A. Whittaker, Ductile design of steel structures, New York: McGraw Hill, 1998.

[44] V. Bertero, E. Popov and H. Krawinkler, "Beam-column subassemblages under repeated loading," *Journal of the Structural Division,* vol. 98, no. 5, pp. 1137-1159, 1972.

[45] K. D. Tsavdaridis, C. Pilbin and C. K. Lau, "FE Paramatetric Study of RWS/WUF-B Moment Connections with Elliptical-based Beam Web Openings Under Monotonic and Cyclic Loading," *International Journal of Steel Structures,* vol. 17, no. 2, pp. 677-694, 2017.

[46] ICBO, Uniform Building Code, Whittier, CA, 1988.

[47] E. Popov, N. Amin, J. Louie and R. Stephen, "Cyclic behavior of large beam-column assemblies," *Earthquake Spectra,* vol. 1, no. 2, pp. 203-238, 1985.

[48] M. Engelhardt and A. Husain, "Cyclic-loading performance of welded flange-bolted web connections," *Journal of Structural Engineering,* vol. 119, no. 12, pp. 3537-3550, 1993.

[49] FEMA, "State of the art report on connection performance," in *FEMA 350, SAC Joint Venture and FEMA*, Washington, DC.

[50] ASCE, "Minimum Design Loads for Buildings and Other Structures," in *SE/ASCE 7-02*, Reston, VA.

[51] AISC, "Load and Resistance Factor Design Specifications for Structural Steel Buildings," Chicago.

[52] AISC, "Seismic Provisions for Structural Steel Buildings," in *ANSI/AISC 341-02*, Chicago.

[53] FEMA, "Recommended seismic design criteria for new steel moment-frame buildings," in *FEMA 350, SAC Joint Venture and FEMA*, Washington, DC.

[54] Z. Lai, "Experimental databases, analysis and design of noncompact and slender concrete-filled tube (CFT) members," Purdue University, West Lafayette, IN, 2014.

[55] L. Choe, C. Zhang, W. E. Luecke, J. L. Gross and A. H. Varma, "Influence of Material Models on Predicting the Fire Behavior of Steel Columns," *Fire Technology,* pp. 375-400, 2017.

[56] E. Fischer, K. Selden and A. Varma, "Experimental Evaluation of the Fire Performance of Simple Connections," *J. Struct. Eng.*, no. 143(2): 04016181, 2017.

[57] Specification for Structural Steel Buildings, Chicagi (IL): AISC, 2016.